T.C.
BURSA TECHNICAL UNIVERSITY
GRADUATE EDUCATION INSTITUTE

DESIGNING AND MANUFACTURING SUPERAMPHIPHOBIC FLEXIBLE SENSORS

PhD THESIS

Fatma Saime ERDÖNMEZ

Department of Polymer Materials Engineering

Doctorate Programme

JULY 2023

T.C.
BURSA TECHNICAL UNIVERSITY
GRADUATE EDUCATION INSTITUTE

DESIGNING AND MANUFACTURING SUPERAMPHIPHOBIC FLEXIBLE SENSORS

PhD THESIS

Fatma Saime ERDÖNMEZ
(152081003)
ORCID: 0000-0001-8961-8525

Department of Polymer Materials Engineering

Doctorate Programme

Thesis Advisor: Prof. Dr. Ayşe ÇELİK BEDELOĞLU
ORCID: 0000-0003-2960-5188

JULY 2023

In accordance with Articles 9/2 and 22/2 of the Postgraduate Education and Training Regulation published in the Official Gazette dated 20.04.2016; for this postgraduate thesis, a report was received in accordance with the criteria determined by the Graduate Education Institute by using the plagiarism software program that Bursa Technical University is subscribed to.

STATEMENT OF PLAGIARISM

I declare that all the information and results presented in visual, auditory, and written form in this thesis were obtained by me in accordance with academic and ethical rules, I have documented all the results and information in the thesis that are not specific to this study, by citing the source in the thesis, and I accept all kinds of legal consequences if the opposite arises.

Student's Name Surname: Fatma Saime ERDÖNMEZ

Signature :

To my parents,

FOREWORD

I would like to offer my sincere gratitude to my advisor, Prof. Dr. Ayşe Çelik Bedeloğlu, for her valuable guidance during my doctoral studies. She has been patient and professional, leading me with her vast experience and knowledge.

I would like to thank members of my thesis monitoring jury, Assoc. Prof. Cemal Hanilçi and Dr. Ömer Yunus Gümüş, for their help.

I would also like to thank Assoc. Prof. Cihan Kaboğlu and Dr. Hüsnü Bademlioğlu for providing me with support and motivation throughout this process.

Academicians, research assistants, and students in BTU Polymer Materials Engineering Laboratories have been helpful during my experimentation and characterization stages therefore I would like to thank the department as well as Dr. Yasin Altın, Research Assistants Ömer Faruk Ünsal, Ayten Nur Yüksel Yılmaz, İnal Kaan Duygun and Kübra Nur Korkmaz for all their help.

I would like to thank Prof. Dr. Şule Altun Kurtoğlu who encouraged me to start on this journey.

And finally, I would like to thank my family for providing moral and material support; and to my nephews and nieces for being a constant source of joy in my life.

July 2023 Fatma Saime ERDÖNMEZ

TABLE OF CONTENTS

Page

ABBREVIATIONS

Ag : Silver
AgNWs : Silver Nanowires
Al : Aluminum
Au : Gold
BTU : Bursa Technical University
CP : Carbon Paper
CS : Chitosan
CTE : Coefficient of Thermal Expansion
Cu : Copper
CVD : Chemical Vapor Deposition
CWM : Cathode Waste Material
DMSO : Dimethyl Sulfoxide
DOD : Drop on Demand
ECG : Electrocardiography
EEG : Electroencephalogram
EMG : Electromyography
GO : Graphene Oxide
GSR : Galvanic Skin Response
HEM : Hierarchical Elastomer Microstructures
IoT : Internet of Things
MIT : Massachusetts Institute of Technology
PA : Polyacetylene
PANi : Polyaniline
PDMS : Polydimethylsiloxane
PEDOT:PSS : Poly(3,4-ethylenedioxythiophene):poly(styrenesulfonate)
PET : Poly(ethyleneterephthalate)
PF : Polyfuran
PI : Polyimide
PLA : Polylactide
PLGA : Polylactic-co-glycolic acid

PPG : Photoplethysmography
PPP : Poly(para-phenylene)
PPV : Poly(phenylenevinylene)
PPy : Polypyrrole
PT : Polythiophene
PU : Polyurethane
PVDF : Poly(vinylidene fluoride)
RGO : Reduced Graphene Oxide
RTV : Room Temperature Vulcanizing
SiO_2 : Silicon dioxide
SNR : Signal-to-Noise Ratio
SWCNT : Single Wall Carbon Nanotubes
Tg : Glass Transition Temperature
Tm : Melting Temperature
TPU : Thermoplastic Polyurethane
ZnO : Zinc Oxide

SYMBOLS

C	**:** Capacitance
ε_r	**:** Dielectric constant of the layer
ε_o	**:** Dielectric constant of the vacuum
A	**:** The overlapped area of the two electrodes
d	**:** Distance between the electrodes

LIST OF TABLES

Page

LIST OF FIGURES

Page

SU VE YAĞ İTİCİ ÖZELLİĞE SAHİP ESNEK SENSOR TASARLANMASI VE GELİŞTİRİLMESİ

ÖZET

Hızla gelişen teknoloji geleneksel üretimde kullanılan tek fonksiyonlu malzemeler yerine farklı fonksiyonel özellikleri bünyesinde barındıran malzemeleri gerekli kılmaktadır. Tekstil malzemelerinde, lif ve polimerlerde biouyumluluk, antibakteriyel, antistatik, iletken özellikler ile fonksiyonları geliştirecek birçok yöntem bulunmaktadır. Çok fonksiyonlu tekstil malzemelerinin geliştirilmesi ile yeni uygulama alanları da ortaya çıkmıştır. Akıllı tekstiller medikal, savunma, endüstriyel ve çevresel olmak üzere çeşitli alanlarda kullanılmaktadırlar. Akıllı tekstiller sensör ve giyilebilir elektronikler geliştirilmesinde de kullanılmaktadırlar. Teknolojideki son gelişmeler esnek ve gerilebilen sensörlerin geliştirilmesini gerektirmiştir ve sensörlerin hassasiyetini kaybetmeden esnekliğini arttırma üzerine tamamlanmış ve devam eden çok sayıda araştırma bulunmaktadır. Esnek malzemeler, giyilebilir sensörler için çok çeşitli uygulamalar sağlar. Doğrusal olmayan yüzeylere uyma yetenekleri, elastikiyetleri, stres ve gerinim kuvvetleri altında dayanıklılıkları ve eğilme direnci, sensör alt tabakaları olarak esnek malzemelerin tercih edilmesinin nedenlerinden bazılarıdır. Giyilebilir esnek sensörler için esnek alt tabakalar, insan derisi üzerindeki uygulamalarla uyumlu olmalıdır.

Bu tez çalışmasında, tekstil ve polimer yüzeylerde su ve yağ itici özelliklere sahip esnek sensörler tasarlanması öngörülmüştür. Süperamfifobik özellik kazandırarak sensörlerin onların yağmur, yağ sızıntısı, korozyon gibi dış etkenlere karşı dayanıklılığını arttırmak hedeflenmiştir, böylece hassasiyeti azaltmadan dayanıklılık ve uzun yaşam süresi sağlanması hedeflenmiştir. Bu çalışmada farklı yüzeyler üzerine esnek sensör tasarlanması ve üretilmesi ve üretilen sensörlere su ve yağ itici özellik kazandırılması üzerine araştırmalar yapılmıştır. Optimal seviyede esneklik için pamuk ve TPU bazlı substrat malzemeler kullanılmış, karbon bazlı (grafit, grafen, katod atık malzemesi) ve polimer bazlı (PEDOT:PSS) iletken mürekkepler farklı konsantrasyonlarda hazırlanmış, doctor blade ve sprey kaplama metodları ile mürekkepler substrat yüzeylerine uygulanmış, elde edilen elektrot su ve yağ itici dispersiyonlarla kaplanarak sonuçlar analiz edilmiştir. Üretilen elektrotlar morfolojik ve elektriksel özellikleri bakımından karakterize edilmiştir.

Sonuçlar, grafenin uygulanan mürekkepler arasında en iyi iletkenliğe sahip olduğunu ve mürekkep dağılımındaki karbon bazlı malzemelerin konsantrasyonu ve uygulanan katman sayısı arttıkça sonuçların iyileştiğini göstermiştir. Tekstil uygulamalarında hidrofobik ve oleofobik kaplamalarda kullanılan bir florokarbon dispersiyon olan Tubiguard, ZnSt ve SiO2 ile karıştırıldı ve sonuçlar, hidrofobik özelliklerin büyük ölçüde iyileştirildiğini ve oleofobik özelliklerin de bir miktar gelişme gösterdiğini göstermiştir. Saf haliyle hidrofilik bir malzeme olan pamuk substrat, TPU substratına kıyasla kaplamalar uygulandıktan sonra daha iyi amfifobik özellikler göstermiştir. Pamuklu kumaşın ştapel lifleri, amfifobik özelliklerini iyileştirmeye yardımcı olan

kaplamaların uygulanmasıyla mikro hiyerarşik yapılar olarak işlev görerek, su ve yağ iticiliği artırmıştır. Genel olarak bu çalışmada kullanılan malzemeler ve uygulanan yöntemler, maliyetleri optimum seviyede tutmayı ve ticari uygulamalar için elektrotların seri üretimine izin vermeyi amaçlamaktadır ve sonuçlar hedefe ulaşılabilir olduğunu göstermiştir.

Anahtar kelimeler: Su itici, Yağ itici, Sensör, Esnek, Tekstil tabanlı, Polimer.

DESIGNING AND MANUFACTURING SUPERAMPHIPHOBIC FLEXIBLE SENSORS

SUMMARY

Rapidly developing technology necessitates materials with different functional properties instead of single-functional materials used in traditional production. There are many methods to improve biocompatibility, antibacterial, antistatic, conductive properties and functions in textile materials, fibers and polymers. With the development of multifunctional textile materials, new application areas have emerged. Smart textiles are used in various fields such as medical, defense, industrial and environmental. Smart textiles are also used in the development of sensors and wearable electronics. Recent advances in technology have necessitated the development of flexible and stretchable sensors, and there is a great deal of research completed and ongoing on increasing the flexibility of sensors without losing their sensitivity. Flexible materials provide a wide variety of applications for wearable sensors. Their ability to conform to non-linear surfaces, their elasticity, durability under stress and strain forces, and bending resistance are some of the reasons why flexible materials are preferred as sensor substrates. Flexible substrates for wearable flexible sensors must be compatible with applications on human skin.

In this thesis, it is foreseen to design flexible sensors with water and oil repellent properties on textile and polymer surfaces. It is aimed to increase the resistance of the sensors against external factors such as rain, oil leakage and corrosion by giving them a superamphiphobic feature, thus providing durability and long life span without reducing the sensitivity. In this study, researches were conducted on the design and production of flexible sensors on different surfaces and the water and oil repellent properties of the produced sensors. For optimal flexibility, cotton and TPU-based substrate materials were used, carbon-based (graphite, graphene, cathode waste material) and polymer-based (PEDOT:PSS) conductive inks were prepared in different concentrations, inks were applied to the substrate surfaces with doctor blade and spray coating methods, The results were analyzed by coating the electrode with water and oil repellent dispersions. The produced electrodes were characterized in terms of their morphological and electrical properties.

Cotton and TPU-based substrate materials were used for optimal flexibility, carbon-based (graphite, graphene, cathode waste material) and polymer-based (PEDOT:PSS) conductive inks were prepared in different concentrations. Inks were applied to the substrate surfaces as 1, 2 and 3 layers of coating by using doctor blade and spray coating methods, the obtained electrode was coated with water and oil repellent fluorocarbon and zinc stearate, silicon dioxide dispersions and the results were analyzed. The produced electrodes were characterized in terms of their morphological and electrical properties.

The results showed that graphene had the best conductivity among the inks applied and the results improved as the concentration of carbon-based materials in the ink

dispersion and the number of applied layers increased. Tubiguard, a fluorocarbon dispersion used in textile applications hydrophobic and oleophobic coatings was mixed with ZnSt and SiO_2 and the results showed that hydrophobic properties were greatly improved and oleophobic properties also showed some improvement. Cotton substrate, a hydrophilic material in its pure form, showed better amphiphobic characteristics after the coatings were applied compared to TPU substrate. The staple fibers of cotton fabric acted as microhiearchical structures with the application of coatings which helped improve their amphiphobic properties.

Overall the materials used and methods applied in this study are aimed to keep the costs at an optimal level and allow mass production of electrodes for commercial applications and the results show that the goal is achievable.

Keywords: Hydrophobic, Oleophobic, Sensor, Flexible, Textile-based, Polymer.

1. INTRODUCTION

Wearable flexible sensors enable electronic devices to be incorporated onto human body through applications on textiles or accessories. Main application areas for wearable devices are health, well-being, sports, automotive, robotics and aerospace. Flexible and wearable electronic devices have shown great technological advancement since their debut in 1960s and they have attracted considerable attention due to their great potential applications. The increase in number and variety of mobile devices, internet and cloud computing has started a new era of Internet of Things (IoT), where researchers study case specific solutions based on the relationships between physical objects and the internet. Since the beginning of 21st century, there has been a rapid increase in development of innovative materials such as conductive polymer and new production methods as well as new knowledge on electrical sensing principles which has caused momentous progress in the research and commercilization efforts towards flexible and stretchable wearable sensors. Some of the key considerations for wearable flexible electronics are that they have to be durable, small, comfortable to wear, safe, and utilizes minimum amount of energy (Cima, 2014; Park and Jayaraman, 2003). Flexible sensors have been a favorite topic for researchers since the beginning of 21st century. Designing wearable, lightweight, multi-modal, durable, comfortable flexible sensors that give reliable measurements and can be fabricated in mass quantities with affordable costs is important for the future developments in flexible sensors' market. Based on market forecast reports flexible sensors market is expected to reach US$ 12.83 billion in 2027 and US$ 18.09 billion in 2029 (maximizemarketresearch), (precedenceresearch). By improving the design and properties of the flexible sensors, addressing the current challenges and reducing costs for manufacturing, new venues for applications will be opened and the market will continue to grow.

1.1 Aim and Scope of Thesis

The purpose of this study is to design and manufacture flexible sensors on textile or polymer surfaces which will also contain superamphiphobic characteristics to enhance their durability against outdoor factors.

Our aim is to find optimal fabrication methods and materials for cost efficient, durable and high precision flexible sensors that can also be applied to sustainable industrial scale production.

1.2 Literature Review

1.2.1 History of wearable electronics

Wearable electronics are devices with electronic components and software that come in the form of clothing or accessories (Godfrey, 2021). Electronic textiles or smart textiles form a part of wearable electronics. Textile materials, which are referred to as the most widely used materials by human beings, have achieved an additional function following the integration of electronic components within textile structures. Conductive materials needed to fabricate electronic textiles, conductive threads and fabrics have been around for over one thousand years. Artisans have been wrapping fine gold and silver foils around yarns used in embroidery for centuries.

The integration of electronics with textile materials started as a fashion statement towards the end of 19th century with items such as “illuminated headbands” in ballet performances, necklaces, hats and costumes for entertainment industry. In mid 1960s Diana Dew, an American model and designer, designed and manufactured the first wearable electronics “rechargeable illuminated clothing” by sewing plastic lamps into her clothing in segments and connecting them to a rechargeable battery pack. Dew’s designs were displayed in New York Museum of Contemporary Craft at an exhibition that centered on the concept of technology and apparel (Syduzzaman et al, 2015).

In 1980, MIT Professor Steve Mann created a wearable camera prototype by integrating photography equipment onto a helmet. Other electronic equipments that could be construed as “wearable electronics” were brought into market in 70s and 80s. In 1973, Motorola engineers invented the first handheld mobile phone; Sony introduced The Walkman in 1979. Polar Electro was founded by a Finnish professor

who invented the first battery operated fingertip heart rate monitor in 1977. In 1982 Polar Electro introduced a wearable heart rate monitor complete with a wristwatch and a sensor belt worn around the chest. (Kite-Powell, 2016)

The designs and function of electronic textiles became more sophisticated over time. Harry Wainwright is one of the leading figures in wearable electronics. He is referred to as the "grandfather of electronic textiles". In 1985 he successfully integrated fiberoptics with textiles and created the first animated sweatshirt. He also invented a machine that could embed plastic optical fibers [POF] into the fabric. He teamed up with a German machine designer Herbert Selbach and together they designed patented CNC machines to embed fiberoptics into textiles (www.hleewainright.com).

Towards the end of 20th century, a groundbreaking development in polymer science "the conductive polymer" invented by Shirakawa et al, provided a variety of innovative applications for electronically embedded textiles (Shirekawa et al, 2003).

What started as a fashion statement, evolved by further innovations and research in this field. A later study in mid 1990s conducted by MIT scientist Steve Mann and his team focused more on a technological end-use by combining computers with textiles to create "wearable computers" (Mann, 1997).

A group of researchers at MIT, including Maggie Orth and Rehmi Post, explored methods to integrate electronic devices into textile materials and on other soft substrates in a more presentable way in order to address some technical, social, and design related challenges. The group explored integration of digital electronics with fabrics that conduct electricity, and they also developed a new technique for embroidering electronic circuits (Orth, et al, 1998). Another researcher from the MIT Media Lab, Buechley, created Lilypad Arduino, one of the first commercially available microcontrollers (Buechley, 2008).

Research by Orth and Post focuses on the advantages of textile-based computing compared to conventional printed circuitries. Their theory was that textile-based substrates exhibit better characteristics such as durability, body-conformability and wearability compared to conventional substrates used in flexible circuits. As an example to this claim they designed a fabric keypad readout with a flexible multichip module. The team of researchers present several different computer displays and computational gadgets that are manufactured using electronic fabrics and conductive

threads. The purpose of the study is to give designers more options and leniency in their creative efforts towards designing new and innovative computational devices. Their team consists of researchers from multidisciplinary backgrounds of arts and sciences. They identified the major design obstacles as rigid physical substrates and bulky switches and batteries used in wearable computers which limit the design parameters of objects designed with these traditional sensors.

"Firefly dress and necklace" design Orth and Post is made with conductive fabric that distributes electricity over the fabric of the dress. As the fabric moves with each motion of the wearer, LED lights with attached fuzzy conductive pads come into contact with the fabric power source and ground layers and create a sporadic lighting effect. The firefly necklace has no power supply of its own but contains conducting beads and tassels that brush against the fabric of the dress as the wearer moves and creates a lighting effect by completing the circuit when they touch the fabric. The scientists call these "opportunistic connections" that allow power to be distributed without rigid and bulky connectors and wires. Using sewn fabric sensors and circuits allowed researchers to eliminate bulky wires, connectors and electronics. It also allowed them to design computers that resembled regular textile materials in shape and degree of comfort (Orth, et al, 1998).

Researchers at Virginia Tech University E-textile Laboratory studied the design of e-textile fabrics both in terms of electronic parts and software associated with the product. The purpose of the study was to improve manufacturing methods and physical attributes of wearable technologies. Other researchers have studied the design variables of sensing components in terms of quantity, type of component and location of components to optimize cost, sensitivity, accuracy, and conformity (Gioberto, 2015).

Later studies focused on integration of electronic components within the textile structure such as functional yarns that contain semi-conductors. Patents from 2005, 2016 and 2017 describe methods to manufacture electronical functional yarns (Hughes-Riley et al. 2018).

At the Smart Fabrics Conference in Washington D.C. in 2007, Wainwright and Byckov presented a machine washable denim jacket with LED/optic displays for ECG

bio-physical data monitoring, using GSR sensors embedded into the fabric and connected to a wristwatch via Bluetooth (Syduzzaman et al, 2015).

Timeline of developments

Miniaturization, increased mobilization, and the inclusion of multifunctional abilities make wearable electronics / sensors an attractive topic of study. Key developments in wearables include:

1500s: Pedometers were first created by Leonardo da Vinci (Ajana, 2017). In 1510, a marine chronometer pocket watch named as 'clock-watches', ornamental timepieces were developed by German craftsmen is credited as the inventor of the pocket watch. (Oseledchik et al, 2017).

1700-1800s: An abacus tool made of a smart ring was also designed as jewelry in the 17th century (Guler et al, 2016).

1800-1900s: Hearing aids in the form of ear trumpets were developed in the 1800s. Hutchinson innveted the first electrical hearing aid "Akouphone" were created, and digital hearing aids were first used in 1890's (Shimokura, 2018).

1960s: Wearable devices like timing devices and to help in gambling, concealed cameras that can foretell game results were created (Guler et al, 2016).

1970: Calculator watches were invented in 1970 and manufactured by Pulsar and Hewlett Packard. (Grabis, 1980).

1977: The introduction of fingertip pulse rate monitors (Nimbalker, 2015). Plar Electro® applied for a patent for a wireless heart-rate monitor in 1977 and the product came into the market in 1982 (https://www.polar.com/blog/40-years-of-incredible-firsts-polar-history/).

1979: Sony's Walkman® came into the market and dominated for several years (Acosta, 2000).

1980-1990s: The clothing designed by Steve Mann has electrical components (1985 fiber-optic sweatshirts, 1995 fiber-optic fabric weaving machine, and in 1997 ductile material) and the Massachusetts Institute of Technology (MIT) developed electronic spectacles (Mann, 1997).

1996: Georgia Institute of Technology has developed Wearable Motherboard™ with the development of electric conductive fibers with integrated body monitoring sensors like pulse rate to detect army casualties from projectiles and gunshot wounds. This sparked the wearables revolution, which included user-friendly gadgets built into clothing to gather data from the human-body and the surroundings (Park, 2002).

2000: Development of cyberia survival suit (Reima®) with electronic features to monitor pulse rate, temperature, humidity and communication system (antennas, the GPS, and the SMS), and position monitoring system (sensors for movement, and posture) (Malmivaara, 2009).

2003: In 2003 the Bioharness™ was developed by Zephyr Technology (NZ) which consisted of a chest-strap with bio-sensors for various applications includes physical work (e.g., first responders or workers). It was used for miners trapped in Chile in 2010 to monitor vital signs (pulse rate, breathing rate, skin temperature, activity, and posture). The collected information is then sent to a personnel monitoring system via wireless connection. (Hailstone and Kilding, 2011).

2008: Celio® club suit which was developed in 2008 with an embroidered fabric patch to control an Apple® iPod (Wilson and Laing, 2018).

2009: Fitness bracelets were introduced as contemporary pedometers. Numerous brands, such as Fitbit®, Samsung®, Jawbone®, TomTom®, and Huawei® have created wearable fitness bands with outstanding end applications including daily step tracking and particular sports modes, such as running, swimming, cycling, yoga, etc. (Wilson and Laing, 2018).

Since 2010: The creation of Apple® smart watches made the company the market leader for wearables as of 2017. Different advancements in sensors, such as pulse rate, steps, GPS, and gyroscope were incorporated. The smartwatches also have additional features including texting, phone calls, a clock, the ability to set alarms, and reminders (Qiu et al, 2017). Google™ Project Glass: Google developed smart glasses which were wearable, voice- and a motion-controlled android gadget that projects information into the user's field of vision and mimics a pair of eyeglasses (Due, 2014). The solar-powered jacket by Tommy Hilfiger was an invention for charging phones. The front patch pocket battery was connected to solar batteries that were sewed inside the jacket. Solar panels may be removed with ease (Zhang et al, 2020). Pulse rate, breathing rate,

body temperature, body posture, and fall detection are all measured by the Health Patch^{TM} MD (Seneviratne et al, 2017). Abbott^{TM} developed the Freestyle Libre Flash wearable glucose monitor (Zu et al, 2022). Various wearable products in sports application from Garmin® such as Vivoactive swimming tracker, Edge 520 cycling bands came into the wearable market. At Disney World, the MagicBand 2 let visitors to make reservations for restaurants and practically stand in line (Borkowski, 2016). Smart hearing aids with enhanced voice detection and noise cancellation have been created. These can link to sound producing devices like televisions, doorbells, and smoke alarms (Nossier et al, 2019). A virtual reality headset for gaming, media, industrial and professional use "Oculus Rift" was manufactured by Oculus. E-textiles and skin patches started to dominate the market. These wearables were functionalized to measure heart-rate, electrocardiography (ECG), electromyography (EMG), electroencephalogram (EEG), hydration, analyte concentration and glucose levels (Skyrme et al. 2022). Figure 1.1 gives a summary of the timeline of developments regarding wearable flexible sensors.

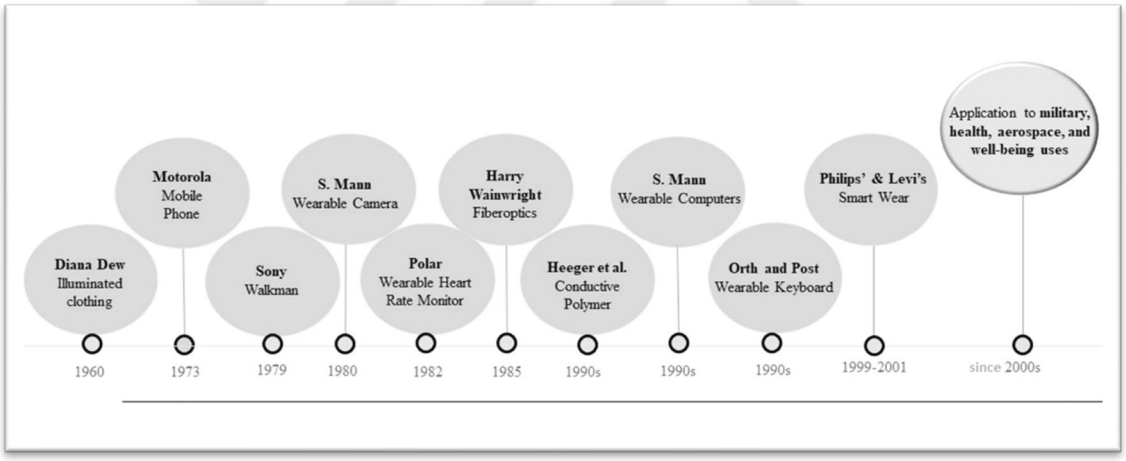

Figure 1.1 : Timeline of developments for wearable sensors.

1.2.2 Types and properties of flexible sensors

Sensors are widely used in many different applications for a variety of purposes. An active use of sensors has resulted in a constant expansion of sensor customization. They are used in numerous sectors including temperature sensing, moisture sensing, gas sensing, environmental sensing, and the analysis of food and beverages. One of the most significant uses of sensors is the monitoring of physiological parameters, since it facilitates the creation of a model of human behavior.

Flexible and non-flexible types of sensors make up the broad classification of sensors. In contrast to the latter type of sensor, which is rigid and built of brittle materials, the former sensor is made up of materials that are stretchable to a certain level without altering their characteristics (Nag et al, 2017). The conventional rigid sensors have been present in the market for a long time and the most popular ones have silicon substrates. Although these sensors have a wide range of uses, they have several drawbacks such as rigidity, constant need for a power supply, low signal to noise ratio, etc (Hu et al, 2021). The true drawback arises, in particular, when the sensor device is used to monitor a person's physiological parameters. Flexible sensors nowadays are readily available and can be used dynamically with no discomfort to the user. They are a superior choice for usage in flexible accessories since they are lightweight, inexpensive to fabricate, and have excellent mechanical and thermal properties (Nag et al, 2017).

Sensors are also classified according to their sensing mechanisms. The following sections describe sensors based on their mechanisms. Figure 1.2 gives a schematic of classification of sensors based on their sensing mechanisms. Main categories of mechanical sensors are stress/pressure sensors and strain sensors.

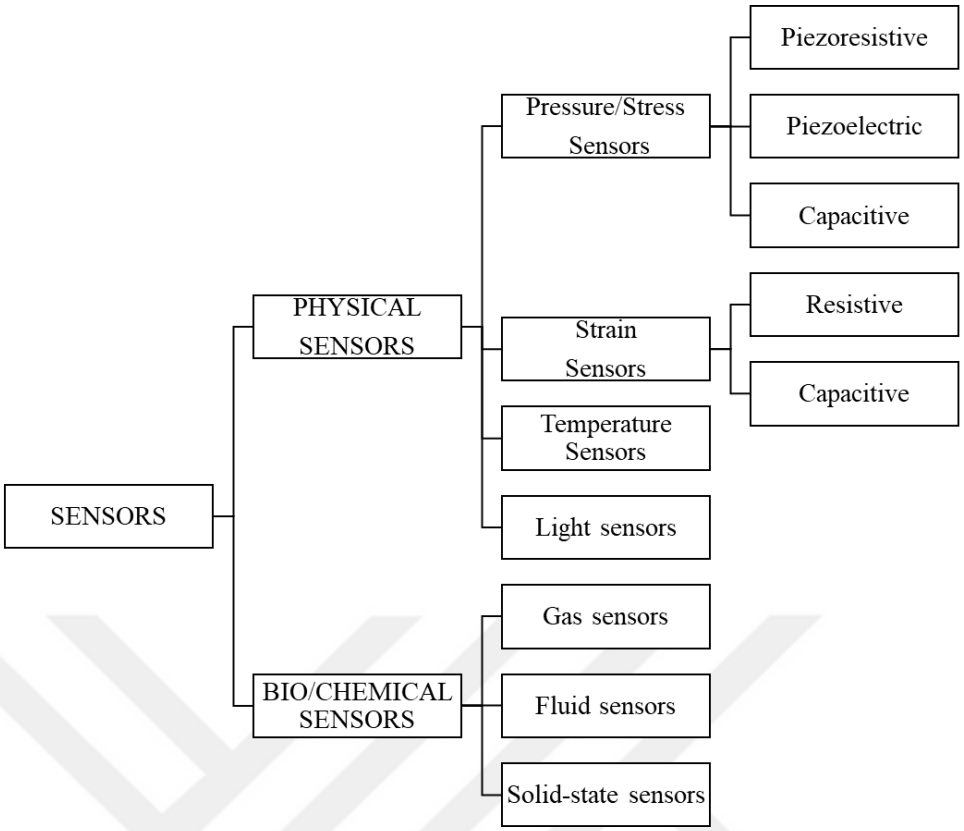

Figure 1.2 : Classification of sensing mechanisms.

1.2.2.1 Pressure/stress sensors

A pressure sensor is a piece of technology that detects, controls, or monitors pressure pulses while transforming the physical information into an electrical signal. Because piezo-electric devices emit an electric charge in proportion to the applied tension, they are commonly utilized in pressure sensors. The level of voltage given out by the sensor depends on the level of pressure applied. Based on the pressure transduction method, pressure sensors are divided into three categories; resistive, capacitive, and piezoelectric pressure sensors. (Huang et al, 2019)

Piezoresistive pressure sensor:

A piezoresistive pressure sensor's sensing technique is based on variations in pressure resistance. Due to its straightforward design, higher sensitivity, and broad estimation range, resistance-based pressure sensors have been the subject of extensive research. Resistive pressure sensors measure the change in the resistance between two conducting layers when pressure is applied (Valle-Lopera et al, 2017).

The working principle of a piezoresistive pressure sensor is that it has a number of tiny silicon wafers sandwiched between shielding surfaces. Outside force applied on the sensor is converted into a variance in resistance that can be recorded. Piezoresistive pressure sensors generally have two parallel electrodes with an active material in between (Li et al, 2020). Figure 1.3 shows a flexible piezoresistive pressure sensor diagram that is used for pulse monitoring (Long et al, 2022).

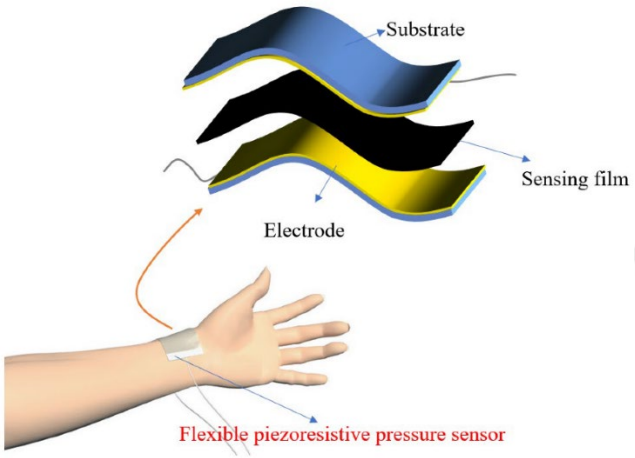

Figure 1.3 : Schematic illustration of a flexible piezoresistive pressure sensor (Long et al, 2022).

Advantages of piezoresistive pressure sensors are their low price and increased durability, good resistance to dynamic pressure fluctuations, vibration and shock and their ability to operate at higher temperatures (Chen and Huang, 2022).

Cho et al. (2016) designed a high-performance piezoresistive pressure sensor using a polydimethylsiloxane (PDMS) coated with a single layer of graphene. They used a cupper sheet and molded it into dome structures with photolithography and wet etching techniques. Later using the chemical vapor deposition (CVD) method they grew graphene on the surface and molded it with PDMS. The cupper sheet was etched away after the PDMS is molded onto the graphene. They used this structure as top layer of piezoresistive sensor and for the bottom layer they used two interdigitated electrodes fabricated from mono layer graphene with CVD method. The bottom layer interdigitated electrodes were seperated from each other and when the PDMS/graphene top layer was placed on top, it completed the conductive circuit. When pressure is applied the contact area between top and bottom layers increases and total resistance decreases thus allowing the current to increase (Cho et al, 2016).

Gao et al. (2019) designed a paper based piezoresistive sensor using nanocellulose based paper as substrate and top layer; and silver nanowire coated tissue paper as

active material. The writers claim that their fabrication method is simple, cost effective and environmentally friendly. They proposed that the sensor can be applied on to the skin and measure physiological parameters such as heart rate and vocal cord vibrations and as e-skin to measure applied pressure. The sensor showed a high sensitivity of 1.5 kPa–1 in the range of 0.03–30.2 kPa and retained excellent performance in the bending state. Availability and low cost of materials used, the uncomplicated fabrication method and fast fabrication time allows this method to be cost-efficient (Gao et al, 2019).

In a study by Li et al. (2019) PU sponge was treated with chitosan (CS). The outcome is a CS/PU sponge with positive charge which later is coated with Titanium Carbide (Ti3C2Tx) Mxene sheets. The resulting MXene@CS@PU sensor has a high compression resilience due to sponge-based structure and stable piezoresistive response because of the Mxene sheets. They are susceptile to both high and low pressure applications such as human motion and physiological parameter detection and insect motion detection. The sensor is viable for fivethousand use cycles with good performance even after washing for 1 hour in water (Li et al, 2019).

Wearable piezoresistive sensors made of three-dimensional graphene are regarded as promising sensors due to their ease of manufacture, straightforward mechanism, less power consumption, and easy signal collection. Piezoresistive sensors based on 3D graphene have shown great potential in the fields such as motion detection, health monitoring, e-skin and artigicial intelligence which are thought to be key technologies in the future artificial intelligence systems (Cao et al, 2021).

Piezoelectric pressure sensor:

Piezoelectric pressure sensors employ the piezoelectric action of the sensor material to turn the measured pressure into an electrical signal. It converts the pressure to be measured into electricity using electrical components and other apparatus. The voltage across a piezo-electric element caused by the applied pressure is measured by the piezo-electric pressure sensor. They are extremely durable and utilised in a variety of commercial applications (Gautschi, 2002).

When a force is applied to a piezoelectric material, a charge is generated across the crystal surface. A voltage inversely correlated with the pressure can be used to monitor this. Most notably, piezoelectric sensors produce power when the pressure adjustments are done. Figure 1.4 shows a schematic of the positive and inverse piezoelectric effects (Wu, 2021) .

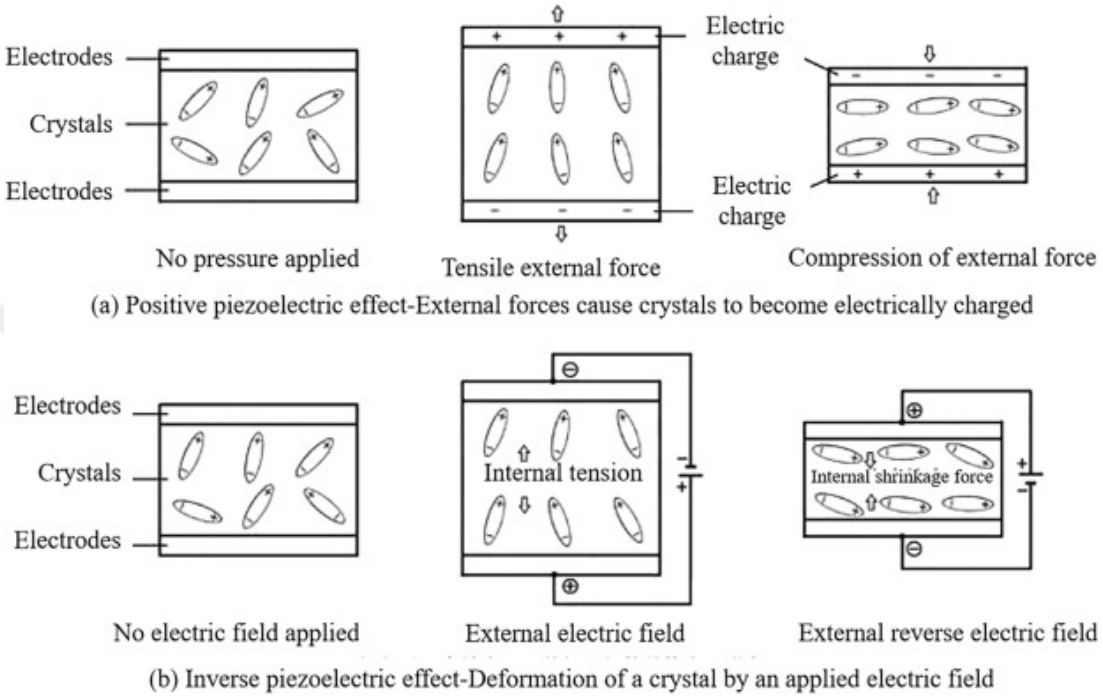

Figure 1.4 : Schematic of positive and inverse piezoelectric effects (Wu, 2021).

Advantages of Piezo-electric pressure sensors are that they are highly sensitive and compact in size. They need a slight disturbance to provide an output and they tolerate temperatures upto 1000 ºC (Liu et al, 2021).

Park et al (2017) studied self powered epidermal piezoelectric sensors for real time arterial pulse rate monitoring. Although conventional pulse sensors are capable of detecting human bio-signals, their significant power consumption disadvantages prevent wearable medical devices from operating sustainably. Thus, the ability to monitor radial/carotid pulse signals in close-to-surface arteries in real-time is demonstrated using a self-operating piezo-electric pulse sensor. The inorganic piezoelectric sensor on an extremely thin piece of plastic makes conformal contact with the rough skin's intricate texture, enabling it to react to the minute pulse variations that appear on the epidermis surface (Park et al, 2017).

In an article in 2021 Luo et al. shared their design for a piezoelectric pressure sensor composed of 5 layers. Top and bottom layers are PDMS substrate and encapsulation

film then comes the cupper electrodes and a PVDF/SWCNTs film in between the electrodes acts as the active film. High sensitivity and quick response features come packed with the flexible piezo-electric pressure sensor. The sensor has a great deal of potential for usage in wearable technology and human motion monitoring as it can be used to track physiological signals and recognize human motion (Luo et al, 2021).

Shirley et al. (2020) designed a piezoresistive textile pressure sensor based on zinc oxide nanostructures for wearable applications. an electrode of conductive woven fabric acts as the electrode and forms the outer layers and ZnO is sandwiched between two conductive layers. The force exerted by sensor may be used to monitor human body motions with wearable textile pressure sensors that have piezo-electric capabilities. (Shirley et al, 2020).

Capacitive pressure sensor:

A dielectric layer is a component of the capacitive type pressure sensor and is crucial to obtaining high sensitivity. The capacitance value is determined by the equation:

$$C = \frac{\varepsilon_0 \varepsilon_r A}{d} \tag{1.1}$$

where ε_r and ε_o are the dielectric layer and the dielectric constants of the vacuum, A is the overlapped area of the two electrodes, and d is the distance between the electrodes. The capacitive sensor is typically based on a parallel-plate capacitor. The capacitance value varies as a result of the dielectric layer deforming when pressure is applied to the sensor, or when d changes. Due to their great deformability, PDMS and Ecoflex are frequently employed as dielectric materials in capacitive pressure sensors (Pierre Claver and Zhao, 2021).

Working principle of capacitive pressure sensors is that two parallel conducting plates are joined together in a capacitor and are spaced apart by a narrow gap. Any change in the variables will result in an equivalent change in the capacitance. The capacitance is controlled by the spacing between the plates. An electric signal of the position of the moving element is provided by a linear change in capacitance with changes in the element's physical position. The separation between the conductor plates, which changes as the pressure changes and thus affects capacitance. Both electrodes are fixed, with one having a pressure-sensitive diaphragm. Making it a part of a tuned

circuit is a simple technique to measure the change in capacitance. Figure 1.5 shows a schematic of capacitive type sensors (Ko, 2021).

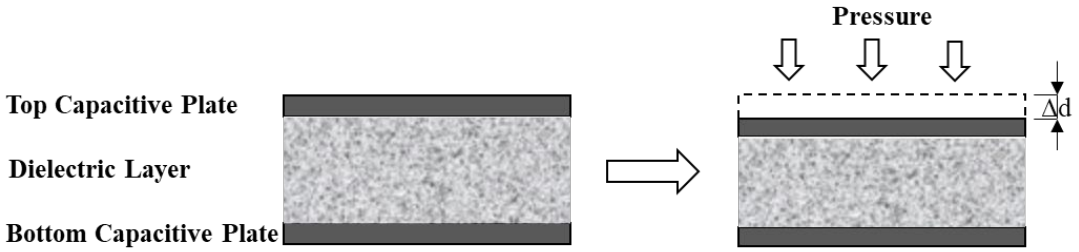

Figure 1.5 : Schematic of capacitive type sensors.

The capacitive sensing method is one of the most popular and researched methods because of their large fabrication area, high degree of sensitivity and less sensitivity to temperature differences. Capacitive sensors are ideal for applications requiring less pressure and moderately severe settings (Mishra et al. 2021).

Wan et al (2017) presented a high sensitivity capacitive pressure sensor based on GO and with graphene electrodes. The dielectric GO was used in foam form between PET sheets. rGO electrodes were patterned on the PET sheets. GO foam with a high relative dielectric permittivity acts as a sponge when air is released as pressure is applied and the distance between the two electrodes decreases causing the dielectric constant to increase. (Wan et al, 2017).

Park et al (2017) design a capacitance type pressure sensor with a dielectric layer to be used as a respiration monitoring system. The sensor electrodes are made of carbon fibre thin films and silver nanowires based on PDMS. Since the suggested sensor is adaptable and flexible, it can be incorporated into clothing and conveniently positioned anywhere on the human body. A porous ecoflex with 36% porosity is used as the dielectric layer. The resulting sensor has a high range of sensitivity and good resiliency for over 6000 cycles. The fabricated product is highly flexible and can be adapted onto textile materials to use in human motion monitoring. The authors placed the sensor into a waist belt to monitor real time respiration of the user. (Park et al, 2017).

Zhao et al. used natural viscoelastic material TPU nanofibers coated with silver nanowires (AgNWs) to build a capacitive pressure sensor used as a touch sensor with high sensitivity and quick reaction time. These advanced features have made it possible to detect a variety of micro pressure changes, including pulse, airflow, and Morse code (Zhao et al, 2020).

Kang et al (2017) designed a 3-Dimensional Capacitive Sensor Based on Graphene for use in wearable electronics. The design consists of a compact sensor with a graphene foundation for capacitive touch and excels at sensing in both contact and non-contact modes. Forearms and palms, two extremely deformable body parts, can be integrated with the device. The touch sensor determines the distance and shape of the incoming object before making direct contact and detects numerous touch signals in acute recordings. The sensor is composed of three seperate layers. Top and bottom layers are graphene electrodes on PET substrates and the dielectric layer is formed with acrylic polymer (Kang et al, 2017).

Sergio et al (2002) designed a textile based capacitive pressure sensor to measure the amount of pressure exerted onto the surface of the fabric. Capacitors were implemented among the rows and columns of conductive fibers patterned on the two opposite sides of an elastic synthetic foam (Sergio et al, 2002).

Keum et al (2021) proposed a textile-based capacitive pressure sensor with good sensitivity over a wide range and stability. They embedded Ag plated conductive fibers on to the textile material as electrodes and a poly(vinylidene fluoride)-co-hexafluoropropylene (PVDF-HFP)/ionic liquid (IL) composite film to construct the textile-based capacitive sensor. (Keum et al, 2021).

1.2.2.2 Strain sensors

Similar to pressure sensors, strain sensors sense the physical deformation in their structure and transmit that deformation as an electrical signal. Most used strain sensors used for textile-based flexible electronics are resistive and capacitive strain sensors. They are used to monitor motion and muscle movements such as respiration and heart rate. Figure 1.6 shows schematics of resistive and capacitive strain sensors (Souri et al, 2020).

The three primary components of flexible strain sensors are a functional composite structure, sensing electrodes, and connecting wires. Utilizing conductive nanofillers in an insulating or conducting polymer matrix while taking into consideration certain properties such as electrical conductivity, mechanical strength, and structural interface, functional stretchable composite structures are predominantly formed from these components (Souri et al, 2020).

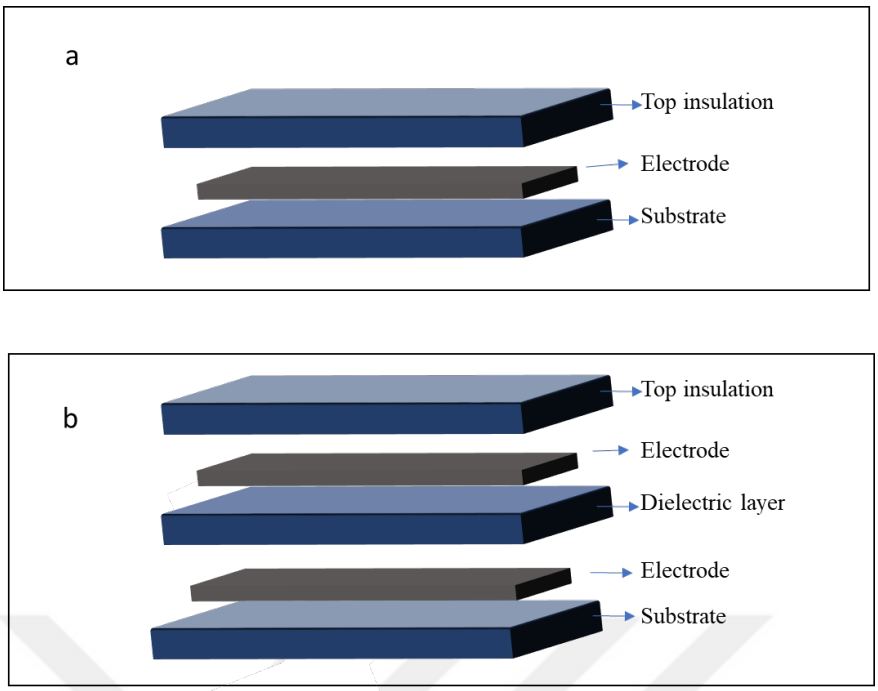

Figure 1.6 : a) Piezoresistive strain sensor, b) capacitive strain sensor.

Resistive Strain Sensor:

The difference between a piezoresistive pressure sensor and a resistive strain sensor is that in a pressure sensor, compression is applied, and in a strain sensor, the sensor stretches or contracts. Resistance of the sensor changes with the change in the sensor's length or area during exposure to strain (Parameswaran and Gupta, 2019).

Capacitive Strain Sensor:

A capacitive strain sensor is also similar to a capacitive pressure center in its structure of two parallel conductive plates with a dielectric material sandwiched in between. When strain is applied to the sensor and the sensor stretches, the difference between the area or length between the parallel plates shifts and changes capacitance values (Parameswaran and Gupta, 2019).

Kwak et al (2017) fabricated a capacitive strain sensor for pulse rate monitoring. The sensor is composed of metallic micro patterns on a flexible substrate which acts as an insulator. When force is applied to the sensor, the substrate and the metallic patterns are deformed, causing the electrical resistance to change. They used PI as substrate and nickel-chrome as electrode and coated the sensor with a silicone elastomer to ensure flexibility. The end product was a highly sensitive pulse rate detection sensor that is thin, flexible, small, and affordable for mass production (Kwak et al, 2017).

In 2016 Li et al used carbon paper (CP) to create a flexible strain sensor . They used pyrolysis technique to turn tissue paper into CP and encapsulated the CP in and PDMS elastomer. As a result, the manufactured PDMS/CP strain sensor has a gauge factor of ~ 25, which is about ten times greater than that of a typical metallic strain gauge and is very sensitive to applied strain. The PDMS/CP strain sensor was successfully used in wearable electronics for robot control and breath monitoring (Li et al, 2016).

Ferrone et al (2016) introduced a strain-based wearable band for hand gesture recognition. A series of strain sensors fabricated from thermoplastic and conductive nanoparticles are extruded into filament form and embedded into the wristband. The sensor does not directly touch the skin but is sensitive enough to detect a series of hand movements essential to the rehabilitation process (Ferrone et al, 2016).

1.2.3 Materials for flexible and wearable sensors

There are numerous materials that can be used to produce sensors. High sensitivity, good flexibility, desirable stretchability, biocompatibility, sustainability, and good stability are some of the important conditions that one should take into account while designing a flexible and wearable sensor (Jian et al, 2017). Physical, mechanical, chemical, and electrical properties of flexible sensors are influential in the decision-making process for material choice, therefore, they should be taken into consideration when choosing the materials and designing the flexible sensor, keeping in mind the fabrication process, application area, and required parameters of the end product. Glass transition temperature and melting temperature should be compatible with processing temperatures. The sensors may require a structure that can conform and adapt to irregular surfaces, depending on the application area of the end product. Elasticity, permeability, tensile strength, surface roughness, adhesion, chemical stability, and electrical conductivity are some of the properties taken into consideration for flexible sensors (Yang et al, 2017). Some of the most common materials used for designing textile-based flexible sensors are conventional natural materials like wool, cotton, and paper, as well as polymeric materials such as polyester, polyurethane, polypropylene, polylactic acid, polycarbonate; conductive polymers polyaniline (PANi), polypyrrole (PPy), polyimide (PI) and poly(3,4-ethylenedioxythiophene):poly(styrenesulfonate) [(PEDOT:PSS]), and metal-based materials, Ag, Au, stainless steel, Cu, and aluminum. Materials for flexible sensors can be examined in two different categories:; substrates and conducting medium (Nag et al, 2017).

1.2.3.1 Substrates for flexible sensors

Printing sensors over flexible substrates is the main part while manufacturing the sensors and materials play a significant role in it. There are many types of substrates that are flexible and can be used in wearables as well. Most of them are polymers as they are of low cost and easy to fabricate. Properties of some of the most common materials used as substrate are mentioned in Table 1.1 (Khan, et al. 2014). Substrates can be in film, yarn, filament, fabric (nonwoven, knitted, woven) form.

Flexible substrates have many desirable qualities but in order to completely replace conventional substrates, flexible substrates are expected to show such properties as a low CTE, dimensional stability, and thermal stability, as well as good solvent resistance and satisfactory barrier properties for moisture and gases. Polymer materials are favorable materials for applications that require high degree of bendability, transparency and emission. Some of the polymers used as substrates in flexible wearable electronics are polyethylene terephthalate (PET), polyethylene napthalate (PEN), polyetheretherketone (PEEK), polycarbonate (PC) and polyimide (PI), silicone and polyurethane (PU). Besides polymeric substrates, metal-based foils, cotton and paper are also used as flexible substrates (Dahiya et al, 2014).

Table 1.1. Properties of flexible substrates (Khan, et al. 2014).

Property	Polyester (PET)	Poly-acrylate (PAcr)	Polyethylen-napthalate (PEN)	Poly-carbonate (PC)	Polyether sulphone (PS)	Poly-imide (PI)
Glass Transition Temperature Tg (^{O}C)	70	105	120	145	203	270
Melting Temperature Tm (^{O}C)	115	175	268	115-160	180-220	250-320
Coefficient of Thermal Expansion CTE (Ppm/^{O}C)	33	70	20	75	54	8-20
Transparency (%)	90	>90	88	92	89	35-60
Water Absorption (%)	0.6	0.2	0.4	0.25	1.4	2-3
Youngs Modulus(GPa)	2.8-4.1	2.4-3.4	0.1-0.5	2.4	-	2.5
Solvent Resistance	Good	Good	Good	Poor	Poor	Good
Surface Roughness	Poor	Fair	Poor	Good	Good	Good
Dimensional Stability	Good	Good	Good	Fair	Fair	Fair

Polyurethane film:

Polyurethane is produced in a polymerisation reaction between diols or polyols which and diisocyanates or polyisocyanates. The result is a molecule with (COONH) bonds. Figure 1.7 shows the polymerisation reaction and chemical structure of polyurethane. The polymer backbone affects the properties of polyurethanes. The properties can be manipulated by the changes to the backbone in order to have high strength and rigidity, or high flexibility and toughness. There are two types of PU, thermoplastic and thermoset. When the diol reacts with diisocyanate, a linear and thermoplastic polymer is formed. If the alcohol consists of three or more hydroxyl groups, the outcome will be a rigid, cross-linked, thermoset molecule. Polyurethane (PU) has many different potential applications due to its properties and processing methods. Thermoplastic Polyurethane (TPU) is highly favored as substrates for flexible electronics due to their elasticity, high tensile strength and abrasion resistance. Table 1.2 gives a summary of properties of TPU (Lee et al, 2020).

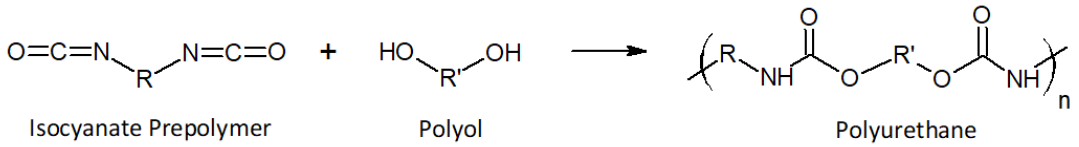

Figure 1.7 : Polyurethane chemical structure (Krol, 2007).

Table 1.2 : Properties of thermoplastic polyurethane (TPU) (Lee et al, 2020).

Properties	Typical Value	Units	Test Method
Density	1.21	g/ml	ASTM D792
Hardness, shore a	67	-	ASTM D2240
Tensile strength	31-62	MPa	ASTM D412
Elongation at break	700	%	ASTM D412
100% modulus	3.5-7	MPa	ASTM D412
300 % modulus	6.3-13	MPa	ASTM D412
Tear strength	371	pli	ASTM D624
Abrasion	40	-	DIN Abrasion Loss, DIN 53516
Tg	-42.0	˚C	DSC

Silicone Film:

Silicone is a semiconductive elastomer. Room temperature vulcanizing (RTV) means that the silicone solidifies at room temperature. RTV Silicone is a type of liquid silicone rubber that vulcanizes at room temperature and is heat resistant up to 180°C. The two types of room temperature vulcanizing silicones are RTV-1 and RTV-2 silicones. RTV-1 is a single-component, ready to use silicone. It starts crosslinking as soon as it comes into contact with atmospheric moisture. RTV-2 is a two-component

silicone which needs a catalyzor to cross-link. Table 1.3 Summarizes properties of RTV-2 Silicone (Dahiya et al, 2014).

Table 1.3 : Properties of RTV-2 Silicone (Dahiya et al, 2014).

Physical Properties	Metric	Thermal Properties	Metric
Density	1.300 – 1,800 kg/m^3	CTE, linear	1.40 - 730 µm/m-°C
Water Absorption	0.050 - 0.50 %	Thermal Conductivity	0.0159 - 140 W/m-K
Viscosity	50 - 880000 cP	Maximum Service Temperature, Air	125 - 300 °C
Mechanical Properties	Metric	Minimum Service Temperature, Air	-115 - -40.0 °C
Tensile Strength, Ultimate	0.310- 6.86 MPa	Glass Transition Temp, Tg	-110 - -40.0 °C
Tensile Strength, Yield	1.17 - 1.72 MPa	Flammability, UL94	HB - V-0
Elongation at Break	15 - 400 %	Optical Properties	Metric
Elongation at Yield	80 - 160 %	Refractive Index	1.39 - 1.42
Electrical Properties	Metric	Transmission, Visible	90%
Electrical Resistivity	1.00e+13 - 1.20e+16 ohm-cm		
Dielectric Constant	2.0 - 5.3		
Dielectric Strength	7.40 - 27.0 kV/mm		

Cotton Fabric:

Textile-based flexible sensors generally use textile fibers, yarns, or fabrics as substrates. Textile materials can also be used as conductive surfaces when they are coated with a conductive layer. One of the desirable properties of flexible sensors is that they conform to the human body. Cotton is a natural fiber that provides the user

with comfort due to its soft, breathable structure (Zhang et al., 2022). Researchers have used cotton yarns and fabrics as substrates for flexible sensors. Cotton fiber is primarily composed of cellulose, a complex carbohydrate made up of repeating units of glucose. Cotton is highly hydrophilic due to the presence of hydroxyl (-OH) groups on the cellulose molecules, which can form hydrogen bonds with water molecules. Cotton fiber is chemically reactive and can undergo a variety of chemical reactions, such as oxidation, reduction, and esterification. This property makes it useful for a variety of applications, such as dyeing, printing, and chemical modification. Cotton has a decomposition temperature of around 280-300°C. This property makes it useful for applications that require high-temperature processing (Hsieh, 2007).

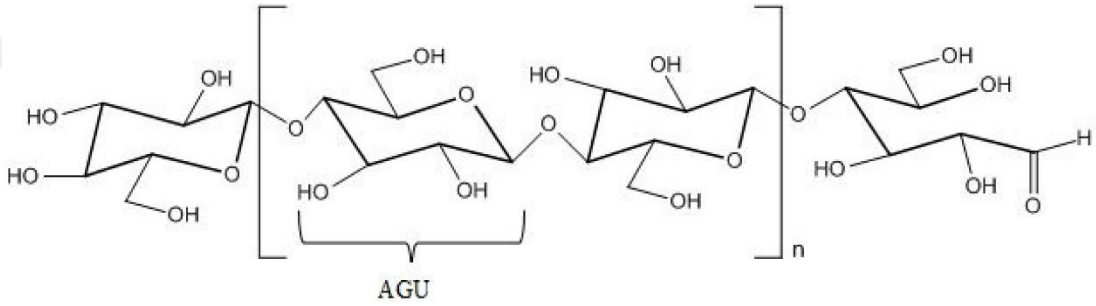

Figure 1.8 : Chemical structure of cellulose (Kramar and González-Benito, 2022).

Cellulose-based materials have excellent physical and mechanical properties, good biocompatibility and biodegradability as well as easy processability and sustainable production on large scales. In recent years these properties have accelerated ongoing developments ongoing developments in wearable and intelligent cellulose-based. Cellulosic materials have been functionalized in a wide variety of architectures such as 1 dimensional (nanofibers, fibers, and yarns), 2 dimensional (paper, films, and fabrics), and 3 dimensional (hydrogels, aerogels, foams, and sponges) structures. Due to the emergence of new material processing and fabrication methods, cellulosic materials can be used as substrates as well as electrically conductive mediums (De France et al, 2021).

1.2.3.2 Conducting medium

A conducting medium can be applied in solution form, melt form, or nanoparticle form as ink or coating material, as well as in fiber, filament, or thread form for knitting, woven, and embroidery applications. Conductive substances that are unaffected by bending or stretching are necessary for a high signal-to-noise ratio and effective

information transfer. For stretchable, flexible, and conducting materials, mechanical flexibility and carrier mobility must be balanced. Organic and inorganic conducting materials can be used to design conducting parts of a flexible sensor. Materials that are used as conducting mediums can be categorized as polymer-based, metal-based, carbon-based, and composites of the first three categories. A conducting medium can be applied in solution form, melt form, or nanoparticle form as ink or viscous material, as well as in fiber, filament, or thread form for knitting, woven, and embroidery applications (Costa et al, 2019).

Polymer-based conductive medium:

Polymers are organic materials that can be processed by convenient and low-cost ways. Chemical structures of polymers can be designed to adapt to various conditions and applications. Some polymers also have excellent biocompatibility and in-body stability, which endow them with health monitoring capability in complicated human conditions. As a result, polymers become one of the most indispensable materials in flexible electronics.Although polymeric materials show many advantages in flexibility, conformality, wearable portability etc., these organic materials still have obvious disadvantages when compared with inorganic semiconductors and metal conductors in terms of electrical properties and device stability (Li et al, 2023).

Conductive polymers, first discovered by Heeger, Shirakawa, and Macdiarmid in the 1970s, have characteristics such as easy applicability, flexibility, light weight, biocompatibility, cost-effectiveness, and lightweight, as well as mechanical properties compatible with flexible surfaces, which gives them an important place in wearable electronics applications. Due to the doping process during polymerization, conductive polymers display relatively high levels of adjustable electrical conductivity. They are also easy to process. Conductive polymers contain monomers that can acquire positive or negative charges by oxidation or reduction that contribute to the electrical conductivity of intrinsically conductive polymers. Some examples of intrinsically conductive polymers are polyacetylene (PA), poly-furan (PF), PANi, poly(phenylenevinylene) (PPV), PPy, polythiophene (PT), and poly(para-phenylene)

(PPP). Figure 1.9 shows the chemical compositions of selected conductive polymers (Namsheer, 2021).

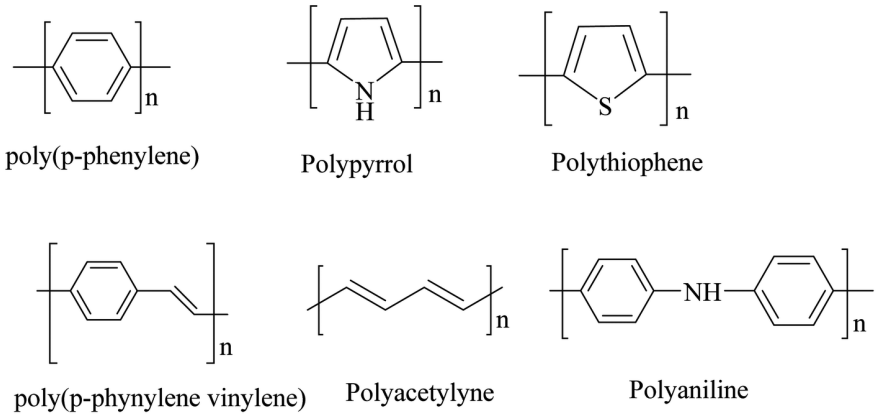

Figure 1.9 : Chemical structures of conductive polymers (Namsheer, 2021).

Metal-based conducting medium:

Metal-based conducting mediums are commonly prepared as conductive inks, conductive fibers and filaments, and metal coatings. Conductive inks are prepared by suspension of metal nanoparticles or metal-organic decomposition (MOD). The process of producing metal -nanoparticles is labor intense and energy-consuming, however, but the positive side is that they are easy to disperse in inks for application in printed electronics. Stabilizers are added to the ink-metal nanoparticle solution to prevent the agglomeration of nanoparticles. Metals can also be used in filament or thread form and woven, knitted, or embroidered onto textile surfaces (Wu, 2022), (Islam et al, 2019), (Wiklund et al,2021).

Carbon-based conducting medium:

Carbon, one of the most prolific elements found in nature, has various allotropic forms. Graphite is one of these allotropes and is favored in electronic applications for its conductivity and thermodynamic stability. The graphite structure is multiple layers of graphene, which is a single-layered two-dimensional honeycomb structured allotrope of carbon atoms, piled together. Other carbon-based materials used in the fabrication of flexible electronics are graphene derivates (graphene oxide (GO) and reduced graphene oxide (rGO)); single and multi-wall carbon nanotube (SWCNT), (MWCNT), carbon black, and activated carbon. Since graphene is a single-layer structure, it can transmit light, is flexible, and has mechanical strength but conductivity increases as the number of layers goes up. Carbon-based materials are used as fillers in composites.

They are also highly favored in conductive inks (Wu, 2022), (Uner and Gürcüm, 2019), (Hatamie et al, 2020).

Composite structures:

In order to maximize desired properties or to functionalize new properties for materials, particles or coatings of conductive polymers, metals, and carbon-based materials can be combined in several ways to form composite structures. Carbon-polymer composites and organometallic conductive inks are an example of conductive composites. Other examples are Ag nanowire/carbon nanotube composite materials; Au NW (Au nanowire) / polyaniline (PANI) conductive inks and Ag NW/poly (3,4-ethylenedioxythiophene): poly (styrene sulfonate) (PEDOT: PSS) conductive inks (Ren et al, 2021).

Some of the more popular and frequently used materials for ink formulation are given in the following paragraphs. These are also the materials chosen for the aim of this thesis study.

PEDOT:PSS:

Poly(3,4-ethylenedioxythiophene) (PEDOT) polymer is a highly conductive polymer with good thermal and electrochemical stability. PEDOT has a wide range of optical properties and high transparency. PEDOT:PSS based solutions have good flexible processing and stable electrical conductivity, good film forming properties and thermal stability therefore they are very popular in flexible sensor studies. The electrical conductivity of PEDOT is caused by delocalized π-electrons within its chemical structure and the presence of PSS.The conductivity of PEDOT:PSS can be improved by secondary doping by thermal and light treatment, or treatments of organic solvents, ionic liquids, surfactants, salts, and acids. Figure 1.10 shows the chemical structure of PEDOT:PSS polymer (Quirós-Solano et al, 2016), (Shi et al, 2015).

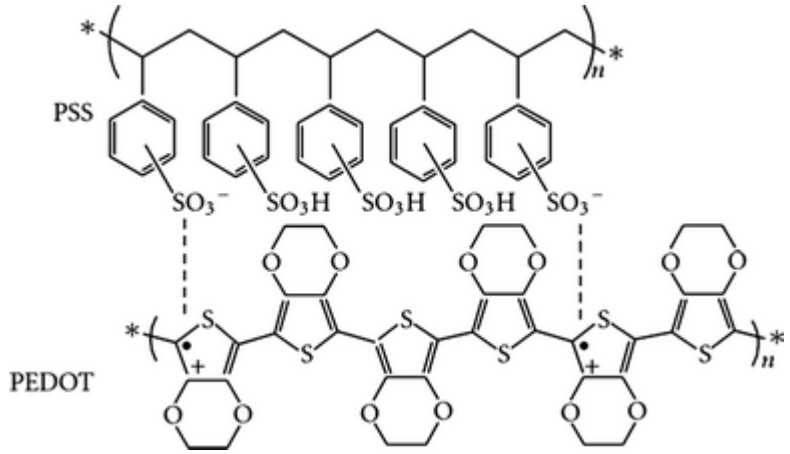

Figure 1.10 : Chemical structure of PEDOT:PSS (Sun et al., 2015).

Graphite:

Carbon is polymorphic material that exists in three basic forms; diamond form, graphite form and fullerene form. In diamond form carbon bonding involves sp3 (tetrahedral) hybridization and in graphite form carbon bonding involves sp2 (trigonal) hybridization resulting in the diamond having a 3D crystal structure whereas graphite consists of stacked carbon layers with covalent and metallic bonding within each layer. Carbon layers are stacked in an AB sequence and are linked by weak van der walls forces produced by delocalized π-orbital. Graphite is an anisotropic material with good electrical and thermal conductivity within each layer but poor electrical and thermal conductivity on a vertical scale. The in planar good conductivity is formed by in-plane metallic bonds, the vertical poor conductivity is due to van der waals forces between the planar layers. The layers in graphite structure are called graphene layers. (Chung, 2022).

Graphene:

Graphene is a freestanding single atomic layer of graphite (Geim, 2009). Andre Geim and Konstantin Novoselov were awarded the Nobel prize in Physics in 2010 as a results of their experiments with graphene. Graphene is a two dimensional nanomaterial with a layer of C atoms covalently bound in a honeycomb lattice structure. The carbon-carbon bond length of graphene is approximately 0.142 nm. Some of the main properties of graphene are large surface area (2630 m2 g-1), high electron mobility (200,000 cm2/(V s), high thermal conductivity (5000 Wm-1K-1) and high young modulus (~1,100 Gpa). Graphene and its derivatives, graphene oxide (GO) and reduced graphene oxide (RGO), have a wide range of applications in

nanocomposites, energy storage devices, transparent films, printable electronics due to their superior properties (Bedeloğlu and Taş, 2016). Transparent conducting electrodes found in flexible electronics can utilize graphene because of its unique electronic and mechanical properties with high optical transmittance. Light-emitting diodes (LEDs), solar cells (SCs), and field-effect transistors (FETs) are other applications for graphene (Han et al., 2017), (Galpayage et al, 2012), (Choi et al, 2010).

Graphene Oxide (GO) and Reduced Graphene Oxide (RGO):

GO is made by exfoliating graphite oxide and RGO by reducing GO. Graphite oxide is mainly produced using the Hummers, Brodies or Staudenmaiers method. In these methods, graphite is intercalated with an oxidizing agent, introducing oxygen functional groups, hydroxyl or epoxy groups in the basal plane, and carbonyl and carboxyl moieties on the edges. After oxidation, graphite oxide is dispersed in water and subjected to sonication or shear, resulting in individual dispersed graphene oxide layers that are homogeneously dispersed in water. The functional groups introduced by the oxidation of graphite help to disperse and stabilize graphene oxide in water. GO is easily dispersed in water and therefore inks prepared with GO can be used in inkjet printers and for production of thin films by spin coating, spray coating and immersion methods (Tas et al, 2019). Li et al (2018) and Huang et al (2019) designed novel GO ink dispersions in water and integrated to inkjet printing. In a similar work, Huang and co-workers used an office inkjet printer to print GO inks onto various plastic substrates, proved that inkjet printing of GO inks is simple and practical (Huang et al, 2019), (Li et al, 2018).

RGO is produced by reduction of GO but even though reducing agents are used some of the functional oxygen groups remain on the surface and edges of graphene (Bo Zhong et al,2022).

GO and RGO are widely used in the fabrication of nanocomposites due to their high compatibility with various polymer matrices. However, harsh oxidation conditions lead to irreversible deformation of the filler, which changes the mechanical and electrical properties, so GO and RGO do not have the same high-quality properties as pristine graphene. While GO shows isolating or semiconducting behavior, rGO has high electrical conductivity. The difference in the conductivities of GO and rGO opens

up different possible applications for these materials.rGO has high surface area and good electrical conductivity. GO also has high surface area and an active surface which increases its conductive properties (Phiri et al, 2018). Figure 1.11 shows the chemical structures of GO and rGO.

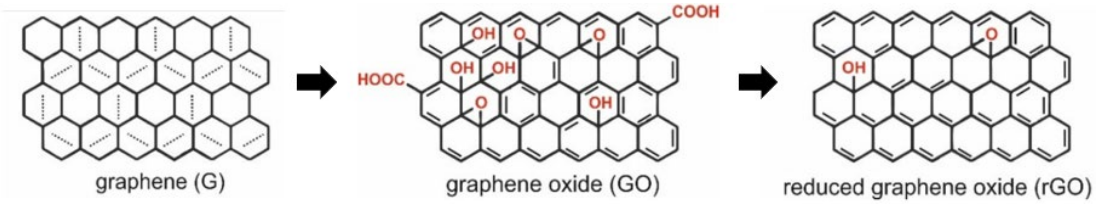

Figure 1.11 : Chemical structures of GO and rGO (Tadyszak et al., 2018).

Cathode waste material (CWM):

Zinc-carbon battery is a type of rechargeable battery that uses zinc and carbon as the anode and cathode materials, respectively. The advantages of zinc-carbon batteries include their high energy density, a low production and watt-hour cost, and come in a large variety of shapes, sizes, voltages, and capacities. Zn-C batteries are reliable and have a moderate shelf life (Dehghani-Sanij, et al. 2019).

The global zinc-carbon battery market is value at US$ 1461.1 million in 2022and projected to grow at a CAGR of 5.5% from 2022 to 2030. The growth in the market can be attributed to the increasing demand for zinc-carbon batteries in flashlights, entertainment, toy and novelty, remote control, and other applications. Key attributes including the convenience of use, size and shape flexibility, and easy disposal of zinc-carbon batteries have resulted in their growing adoption in various consumer electronics products, including home electronics, flashlights, cameras, garage door openers, fluorescent lanterns, remote controls, kerosene heater igniters, security devices, lamps, personal care devices, radios, stereo headsets, smoke detectors, and others. Moreover, these batteries are being comprehensively preferred by consumers living in low-income countries due to their low cost, which in turn is aiding in the vast expansion of the global zinc-carbon battery market (Dataintelo website).

Zinc carbon batteries have a carbon (C) cathode in contact with a paste of MnO_2 with an acid electrolyte, enclosed in a zinc (Zn) case servin g as the anode. Figure 1.12 shows a crosssectional diagram of a zinc carbon battery. Large quantities of zinc and manganese are contained in the batteries and they require proper landfill disposal or

metals recovery (Dehghani-Sanij, et al. 2019). One way to recycle spent zinc carbon batteries is to extract the cathode waste material and use it to fabricate conductive ink.

In a study, the cathode of CWM was extruded from the battery pack and mixed with epoxy to produce conductive paint (Ismail, et al. 2016). In another study graphite rods removed from the spent batteries were cleaned with acetone to remove the plastic coating, and dried prior to electrochemical exfoliation by applying 10 V and 2 A while immersed in a H_2SO_4 solution (1 M). The resulting powders were filtered, rinsed with distilled water until neutral pH and oven dried (80°C). These were then dispersed in a silver-ammonia solution and hydrothermally reacted at 150°C for 5 hours. Sodium silicate solution was used as the dispersing medium for the reduced graphene oxide (rGO) powder to produce conductive ink. The ink showed good surface adhesion, very low resistivity and remained constant even after 500 flex cycles (Amon et al., 2020).

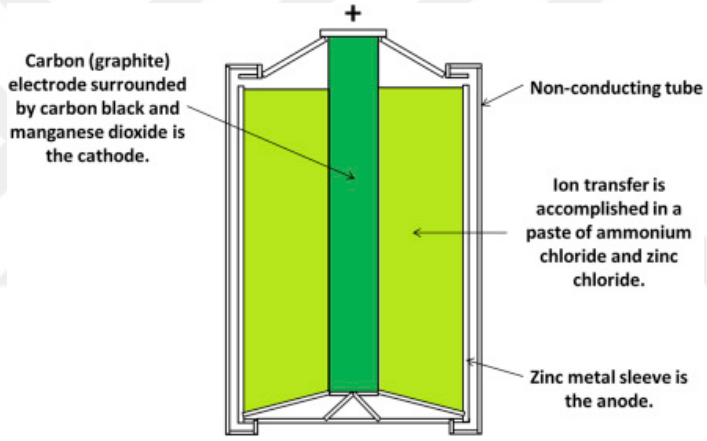

Figure 1.12 : Crosssectional diagram of a Zinc Carbon battery (Sunden, 2019).

1.2.4 Fabrication methods for flexible sensors

To produce flexible wearable devices in more efficient manner using simple procedure, new manufacturing technologies have been developed as discussed below:

1.2.4.1 Yarn type methods (Weaving, knitting, embroidery)

The development of fabric-embedded sensors has mostly utilised this technology. Any weaving machine or handloom can be used for this operation. This technique has been used for centuries for decorative purposes but due to the fragile nature of thin flexible materials and the structure of the flexible sensor integration onto textile the weaving machines that create flexible fabric integrated sensors are still expensive and require specialised handling. Some of the benefits of using this technique are because the

sensor is integrated into the textile, the user does not need to wear an extra layer or device. The sensor can be made in only one step. The electrodes and substrates are not developed separately by different processes. The features of the sensors may be paired with any substrate without much consideration. This is because the clothing is made with conductive material (Takamatsu et al, 2011).

1.2.4.2 Film deposition, casting and photolithography

Thin film deposition

Depending upon the material phase utilized, the two types of thin film preparations are vapour deposition and phase deposition. Chemical deposition is the fabrication of a desired coating on a surface using a highly reactive fluid precursor. Using mechanical or thermodynamic methods, a source material is released and laid down on a substrate in a process known as physical vapour deposition (PVD). Whether or not a chemical reaction occurs during the deposition process determines whether a method is classified as physical vapour deposition (PVD) or chemical vapour deposition (CVD) (Su et al, 2020).

PVD is the process of depositing atoms by physical means onto a substrate in a vacuum to create a paper-thin film, which is typically used to create active metal layers or electrodes. Vacuum sputtering, vacuum evaporation, and ion plating are frequently used deposition techniques. Ionized gas molecules create plasma, and as the electric field accelerates, the cations assault the metal target, and the metal target ion sputters under high voltage of 1500 V, causing the metal atoms to sputter and create a conductive layer on the sample's surface (Su et al, 2020).

Photolithography

One of the widely used methods for creating flexible sensors is lithography or photolithography. This is accomplished by patterning a structure on a substrate with UV light. The structure created on the photomask or uploaded to the system is transferred by the light. Based on the template, photolithography methods can be divided into two categories; masked photolithography and maskless photolithography (Mukhopadhyay and Gooneratne, 2021), (Herzer et al, 2010).

Masked lithography: In this technique, the resist-coated substrate is deposited on top of a mask or template. Through the template, UV light is directed onto the substrate, creating the desired pattern (Mukhopadhyay and Gooneratne, 2021).

Maskless lithography: Here, the system receives the design that will be etched onto the resist. The uploaded pattern is formed on the resist as the UV light scans over it on the substrate (Mukhopadhyay and Gooneratne, 2021).

There are two forms of photoresist that may be used to cover a substrate; positive photoresist (+) and negative photoresist (-). In a positive photoresist, the substrate's UV light exposed areas are removed during a future treatment while other areas are retained. The design is then permanently engraved on the substrate using this resist, which is then treated. In a negative photoresist, the part of the resist exposed to the UV light remains on the substrate while the unexposed part is removed (Herzer et al, 2010).

Casting

This procedure uses a template to create a mould in the preferred design. Then a liquid or semi-liquid substance is placed onto the mould, which causes it to solidify in the mould’s shape. After it has set, the material is cast out of the mould and employed as a separate device. In the case of flexible sensors, the conductive material is poured in liquid or semi-liquid form and then hardened to make the electrodes. To create the substrate for the sensor, a layer of a different material such as a polymer is poured, solidified, and cast on top of the formed mould (Eswaraiah et al, 2011).

Some of the advantages of using this technique are, complex structures can be created with this procedure because the mould is designed to accommodate the needed electrodes. It is more affordable than other widely used manufacturing techniques, such as photolithography and laser printing. Using this technique, prototypes of any shape may be produced. Despite the casting technique's considerable use in recent years, there are significant restrictions that prevent its widespread application (Scot and Ali, 2021).

Some of the considerable limitations are that using this method, microstructures cannot be produced and the electrodes' sensitivity is lower than the electrodes made using laser cutting or printing processes (Eswaraiah et al, 2011).

1.2.4.3 Printing and coating methods

Microcontact Printing: Microcontact printing technology uses a Polydimethylsiloxane (PDMS) material stamp to contact a composite ink and transfer the pattern to the chosen substrate, whereas pattern printing is a general term that applies to a variety of processes, such as having the characteristics of additive transferring, subtractive transferring, or deterministic assembly of materials. Microcontact printing can be used to create composites of carbon nanotubes and PDMS that have a carbon nanotube film incorporated into the material (Fernandes, et al. 2013).

Screen printing: Screen printing technology has been in use since the start of 19th century, when it was primarily employed for commercial purposes. This method has been widely used in flexible electronics for the past 20 years. Screen printing uses a mesh or stencil to apply inks from top to bottom. The design is printed on to the mesh by blocking certain parts of the mesh and when the ink is applied the blocked areas do not transfer the ink, thus forming the design on the substrate. A figure of screen printing is shown in Figure 1.13 where the design created on the coated screen is transferred onto the substrate by pouring ink over the screen (Ohta et al, 2013).

Silver and graphene are two examples of the many commercially available conductive inks used to generate electrodes by screen printing on the substrate. Conductive ink that is applied in screen printing consists of a dispersion of conductive particles and suitable resins in an organic or inorganic solvent. The substrate material can be chosen according to the desired parameters of the sensor. One of the advantages of screen printing is that it can be applied on any flat surface. The properties of the substrate material may affect the outcome of the printing process (Kazani et al, 2012).

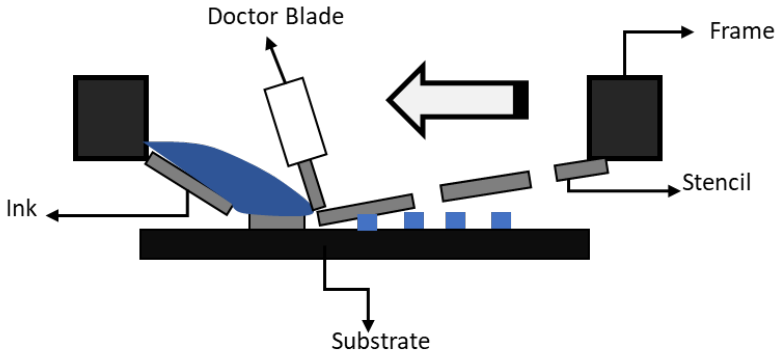

Figure 1.13: Schematic of screen printing.

Spray coating: Spray coaters atomize the solutions or dispersions into mist and spray this mist on to surfaces at high pressure. Spray coating device's nozzle dimensions' change, allowing dispersion of different particle size molecules to be applied. Because of their sophisticated and diverse design, spray coaters have been used for a wide range of applications, from thin film coating of flat sheets such as transparent conductive films for touch panels, to solar cell components and semiconductor photoresist (https://www.keyence.com/ss/products/measure/sealing/ coater-type/spray.jsp).

Laser printing: The substrate is placed under the laser device to be scanned or carved out in order to transfer the design from the software to the substrate. The type of laser system used determines the outcome of the image transfer such as the depth of the sample. Other important attributes that affect the depth of the curved sample are the z-axis; speed and frequency. Z-axis determines the platform height below the laser nozzle. Speed controls how quickly the nozzle passes the sample. In order to get the best characteristics from laser printing, there needs to be a balance between the input power and nozzle speed. Frequency establishes how frequently the laser nozzle will pass the sample (Duocastella et al, 2012).

This technique is dominant and superior compared to the other techniques for the following reasons; contrary to photolithography, there is no need for sample preparation. This method allows for the cutting of very thin and flexible materials, which cannot be done with methods for example screen printing. The final products have reasonably clean edges perpendicular to the substrate surface. Therefore, no further procedure is necessary to polish the finished product (Antikainen et al, 2022).

Ink-jet printing: The concept of using ink-jet printers came out by developing the sensing component on any sensing substrate by swapping the ink for any conductive ink. Silver, carbon, and copper are a few of the popular conductive ink types utilised in ink-jet printing (Hossain et al, 2009).

There are two basic kinds of ink-jet printers; continuous and drop on demand (Sridhar et al, 2011).

Continuous: A piezo-electric crystal inside the laser generates a wave that breaks down a continual stream of ink being extracted from a reservoir into liquid droplets. An electrostatic field produced by a charging electrode charges these droplets. Another

electrostatic field is passed through these charged droplets, this allows them to be redirected onto the printing substrate material (Sridhar et al, 2011).

Drop-on-demand: The drop-on-demand (DOD) technique is further divided into two categories: thermal and piezoelectric. In thermal DOD, a pulse of current is used to heat up the cartridges, which are made up of a number of mini heaters. Ink in the reservoir is then heated as a result, raising its pressure, and producing an ink bubble. This bubble pushes out as a droplet on the substrate. A sequence of droplets is produced on the substrate as a result of the ink being drawn out of the reservoir by an increase in pressure, heating, condensation, and surface tension (Sridhar et al, 2011).

The key difference of piezo-electric DOD lies in the piezo-electric material that takes on a different shape in response to a voltage in place of the mini-heaters. Due to the pressure rise brought on by this change in shape, the droplet of ink is forced out of the reservoir in the form of a bubble. Figure 1.14 shows a diagram of continuous and dod inkjet printing methods. Several advantages of using this technique for construction of sensors compared to other techniques are that these devices are less expensive, they consist of a printer that can use various conductive inks. High quality prints can be fabricated through this method. Printing time is relatively short which is an advantage for large scale fabrication. Due to the simplicity of the device and technique, ink jet printers require less skill to operate (Wang et al, 2022).

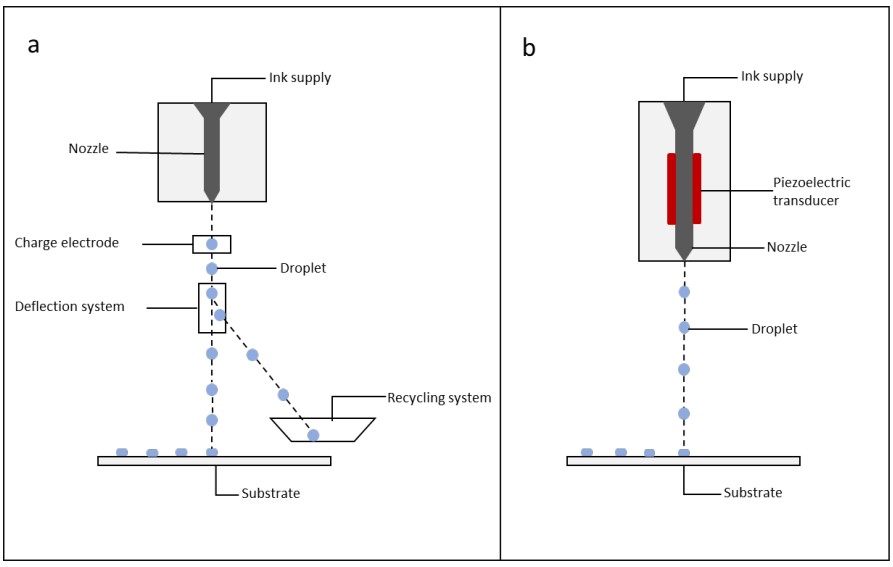

Figure 1.14 : Inkjet printing schematic a) continuous b) drop-on-demand.

Doctor Blade coating technique: Doctor Blade coating technique uses a blade at a fixed distance from the substrate material. The solution that will be used for coating is poured in front of the blade and the blade is swiped along the surface of the substrate creating a film with a certain thickness (Cherrington et al, 2016). Similar to screen printing, a mask or stencil can be placed on the substrate surface to form the desired patterns. This method is simple and effective, low-cost with minimum complications. It can be used in wide area applications. Figure 1.15 shows a schematic of doctor blade technique.

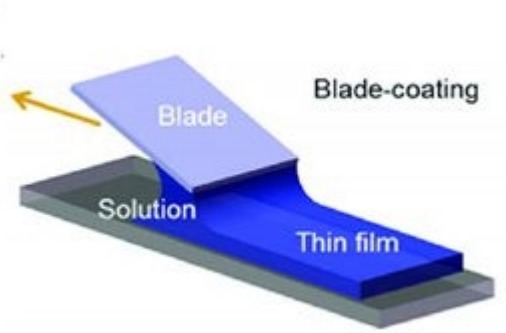

Figure 1.15 : Doctor Blade coating schematic (Hu et al, 2020).

1.2.5 Main applications for flexible sensors

Wearable technology is a novel way for people to engage with computers and has many uses. These have been extensively employed in the medical and healthcare industries for a variety of purpose, like physiological signal monitoring, sports, and environmental detection, greatly enhancing people's lives and the standard of living. Sensors in the medical profession may track and measure certain parameters, allowing for ongoing advancements in the efficacy and practicality of medical care. (Aroganam et al, 2019).

Materials used for flexible sensors depend on the application areas of the sensors. They can be divided into three different segments; biophysical monitoring, biochemical monitoring, and detection of data in real-time data (Costa et al., 2019), (Zazoum et al., 2022).

Biochemical monitoring comprises blood monitoring, pH tracking, and biomolecule recording, whereas biophysical monitoring includes pulse rate monitoring, temperature monitoring, and human motion detection. Each monitoring sensor needs a particular type of material to be fabricated (Nasiri and Khosravani, 2020). Since wearable sensors are in close proximity to the human body, they need to be

comfortable, flexible, and compatible, or the material used to make the sensors needs to be flexible (Yang et al, 2018).

1.2.5.1 Biophysical sensors

Wearable biophysical sensors are used to measure a wide range of physiological and physical parameters of the human body. Some common examples of wearable biophysical sensors include electrocardiogram (ECG or EKG) sensors, heart rate monitoring and blood pressure monitoring (Prieto-Avalos et al, 2022). Some examples of research conducted on biophysical sensors are given in the following paragraphs.

Pulse rate monitoring:

When it comes to cardiovascular diseases, information on pulse rate is crucial, and the two simplest measures of pulse rate are beats per minute and pulse. Mentioned parameters are easily estimated via pressure and strain sensors (Prieto-Avalos et al, 2022). The materials utilized in fabricated pulse rate monitoring sensors are:

An electrocardiogram (ECG) is used to assess the electrical activity of the heart and also yields important information about heartbeat. Pang et al. use polydimethylsiloxane (PDMS) composites made of carbon nanotubes (CNT) to connect to the ECG with electrode. A flexible, sensitive wearable sensor that can track heartbeats is created. Polymeric nanofibers are integrated onto thin PDMS layers. The made-up sensor can readily keep track of a heartbeat's physical force (Pang et al, 2012).

Boutry et al used Polyglycerol Sebacate (PGS, a biodegradable elastomer, for the fabrication of pressure sensors particularly for pulse rate monitoring. PGS has a low viscoelastic response, allowing for quick device reaction times and high repeatability during cycling (Boutry et al, 2015).

Chen et al used self-powered Hierarchical Elastomer Microstructures (HEM) to provide continuous monitoring of heart and vascular health. Due to its lightweight, low cost, self-powering, and high overall sensitivity performance features, the HEM sensor exhibits a great deal of value and potential in the field of flexible wearable sensors (Chen et al, 2020).

Temperature monitoring:

The human body temperature differs in case of different diseases. Additionally, body temperature has an influence on how well therapies work. A temperature sensor is

fixed on human skin to read the temperature in real-time (Dolibog e al, 2022). Sensor material also plays an important role while designing a temperature sensor. Some of the materials utilized in temperature monitoring sensors are as follows.

Hong et al. use a **s**tretchable polyaniline nanofiber temperature sensor with polyethylene terephthalate (PET) films for the construction of a temperature sensor. The temperature sensor has good resistance sensitivity, and mechanical stability, and according to the article the resulting sensor does not exhibit any mechanical or electrical degradation (Hong et al, 2016).

The lower thermal stability of biodegradable polymers such as Polylactic-co-glycolic acid (PLGA) or Polylactide (PLA) limits their use in the fabrication of sensors. Wu et al. coupled the In order to increase heat sensitivity and achieve high-pressure sensitivity, the dielectric layer of organic field-effect transistors (OFETs) is coupled with PLA sheets to create biodegradable temperature sensors. Compared to PLGA, PLA has better inherent thermal stability, therefore it might be used more frequently in future scenarios (Wu et al, 2015).

Sensors that come into direct contact with skin must have good air permeability and excellent water resistance. For the manufacturing of temperature sensors, silicon wafer and polyimide are used which makes the sensor biocompatible, ultra-flexible, and stretchable (Chen et al, 2015).

Human motion detection:

Tracking motion provides significant and useful information about human health. Wearable and flexible sensors are essential for identifying abnormal movement patterns or sudden tremors. Two categories used in detecting human motion are; large-scale movements like the movement of knees or hand, small scale movement like the movement of the chest while breathing (Homayounfar and Andrew2020).

Yang et al. spray coated MXene/SnS2/SA material on a PDMS substrate and encapsulated the top layer by PDMS. A bidirectional sandwich structured sensor with high stretchability, ultra-high sensitivity, excellent repeatability and stability as well as quick response was obtained. According to the authors the sensor has superior application potential in detecting small scale signals and large-scale motion signals (Yang et al, 2022).

Huang et al. constructed a self-powered active pressure sensor with biomass-based bacterial cellulose/chitosan (BC/CS) composites and copper nanoparticles-doped polydimethylsiloxane (PDMS/Cu) film as positive and negative triboelectric layers, respectively (Huang et al. 2021).

Li et al manufactured a novel piezoresistive pressure sensor from thermoplastic urethane (TPU) within electrospun fibrous network (TPUN), where the TPUN was decorated with c-MWCNTs to increase conductivity. The pressure sensor exhibited a high sensitivity to acquire human physiological signals such as various muscle activities and pulse (Li et al, 2021).

1.2.5.2 Biochemical sensors

Wearable and flexible sensors are now used for simultaneous biophysical and biochemical monitoring. In healthcare monitoring, biochemical sensors predominate, and each sensor has a unique set of applications, such as blood monitoring, pH tracking, bio-molecule tracking, etc. In order to fabricate a biochemical sensor, the material selection is crucial (Nasiri and Khosravani, 2020).

Blood monitoring: Some of the materials that have been used for manufacturing blood monitoring sensors are given in following paragraphs.

Blood monitoring is crucial for spotting cardiovascular illness at its earliest stages, and lead zirconate titanate-based sensors are used and quickly customized for continuous usage throughout everyday activities. With high dielectric permittivity, substantial piezo-electric, electromechanical coupling coefficients, and ferroelectric/piezo-electric properties, lead zirconate titanate is a wise option for blood pressure and strain sensors (Dagdeviren et al, 2014).

In another study an isopore flexible gas permeable membrane with electrolytic solution (KCl) is used for the construction of flexible and wearable oxygen sensor that measure partial pressure of Oxygen in arterial blood for non invasive medical monitoring (Iguchi et al, 2015).

pH tracking: It is essential to examine pH since the human body's pH must be maintained within a range. Wearable and flexible sensors provide a precise way to measure pH (Manjakkal et al, 2020).

The following materials have been utilized as pH monitoring sensors:

Flexible electro-chemical pH sensors made of CuO are based on nanorod-shaped CuO nanostructures. These sensors have exceptional capacitance and impedance sensor performance. For fabrication, CuO-based sensors are printed on surfaces, and the pH is then measured (Manjakkal et al, 2018).

The advantages of organically modified silicate-based optical pH sensors are extended lifetime, reversible and quick reactions, durability, affordability, safety, simplicity of downsizing, and mechanical robustness. For the creation of pH monitoring sensors, 3-glycidoxypropyltrimethoxysilane (GPTMS), a pH-sensitive ORMOSIL, is employed as a siloxane precursor. In order to make the sensor wearable and flexible, it has to be gently attached to the smart fabric (Caldara et al, 2016).

The pH of the skin can be continuously monitored using polyaniline (PANi), a pH sensitive material. Cotton fibers are modified using an immersion and drying process and then coated with the substrate poly(3,4-ethylenedioxythiophene)-poly (styrene sulfonate) to form a pH sensor (Smith et al, 2019).

Bio-molecule tracking: The identification of dangerous bacteria, cancer molecules, enzymes, etc. in the human body is done using biomolecule tracking sensors (Castillo-Henríquez et al, 2020; Bohunicky and Mousa, 2010). Some of the materials in the research and development stage for bio-molecule tracking are listed below:

Because of its nanoscale structure, graphene can identify analytes with extreme sensitivity. Resonant coils inside the sensor make it wireless and do away with the need for an external connection. The sensor is used for salivary bacteria detection and respiratory monitoring (Mannoor et al, 2012).

PEDOT:PSS is used to manufacture a sensor to monitor the lactate oxidase enzyme's physiological activity, integrated with an organic electrochemical transistor (OECT), and Kapton as a substrate. This sensor shows high sensitivity to lactase enzymes (Currano et al, 2018).

Agarose hydrogel-based sensors are now used for sweat component detection. When human skin comes in contact with an agarose hydrogel, the sweat components can be simply and continuously collected, followed by in-situ detection. This helps in the identification of salts or enzymes present in human sweat (Nagamine et al, 2019).

1.2.5.3 Real-time data detection sensors

Real-time sensors play an important role in Industry 5.0 where human-beings and robots are expected to coexist in the factory floor, where it is important to detect, transmit and analyze data and take appropriate action in real-time. Real-time sensors are also functional in autonom devices like automobiles where they need to track the pedestrian and traffic movement in real-time and take immediate action. They are also widely used in agriculture. In a world where water-shortage is a real threat irrigation systems based on real-time sensors provide a sustainable solution. Monitoring the physical status of patients, elderly people with medical conditions and athletes in training are several other ways real-time sensors are used (Javaid et al, 2021; Vellidis et al, 2008; Zou et al, 2023).

Honda and friends developed a flexible humidity sensor with ZnIn2S4 nanosheets attached to a mask to monitor sleep apnea at home. The resistive flexible humidity sensor consists of a polyimide (PI) film, laser-induced graphene (LIG) electrodes, a ZIS stacking layer, and a humidity pass filter. A wireless system with a battery measures a voltage change converted from a sensor resistance change, and resulting measurements are transmitted to a smart phone using Bluetooth (Honda et al, 2022).

Müezzinoğlu and Karaköse designed two wearable smart gloves working in real time to obtain signal data and process with machine-learning-based methods and classified multi-mode commands The authors concluded that a flexible design is optimal for the wearable smart glove. They installed five flex sensors, one IMU, and one STM 32 microcontroller in each glove to collect precise data safely and with high accuracy (Müezzinoğlu and Karaköse 2021).

1.2.6 Challenges and opportunities in flexible wearable sensor technology

Although carbon-based materials have many benefits in the progress of different wearable sensors, fully embedded carbon-based wearable electronics still face difficulties in terms of close-packed design, low-cost fabrication, device layers protection, multi-functional sensing, and integration techniques. Demand is growing, especially for wearable flexible sensors that are mass produced at low cost. Although several efficient preparation methods have been researched for cost-effectiveness and mass production, yet these new techniques have significant flaws that could result in the degrading performance of carbon-based materials (Heo et al, 2020).

Thus, to secure acceptable materials for wearable sensors, efficient procedures like functional material optimization and hybridization are needed. In addition to the economic challenges, it is crucial to develop the high sensitivity and prolonged operational stability of carbon-based sensor devices in order to implement practical applications that can precisely detect human activities or physiological signals (Homayounfar and Andrew, 2020).

Although contemporary textile-based sensors frequently require additional lamination or interlayer to produce sensors directly on the fabric substrates, they are highly cost-effective than carbon-based technologies. This is frequently caused by the rough surface of textiles, which can weaken the adhesion, cause materials to delaminate that have been coupled to the textiles, and degrade electrical performance. Textile-sensors have lost their distinctive qualities as a result of the extra layering of textiles. Therefore, the aforementioned materials, fabrication technologies, and different sensor devices must all be developed in combination in order to make textile-sensors. Additionally, textile-sensors are flexible, however due to the mechanical deformations caused by washing, the electric performance of textile-based wearable sensors may get compromised (Nasiri and Khosravani, 2020).

Moreover, it is still difficult to align textile-based sensors with electronics. Since the bulk of silicon-based electronics are constructed on rigid or non-stretchy substrates, the issue of creating connections between electronics and stretchable textile-based sensors arises. The development of active devices on thread or transistor-based active sensor arrays might be the appropriate answers since on-thread or on-sensor amplifiers can increase the Signal-to-Noise Ratio (SNR) of the measured signal (Miah et al, 2022).

The fact that sensors produce data is another significant feature that is occasionally overlooked while discussing the topic of flexible sensors. The processing and decoding of this data is a crucial component of sensor technology development. To deliver the final feedback to the end user in real time, the detected data must be analysed and processed using artificial intelligence, deep learning, or other methods for managing "big data“ (Comini, 2021).

Some of the major challenges of flexible sensors are low level of accuracy and sensitivity, lack of standards for fabrication and data reliability. Sensitivity, reliability,

response time, data accuracy, durability, the difficulty of mass manufacturing, and high costs are some of the main areas that need to be developed. The structure of the textile material that provides comfort to the user also provides a handicap for the sensor. The flexible, soft, breathable materials cause extra stress to the sensor and decrease its sensitivity and accuracy. In conventional sensors, because of their rigid structure, there is no extra bending and twisting, therefore, they have higher sensitivity and accuracy, and the results can be repeated and are more reliable (Nag and Mukhopadhyay, 2021).

Another disadvantage of flexible wearable sensors is that they need to be washed for re-use and the washing cycles shorten the lifespan of the sensor. If a sensor is not a single-use sensor, it needs to provide the same data accuracy and reliability after several cycles of washing as it did pre-washing (Zhang et al,2022).

Since the fabrication of textile-based sensors is a relatively new technology, it is difficult to compare the performance of sensors due to a lack of methods and standards. Most of the testing and standards are developed for conventional sensors or conventional textile materials, therefore, the results are not conclusive (Miah et al, 2022).

1.2.7 Future of flexible wearable sensors

Technologies for remote monitoring and wearables are being developed at an exponential rate. These platforms may soon have an influence on a number of health care practises, including illness management, early identification, and prevention (via the tracking of food and exercise patterns, stress level monitoring, and dehydration warnings). These platforms will deliver more precise measures of physiological indicators and physical state in more practical ways (e.g., drug dose monitoring and reminders). In particular, efforts are being made to create the next generation of wearable sensors to detect cancer-related compounds and biomarkers. (Yang et al, 2018). However more work is required to resolve all technical limitations, particularly the following: (a) data measurement accuracy and reliability (noise reduction); (b) data transfer reliability, safety, and security; (c) system simplification through multifunctional textiles; (d) power management efficiency, including power generation; (e) system durability, including washability and long-term accuracy in performance; and (f) user-friendliness, including the ability to use/wear the garments

without assistance (Erdonmez and Bedeloglu, 2023). Some of the future applications for wearable flexible sensors are given in the following sections.

1.2.7.1 Injectable sensors

The temperature of the internal organs located deep within the body, such as the liver, is referred to as core temperature (Tc). The human body's core temperature is kept within a very tight range of 36.5-38.5 °C. This is the optimal temperature range for the body's metabolic functions. Core body temperature can be measured by inserting a measuring device like a probe into the body which can generally only be done at a hospital setting. Majority of wearable physical sensors are fully non-invasive therefore it is not possible to assess significant parameters like core body temperature. Researchers are working on injectable, minimally encroaching sensors that may be placed beneath the human skin to make measurements within the body to address these issues (Dolson et al, 2022).

1.2.7.2 Microneedle patch type sensors

With long-term symptoms, chronic diseases (CDs) are noncommunicable disorders that cause around 70% of all fatalities globally. Accurate biomarker detection is crucial for the diagnosis and prognosis of CDs. At the moment, the performance and usability of the sophisticated platforms used for CD-associated biomarker identification are constrained. Therefore, there is an unmet need to present creative strategies that can be used in point-of-care (PoC) settings and that also offer accurate biomarker detection. In recent years, there has been a lot of interest in the development of MN-based biosensors for real-time monitoring of CD-associated biomarkers. In order to access the biomarkers, microneedles pierce the skin's outer layer. This minimally invasive procedure enables a more thorough examination of the body's homeostasis, a state of balance among all systems within the body. For a straightforward electro-chemical study of biomarker concentrations, microneedles serve as electrodes. These patches are worn similarly to plasters and remove with little trace, making them perfect for use in point-of-care analysis (Erdem et al, 2021).

1.2.7.3 Smart tattoos

Smart tattoos are an innovative method to monitor analytes in the body. Under the epidermis, ink used for regular tattoos comes in touch with analyte solution. The

tattoos incorporate pigments that are sensitive to changes in biomarkers, changing colour in response to such changes. This eliminates the need for bulky analytical equipment, improves device portability, lowers costs, and increases accessibility by enabling straightforward analysis with the naked eye. Yetisen et al (2019) studied this method which minimizes invasive procedures and is an injectable dermal biosensors for measuring pH, glucose, and albumin concentrations. Quantitative readouts were acquired using a smartphone camera after the sensors were layered in ex vivo skin tissue. In point-of-care settings, these sensors can be used to manage diabetes, liver failure, and acid-base homeostasis (Yetisen et al, 2019).

1.2.7.4 Diabetic monitoring

Diabetes management is an example of how wearable technology is presently enhancing medical care. Diabetes is a disease whose prevalence is rising to the point that, by 2045, 10% of the world's population is expected to be diagnosed with it. To maintain levels within a safe range, blood glucose levels must be constantly monitored (Rodriguez-León et al, 2021).

All currently available continuous glucose monitoring (CGM) solutions demand an invasive analytical instrument and action when asked, both of which reduce adherence. The main topic of current research is non-invasive glucose monitoring. It is hoped that simple wearable devices, like Abbott's FreeStyle Libre, which enable CGM via minimally invasive methods, will increase monitoring adherence. One example of how wearable technology has started to improve lives is CGM, which either directs therapy for type 1 diabetes patients or diet and lifestyle decisions for type 2 diabetes patients (Tang et al, 2020).

1.2.7.5 Wearable systems for pets

Wearables with accelerometers offer more detailed information on the behaviour of the animal, however, tracking data may get lost. Due to the lack of information regarding the animal's location, navigation is only possible based on the estimated distance travelled (calculated from the number of steps taken). Researchers are developing a wearable canine navigation device that enables low-power offline animal position tracking and activity monitoring. (Fonseca et al, 2022)

Wireless auscultation of canines is another potential future application for flexible sensors. Auscultation is the process of listening to the sounds of the body during a physical examination. A flexible, wearable polymer composite object that can be utilised for wireless canine auscultation has been developed. To increase signal conduction on the touch surface and enable the recording of heart sounds, the wearable sensor conforms to the shape of the body and removes air bubbles from within the fur. The literature has incorporated the most recent discovery of an extra sensor for tracking respiratory patterns, including sniffing and panting (Cotur et al, 2020).

1.3 Superamphiphobic Coating

Flexible sensors are used in many different applications where they need to be in contact with human body parts therefore are expected to provide a comfortable texture and breathability. In real life situations, a flexible sensor is subjected to extrinsic parameters such as sweat, blood, rain, oil. The sensor can soak water and organic fluids thus affecting the functionality and sensitivity (Wang et al, 2023). Superamphiphobic coatings are superhydrophobic and superolephobic where they repel both water and organic fluids (Chu and Seeger, 2014).

1.3.1 Attributes of superamphiphobic surfaces

Materials that repel water are called hydrophobic, non-wettable surfaces with high water contact angles are called superhydrophobic. Similarly, materials that repel oil and other organic liquids are called oleophobic and oil-repellant surfaces with high contact angles are called superoleophobic. Superamphiphobic surfaces are both superhydrophobic and superoleophobic (Su and Seeger, 2014).

Superamphiphobic surfaces also carry self-cleaning attributes. Other desirable attributes of superamphiphobic surfaces are antifouling, stain resistance, spill-resistance, drag reduction, corrosion prevention, and liquid separation. Lotus leaf is given as the inspiration behind water-repellant self-cleaning materials and it is called the lotus effect. In 1997 Barthlott and Neinhuis examined the hydrophobic surface and self cleaning property of the lotus leaf. They determined that the relationship between “surface roughness, reduced particle adhesion and water repellency” is the main reason

behind the self-cleaning properties of the lotus leaf (Sahoo et al, 2018), (Barthlott and Neinhuis, 1997).

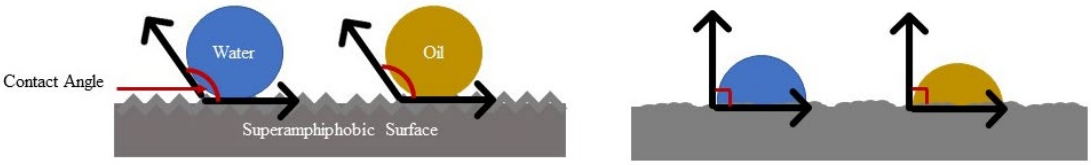

Figure 1.16 : Diagram of contact angles for superamphiphobic and amphiphobic surfaces

1.3.2 Fabrication strategies and materials

It is more difficult to fabricate oil-repellant surfaces because they have a lower surface tension than water. Researchers concluded that a combination of surface roughness and surface chemistry is the key to manufacturing superamphiphobic surfaces. The surface can be roughened by methods like etching, lithography or sputter deposition. After roughening with these methods it is then coated with a low surface energy compound. Another method is to coat smooth flat surfaces directly with compounds that will give it a rough surface structure with low surface energy by using dip-coating, spin-coating and spray-coating methods (Ghaffari et al, 2019).

Some of the materials used in superamphiphobic coating solutions are tetraethoxysilane (TEOS) and methyltriethoxysilane (MTES), nanosilicas, silicone nanofilaments, carbon nanotubes, carbon nanofibers, fluorinated silica nanoparticles, copper perfluorooctanoate, fluoroalkyl polyhedral oligomeric silsesquioxane, fluoroalkyl silane/fluorinated-decyl polyhedral oligomeric silsequioxane (FAS/FD-POSS) (Ghaffari et al, 2019).

A stretchable film with excellent superhydrophobicity is proposed for reliable strain sensors based on a 3D conductive network. First, superconducting carbon black (SCB) nanoparticles are assembled onto electrospun thermoplastic polyurethane (TPU) fibers to form a conductive TPU/SCB film. Then, a dispersion of carbon nanotubes (CNTs) and fluorinated silica (F-SiO2) is sprayed onto the TPU/SCB film to form a TPU/SCB@CNTs/F-SiO2 conductive composite film. After immersing the composite film in a mixed solution of poly(dimethylsiloxane) (PDMS) and perfluorodecyltrichlorosilane (PFDTS) and drying, a flexible conductive superamphiphobic film was obtained. When used as a strain sensor, the film showed superior sensitivity (12.0560.42), wide strain range (0100%), fast response time

(75100 ms), and good stability in strain-relaxation cycles. Due to favorable superamphiphobia, the strain sensor obtained could be effectively used to display stable electrical signals underwater and to monitor human movements under dry/sweat exposure, showing significant potential for practical wearable sensors for stretchable, breathable, and reliable monitoring of human behavior (Ding et al, 2022).

One of the main objectives of this thesis study is to obtain a superamphiphobic surface by coating the sensor surface with a material that has hydrophobic and oleophobic properties. Some of the materials mentioned in literature are discussed in more detail in the following sections.

1.3.2.1 Kaolin

Hydrophobic and oleophobic materials have gained interest due to their ability to repel water and oil drops and self cleaning properties. Scientists are inspired by lotus leaves in nature and the effect is called the lotus effect. Surface roughness caused by micro and nano hierarchical roughness. Formation of superhydrophobic surfaces is attributed to the dual function of micro/nano- hierarchical roughness and low surface energy. Up to now, a variety of methods have been developed to fabricate superhydrophobic surfaces on wood-based materials, such as hydrothermal treatment, sol-gel method, dip or spray-coating, soft lithography, “paint + adhesive” method, and so on. Among “paint + adhesive” methods, PDMS as adhesive has been successfully used to fabricate various robust and durable superhydrophobic surfaces. In a study conducted by Koch and friends after stearic acid (STA) was solubilized in absolute ethanol solution kaolin particles were added to the stearic acid solution to obtain STA modified kaolin suspension. Afterwards, the STA-kaolin particles were obtained from the suspension by filtering. Finally, the STA-KL particles were dried at 120 ◦C for 2 h. Kaolin is a chemically inert (over a relatively wide pH range), soft and non-abrasive material with low heat and electricity conductivity (Koch et al, 2009). Figure 1.17 Shows the chemical structure of kaolin (Murray, 2006).

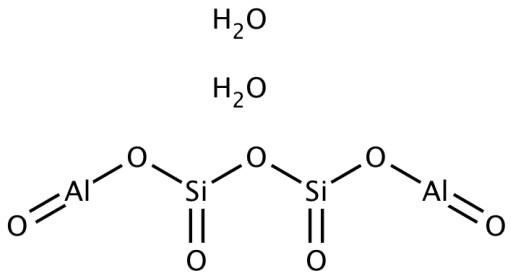

Figure 1.17 : Chemical structure of kaolin (Murray, 2006).

1.3.2.2 Zinc stearate

Zinc stearate (Zinc distearate) is a fine white soft and muctuous odourless bulky powder, molecular weight 632. Its outstanding characteristic is the extremely small particle size of the top quality material, which can be less than one micron in diameter, giving it a high specific surface e.g. the order of 25,000 sq. cm. per gram. The stearate finds the widest use in more diversified applications than any other metallic stearate, except probably aluminium stearate, due to the fact that it exhibits to a high degree all the unique properties of all the metallic stearates in general. It is more 'slippery', more muctuous, more water repellant and least solvent soluble of the common metallic soaps. Zinc stearate has been used in making antiskid adhesives with low cohesion for the fixation of packaging bags made of polyethylene or polyviny l chloride), an example consisting of polyvinyl alcohol, zinc stearate and ethylene glycol, and adhesives for floor and wall coverings have been formulated from cellulose ethers and zinc stearate, as a hydrophobe additive (Lower, 1982).

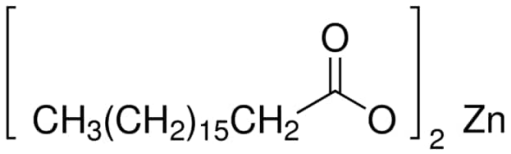

Figure 1.18 : Chemical structure of zinc stearat.

1.3.2.3 Silicon dioxide nanopowder

Silane coupling agent-coated silicon dioxide nanoparticles are extremely oleophilic and hydrophobic. Commonly known as silica, silicon dioxide (SiO2) is a combination of silicon and oxygen. The elements are joined by a covalent connection. It is one among the ingredients in sand and is naturally present in quartz. It is typically colorless or white and is not soluble in ethanol or water. It creates the silicate family when it joins forces with minerals. There are many industrial uses for silicon dioxide (SiO2),

including as a food additive. It serves as an excipient of vitamins and pharmaceuticals as well as an anti-binder, anti-foaming agent, viscosity controller, desiccant, and beverage clarifier (Nanografi website).

Silicon dioxide has a crystalline structure, high acid resistancy and does not react with water. Some of the main properties of SiO_2 are as such; SiO_2 nanoparticles are transparent and have a density of 2634 kg/m^3. The molar mass of SiO_2 is 60.0843 g/mol; melting point is 1712 ˚C, whereas the boiling point is 2229 ˚C. Table 1.4 gives physical properties of SiO_2 (Goda et al, 1987).

Table 1.4 : Physical properties of SiO_2 (Goda et al, 1987).

Purity (%)	97.3+				
Color	white				
Average Particle Size (nm)	16				
Specific Surface Area (m^2/g)	150-550				
Loss of Weight in Drying (wt%)	5,4				
Loss of Weight on Ignition (wt%)	9,4				
pH	6.0				
Bulk Density (g/cm3)	<0.05				
True Density (g/cm3)	2,2				
Elemental Analysis (%)	SiO_2 : Silane	Mg	Ca	S	Fe
	97.3 : 2.0	0.005	0.022	0.0126	0.0056

1.3.2.4 Fluorocarbon dispersions

Fluorocarbons are known to provide Durable Water and Oil Repellency (DWOR) and are therefore used in water and stain repellent fabrics for clothing. For fluorocarbon products it is typical behaviour that they repel both oil and water. In the past, products based on C8 fluorocarbons (eight carbon atoms in the structure) were mainly used. However, there have been health, safety and environmental concerns associated with these C8 fluorocarbons, particularly with regard to PFOA (perfluorooctanoic acid or pentadecafluorooctanoic acid) and PFOS (perfluorooctane sulfonate or

heptadecafluoro-1-octane sulfonic acid). PFOA is classified as CMR and PBT meaning it has carconogenic, mutagenic and or toxic properties and it is persistent, bioaccumulative and toxic (De Smet et al, 2015).

PFOA has been classified as a substance of very high concern because it has CMR (carcinogenic, mutagenic, or toxic for reproduction) and PBT (persistent, bioaccumulative, and toxic) properties. Although there are many different fluorocarbons, many of them have similar potential health risks. Known effects of fluorocarbons include skin irritation with dryness, cracking, redness, and rash formation. Fluorocarbon gases present in the air at levels above a certain level can also cause irritation of the throat, nose and eyes. Short-term consequences of exposure to high levels of fluorocarbons can include nervous system effects with symptoms reminiscent of intoxication, while long-term exposure can result in more permanent damage. In general, highly fluorinated organic compounds are hydrophobic and have water-repellant and stain-repellant properties. The original formulations of products such as Scotchgard contained fluorocarbons including perfluorobutane sulfonate and perfluorooctane sulfonate (PFOS). According to OECD report many of these uses have been phased out due to environmental concerns, such as those associated with PFOA, an intermediate in the manufacture of PFOS. Gore-Tex and Teflon are also made from fluoropolymers (OECD website).

The tendency is to replace the C8 fluorocarbon chemistry by C6 or C4 fluorocarbon products or even fluorine-free water repellents. Currently, new commercial amphiphobic finishes are coming onto the market based on short chain fluorocarbons (C6 or C4 fluorocarbon chemistry), hybrid systems, or they are fluorine free (De Smet et al, 2015).

2. MATERIALS AND METHODS

In the following chapter materials and methods used for superamphiphobic flexible sensor design are discussed in detail. Figure 2.1 gives the graphical abstract of the proposed thesis study.

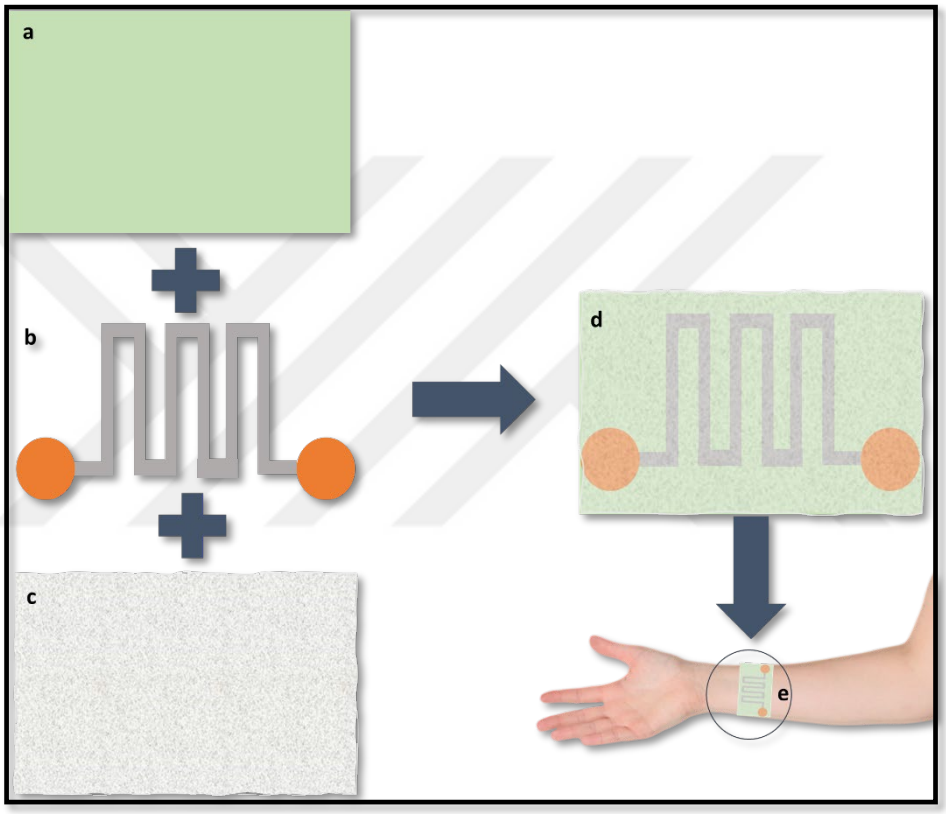

Figure 2.1 : Graphical abstract a)flexible substrate b)printed electrode c)superamphiphobic coating d)flexible sensor e)flexible sensor on application.

2.1 Materials Used for Designing and Fabrication of Flexible Electrodes

2.1.1 Substrates

For the purposes of this study, polyurethane medical wound dressing and cotton fabric were used as substrates.

Thermoplastic Polyurethane Film: Suprasorb® F trademark Polyurethane Film was obtained from Lohmann-Rauscher International GmbH & Co, in three different sizes. 5*7 cm, 10*12 cm, and 10 cm*1 m.

Cotton Fabric: Cotton fabric was supplied from local fabric retailers with a 20 weft/30 warp yarns 1x1 fabric density. The cotton fabric was mercerized and highly hydrophilic. The fabric was cut into 5cm x 5 cm squares.

2.1.2 Inks

In this study, PEDOT:PSS polymer and carbon-based materials (Graphite, Graphene, and Cathode Waste Material) are used to prepare conductive inks. PEDOT:PSS is applied on its own as conductive polymer. PEDOT:PSS is also used as binder for carbon based inks. PEDOT: PSS was purchased as high conductive grade (Clevious PH 1000) with <0.0012 Ω cm bulk resistance from Heraeus company. Graphite was purchased from Chem Pure and had a composition of 16-60 µm sized particles. Graphene was purchased from Graphene Chemical Industries Co. Graphene nanoplatelets had 5-8 nm thickness and 5 µm diameter. Surface area of the platelets were 120-150 m^2/g. Spent zinc carbon batteries were collected from battery recycling units at BTU. In order to provide uniformity Panasonic trademark Zn-C batteries were selected. Oxgall wetting agent was purchased from Oxgall was purchased from Ayan Ebru Ltd. Co. located in Istanbul. A generic automatic coffee grinder was purchased from a local electronics store to grind CWM particles.

Several different concentrations and compositions of conductive ink were prepared for the purposes of this study. Table 2.1 gives a summary of different compositions and concentrations of inks prepared.

Table 2.1 : Summary of ink preparations.

	PEDOT:PSS	GRAPHITE	GRAPHENE	CWM
INK 1	10 ml	-	-	-
INK 2	10 ml	1 gr	-	-
INK 3	10 ml	2 gr	-	-
INK 4	10 ml	-	1 gr	-
INK 5	10 ml	-	2 gr	-
INK 6	10 ml	-	-	1 gr
INK 7	10 ml	-	-	2 gr

2.1.2.1 PEDOT:PSS ink

As mentioned in previous chapters, PEDOT:PSS can be doped with organic solvents to increase its conductivity. In this study, PEDOT:PSS was doped with 5% DMSO. DMSO (≥99.9 wt%) was supplied from Sigma Aldrich. 100 ml PEDOT:PSS was placed on the stirrer and stirred at 500 rpm while 5 ml DMSO was added to the solution. In order to obtain a homogeneous solution, PEDOT:PSS and DMSO were stirred for 1 hour and no heat was applied during stirring (Bedeloglu et al, 2016).

2.1.2.2 Graphite ink

Graphite was prepared at two different concentrations. 1 gr and 2 gr of Graphite was mixed with 10 ml of doped PEDOT:PSS. The dispersion was mixed in the stirrer at 500 rpm for 1 hour. Following the stirring the dispersion was placed in the sonicator for 30 minutes.

2.1.2.3 Graphene ink

Similar to graphite, graphene was also prepared at two different concentrations. 1 gr and 2 gr of Graphene was mixed with 10 ml of doped PEDOT:PSS to form a dispersion. The mixture was stirred at 500 rpm for 1 hour prior to sonication for 30 minutes.

2.1.2.4 Cathode waste material (CWM) ink

Panasonic trademark Zn-C batteries collected from BTU spent battery recycling stations were dismantled and the carbon-based cathode was separated from the assembly. The MnO_2 paste was also collected. Cathode was grinded using the generic automatic coffee grinder. The particles were transferred to a mortar and oxgall was added via a dropper. Oxgall is a wetting agent used for preparing organic dyes used in traditional Turkish Marbling art. 5 drops of oxgall was added to the CWM particles. Distilled water was also added to the mixture to form a paste. The mixture is grinded with a pestle and later transferred to a vial. Distilled water is added to the paste and centrifuged at 500 rpm for 30 minutes. The excess water is drained to wash away impurities. 1 and 2 gr of the resulting CWM particles are added to 10 ml of doped PEDOT:PSS and stirred at 500 rpm for 1 hour and sonicated for 30 minutes to form ink dispersions. Figure 2.2 shows the ink preparation steps for CWM.

Figure 2.2 : Ink preparation steps for CWM a) Spent zinc carbon battery b)coffee grinder to turn into powder form c)oxgall d)mortar and pestle to grind the cathode powder e)sonication process.

2.1.3 Electrode fabrication

INSMA Laser Cutting/Engraving device was purchased from Banggood.com website. The device was used to cut stencils from different materials. Electrode design was prepared using powerpoint and paint software. The electrode images were transferred to INSMA Laser Engraving Software. Acetate, particleboard, PVC, lamination film, masking tape and labels were tried as stencil material. A film applicator was purchased from alibaba.com website to use in Doctor Blade coating. Thickness options for this particular applicator were 50 µm, 100 µm, 150 µm and 200 µm. A motorized propulsion device designed at BTU Polymer Materials Engineering Lab for a previous study was used to push the film applicator at a constant speed for Doctor Blade application. Some of the materials for electrode fabrication are in Figure 2.3.

In order to form conductive paths on the substrate, an electrode design was burned onto transfer paper and masking tape via Insma laser device to use as stencil. The stencil is then transferred to the substrate surface. The ink is applied by the film applicator using a motorized propulsion device to ensure an evenly applied coat of film. When more than one layer of ink coating is applied the material is dried at room temperature for 2 hours. The process is shown in Figure 2.4.

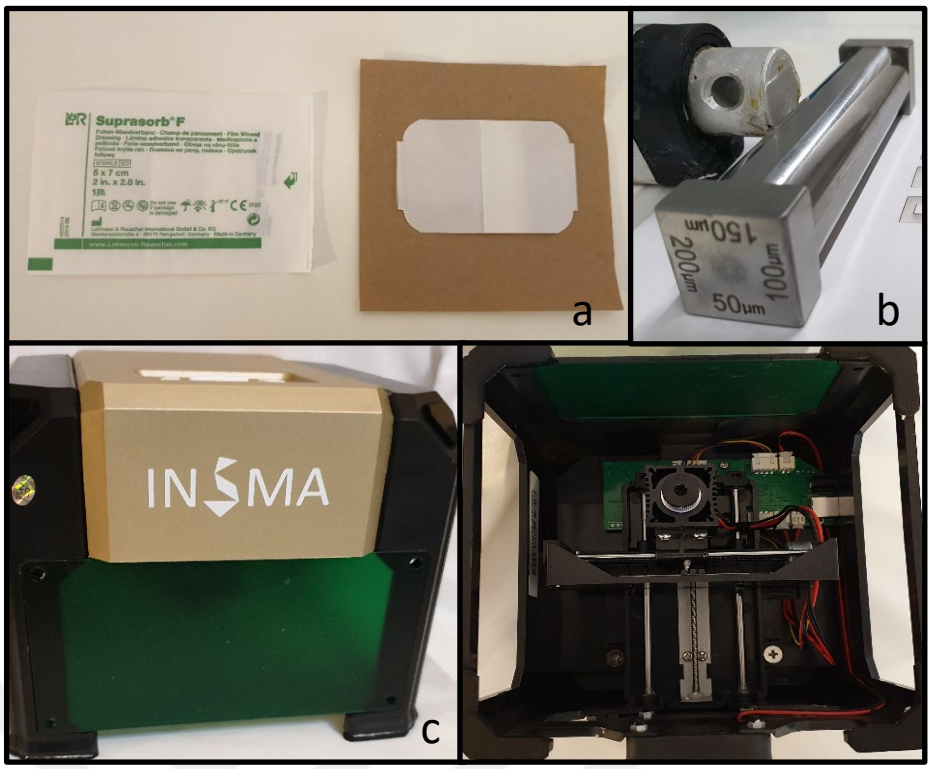

Figure 2.3 : Materials for electrode fabrication a) Polyurethane film b) film applicator c) INSMA laser device.

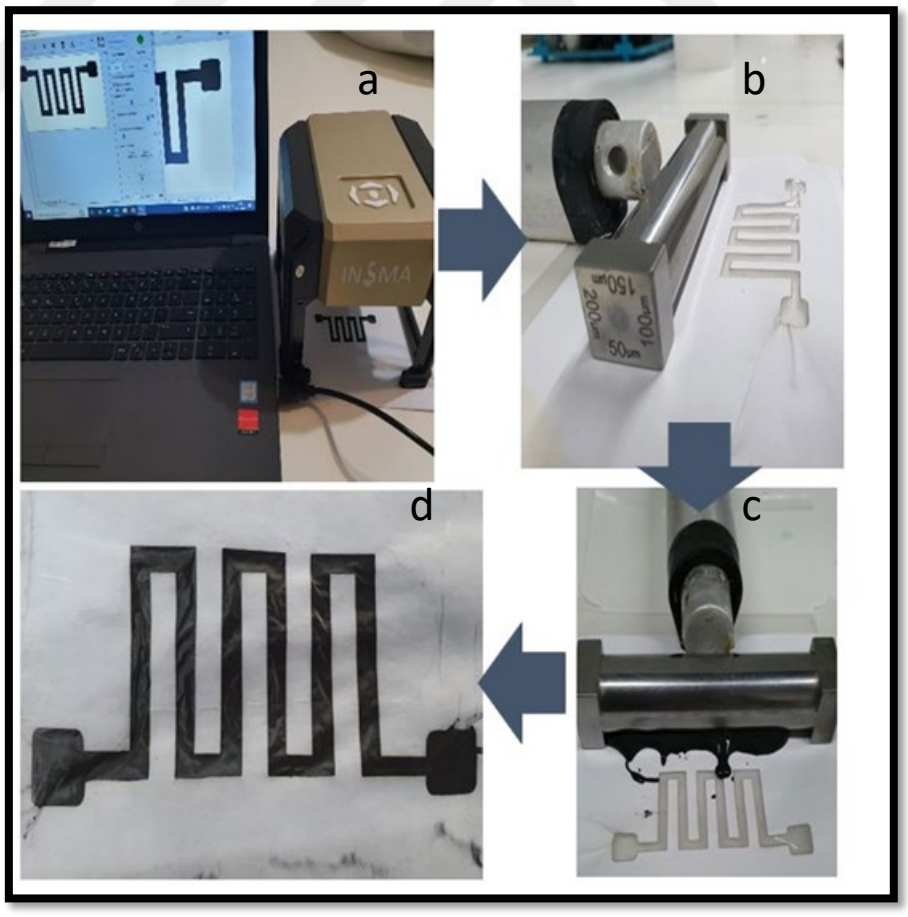

Figure 2.4 : Electrode printing steps a) stencil/mask preparation b) film applicator and propulsion device c) ink applied via doctor blade method d) printed electrode pattern.

7 different ink dispersions were applied on 2 different substrates. Each ink was applied at 3 different layers; 1 layer coating, 2 layers coating and 3 layers coatings. Table 2.2 gives a summary of different ink applications on different substrates.

Table 2.2 : Different applications of ink dispersions on cotton and TPU substrates.

	COTTON		TPU	
PEDOT:PSS	1 layer coating (c)		1 layer coating (c)	
	2 layers coating (c)		2 layers coating (c)	
	3 layers coating (c)		3 layers coating (c)	
GRAPHITE/ PEDOT:PSS	1 gr Grx1 c	2 gr Grx 1c	1 gr Grx1 c	2 gr Grx 1c
	1 gr Grx2 c	2 gr Grx 2c	1 gr Grx2 c	2 gr Grx 2c
	1 gr Grx3 c	2 gr Grx 3c	1 gr Grx3 c	2 gr Grx 3c
GRAPHENE / PEDOT:PSS	1 gr Gx1 c	2 gr Gx 1c	1 gr Gx1 c	2 gr Gx 1c
	1 gr Gx2 c	2 gr Gx 2c	1 gr Gx2 c	2 gr Gx 2c
	1 gr Gx3 c	2 gr Gx 3c	1 gr Gx3 c	2 gr Gx 3c
CWM	1 gr CWMx1	2 gr CWMx1	1 gr CWMx1	2 gr CWMx1
	1 gr CWMx2	2 gr CWMx2	1 gr CWMx2	2 gr CWMx2
	1 gr CWMx3	2 gr CWMx3	1 gr CWMx3	2 gr CWMx3

2.1.4 Characterization of electrodes

Characterization of printed electrodes was carried out at BTU Polymer Materials Engineering Laboratory using the test devices available. The viscosity values of the prepared inks were measured using Digital Rotational Viscosimeter PCE RVI-2. 3 readings were taken from each ink solution. PCE RVI-2 can be operated with an adjustable speed in the range between 6-60 RPM. Viscosity of conductive inks were measured at 12 rpm speed except for PEDOT:PSS which was measured at 60 rpm and

Graphene (2 gr) at 30 rpm. Density of CWM, Graphite and Graphene powders were measured at Metalurgy and Materials Engineering laboratory using a gas pcynometer, Micromeritics - ACCUPYC II 1340. Carbon-based powders were pressed into disc shapes by using a manual press and the resistance of discs were measured. Resistance of electrodes were measured with Keithley 2400 Source Meter. FT-IR measurements were taken for electrode materials using FT-IR NICOLET - IS50. The resistance under strain was measured with tensile testing device Shimadzu - AGS-X and Keithley 2400. 1 kN force was applied to the samples at the speed of 6mm/min for 5 circles. Two probes were attached to the flexible electrode at 1 cm distance. The probes were connected to Keithley 2400. Ketihley 2400 was also connected to a laptop. The electrical resistance results from the probes were analyzed by Sweep Me application.

2.2 Applying Superamphiphobic Coating on Electrode Surfaces

2.2.1 Materials for superamphiphobic coating

Zinc stearate powder and silicon dioxide (SiO_2) nanoparticles with silane coating were purchased from Kimya Deposu. ZnSt has particle size of 4-6 μm and purity is 90%. SiO_2 has 97% purity, 16 nm particle size and is 2% Silane coated. Tubiguard ™ Coating, a commercial fluorocarbon dispersion by CHT was obtained from CHT branch in Bursa. Tubiguard is a non ionic, self crosslinking, sprayable C6 fluorocarbon based coating used in textile coatings with high effectivenes. Pressurized spray coating device was located at BTU Polymer Materials Engineering Department laboratory.

2.2.2 Methods for superamphiphobic coating

3 different coatings were prepared : Tubiguard, Tubiguard and ZnSt dispersion; Tubiguard and SiO_2 dispersion. 0.5 gr on ZnSt was added to 25 ml of Tubiguard solution. 0.25 gr of SiO_2 was added to 25 ml of Tubiguard fluorocarbon dispersion.

Both dispersions were mixed at stirrer without applying heat. When the dispersions become homogeneous after 1 hour of mixing at 500 rpm they are applied onto the fabric and film surfaces. In order to determine the effect of coating on the degree of contact angle the substrates were coated in their pure form, without printing the electrode.

2.2.3 Characterization of superamphiphobic coating

Contact angle was measured at BTU Chemical Engineering Laboratory with Attension Theta Lite by Biolin Scientific contact angle measuring device and BTU Central Laboratory (MERLAB) using Biolin Scientific Attension Theta Flex using the Young-Laplace method that analyzes the droplet shape to determine the contact angle. All samples were measured at 5µl droplet volume. Samples measured for contact angle are given in Table 2.3.

Table 2.3 : Test samples prepared for contact angle measurement.

Cotton Substrate	TPU Substrate
Tubiguard and ZnSt (for H_2O)	Tubiguard and ZnSt (for H_2O)
Tubiguard and ZnSt (for Oil)	Tubiguard and ZnSt (for Oil)
Tubiguard and SiO_2 (for H_2O)	Tubiguard and SiO_2 (for H_2O)
Tubiguard and SiO_2 (for Oil)	Tubiguard and SiO_2 (for Oil)
Tubiguard (for H_2O)	Tubiguard (for H_2O)
Tubiguard (for Oil)	Tubiguard (for Oil)
Control Sample (for H_2O)	Control sample (for H_2O)
Control Sample (for Oil)	Control Sample (for Oil)

3. RESULTS AND DISCUSSION

3.1 Viscosity Measurements

Average viscosity values and standard deviation values are given in Table 3.1.

Table 3.1 : Average viscosity and standard deviation of conductive inks

Ink	Average Viscosity (cp)	Standard Deviation (σ)
PEDOT:PSS	10 cp (60 rpm)	0.75
Graphite (1 gr)/PEDOT:PSS	61 cp (12 rpm)	0.83
Graphite (2 gr)/PEDOT:PSS	406 cp (30 rpm)	8.12
CWM (1gr)/ PEDOT:PSS	1455 cp (12 rpm)	55
CWM (2gr)/ PEDOT:PSS	1804 cp (12 rpm)	180.9
Graphene (1 gr)/PEDOT:PSS	5130 cp (12 rpm)	136.36
Graphene (2 gr)/PEDOT:PSS	7712 cp (12 rpm)	205

Viscosity of the inks increases as the weight-volume fraction of the carbon based particles in the dispersion increases. As particle size decreases, the surface to volume ratio increases thus increasing the degree of interactions between the particles (Koca et al, 2018). Graphene has smaller particle size than Graphite and CWM therefore the viscosity of graphene/PEDOT:PSS dispersion is higher than Graphite and CWM. Graphene dispersion has the highest viscosity among all dispersions.

Viscosity of the ink dispersions play a critical role in their behaviour as conductive electrodes. Therefore the viscosity of the inks should be taken into consideration. For optimum performance an ink paste is expected to have high viscosity at resting state, a low viscosity at high shear rate, and a fast viscosity recovery time (Chodhurry et al, 2019).

3.2 Weight Analysis

Samples were weighed with a precision scale before and after printing the ink, to determine the amount of ink on the substrate surface. Table 3.2 gives the weight analysis results.

Table 3.2 : Weight (g) of inks printed on substrates

	Sample weight (g)					
	TPU			Cotton		
	1x	2x	3x	1x	2x	3x
CWM 1	0.0068	0.0082	0.0098	0.0076	0.013	0.0182
CWM 2	0.0152	0.0186	0.0231	0.0455	0.0473	0.0852
Graphite 1	0.0025	0.0056	0.0092	0.0045	0.0105	0.0211
Graphite 2	0.0065	0.0107	0.0168	0.0161	0.0231	0.0301
Graphene 1	0.0115	0.0161	0.0226	0.0077	0.0253	0.0291
Graphene 2	0.0123	0.0181	0.0245	0.0594	0.0812	0.0971
PEDOT:PSS	0.0021	0.0037	0.0065	0.0035	0.0071	0.0133

The results indicate that graphene ink dispersion with the smallest particle size has the highest weight among the printed inks.

3.3 Density and Disc Resistance Analysis

CWM, graphite and graphene powders were analyzed based on their density and disc resistance values. Table 3.3 gives density values and resistance values for each material.

Table 3.3 : Density (g/cm^3) and Resistance (Ω) of CWM, graphite and graphene

	Density		Resistance	
	g/cm^3	Std. Dev.	Ω	Std. Dev.
CWM	2.4754	0.0050	8.13	1.73
Graphite	2.3736	0.0061	7.95	1.57
Graphene	2.0722	0.0172	3.01	0.41

The results show that graphene powder with the lowest particle size has the lowest density. Graphite and CWM have similar density values. Resistance of graphene powder in pressed disc form is the lowest at 3.01 Ω and resistance of CWM and graphite are 8.13 Ω and 7.95 Ω respectively.

3.4 FT-IR Analysis

Conductive inks applied on cotton and TPU substrates were analyzed with Fourier transform infrared spectroscopy (FT-IR) with a full scale spectrum between 400 cm^{-1} and 4000 cm^{-1} wavenumbers. FT-IR Analysis of cotton-based samples are given in Figure 3.1, and TPU based samples are given in Figure 3.2.

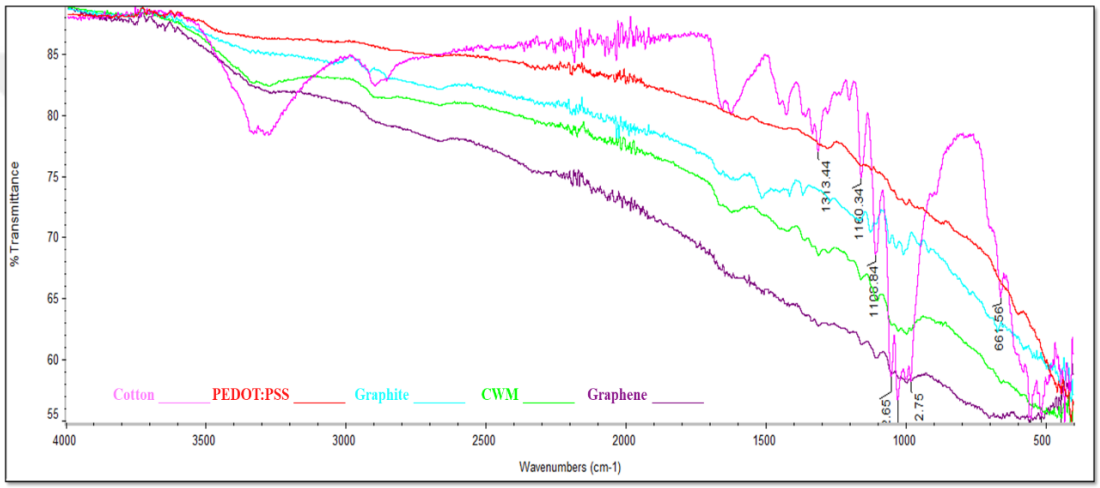

Figure 3.1 : All spectra FT-IR images of cotton substrate.

According to literature the strong peak observed at 3330 cm^{-1} for cotton is characteristic of the hydroxyl (OH) groups of cellulose, lignin, and water. The peak at 2896 cm^{-1} is characteristic of the stretching vibration of C-H present in cellulose and hemicellulose, and the band at 1622 cm^{-1} may be related to the presence of water in the fibers. The absorption band at 1428 cm^{-1} is associated with the CH_2 symmetric bending of the cellulose. The absorption bands at 1360 and 1315 cm^{-1} are relative to bending vibrations of the C-H and C-O groups, respectively, of the aromatic rings in cellulose polysaccharides. Intense peak vibrations observed at 1032 cm^{-1} are related to the (CO) and (OH) stretching vibrations of the polysaccharide in cellulose (Portella et al., 2016). According to literature in the FTIR spectrum of graphite or graphene there are no significant peaks relevant to any functional groups, but weak bands may appear, which can be assigned to adsorbed water molecules (Son et al, 2001; Vaghri et al, 2012).

In case of TPU the signal at 2959 cm^{-1} represents stretching vibration of C-H bond. Typically, carbonyl group can be confirmed at the wavelengths of 1727 cm^{-1} and 1698 cm^{-1} followed by C = N stretching peak at 1529 cm^{-1}. C–C stretching of the aromatic ring is assigned by the wavelengths at 1413 cm^{-1}, 1168 cm^{-1} and 1074 cm^{-1} for C–O–C stretching (Rehman, et al. 2022).

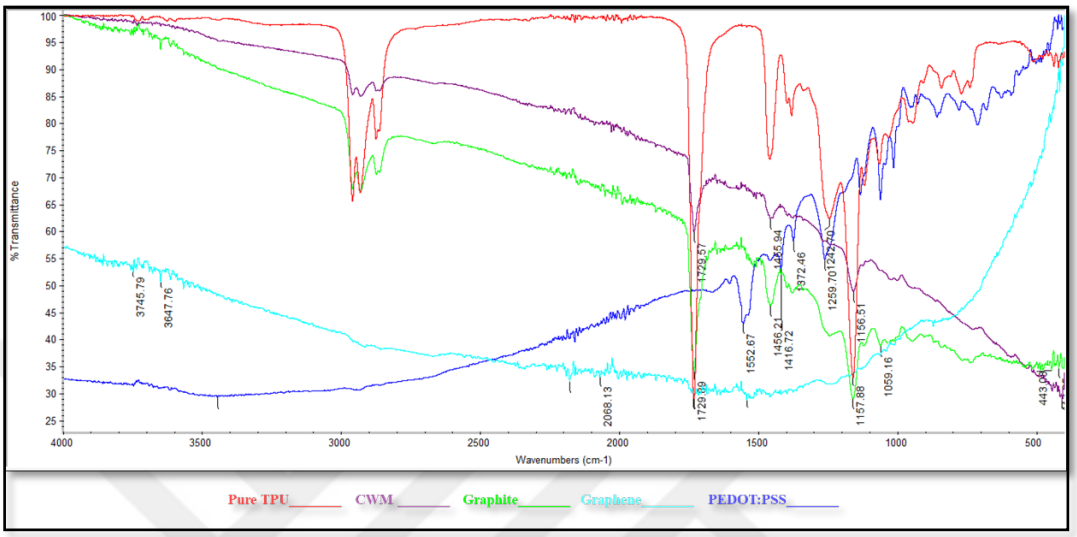

Figure 3.2 : All spectra FT-IR analysis of TPU.

As can be seen from the Figure 3.3, peak values for graphite and CWM are very similar. This is due to the fact that the main component of CWM is the graphite rod extracted from the spent batteries. Both materials show similar characteristics. CWM and graphite share a similar curve and similar peaks. The differences in the curve may be due to the irregularities found in recycled CWM composition.

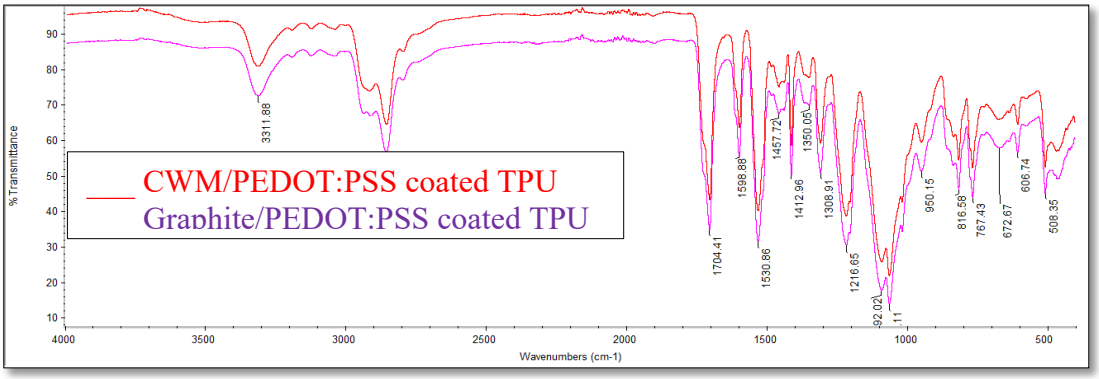

Figure 3.3 : FT-IR analysis of graphite and CWM coated TPU .

3.5 Electrical Measurements

Resistivity measurements of 7 types of ink applied on 2 different substrates for 3 total layers of coating are given at Table 3.4- 3.10. The column charts in Figures 3.4-3.7 give a comparative analysis of two different concentrations of inks on two different substrates.

Table 3.4 : Resistivity of PEDOT:PSS on cotton and TPU substrates.

Number of Coatings	Cotton	Standard Deviation	TPU	Standard Deviation
1 Layer	587.2 $k\Omega cm^{-1}$	61.3	127.46 $k\Omega cm^{-1}$	22.66
2 Layers	140.5 $k\Omega cm^{-1}$	16.5	84.70 $k\Omega cm^{-1}$	8.49
3 Layers	50.47 $k\Omega cm^{-1}$	3.08	30.12 $k\Omega cm^{-1}$	7.63

Table 3.5 : Resistivity of CWM (1gr)/ PEDOT:PSS on cotton and TPU substrates.

Number of Coatings	Cotton	Standard Deviation	TPU	Standard Deviation
1 Layer	40.2 $k\Omega cm^{-1}$	6.49	47.28 $k\Omega cm^{-1}$	5.53
2 Layers	38.02 $k\Omega cm^{-1}$	3.2	35.64 $k\Omega cm^{-1}$	5,39
3 Layers	9.94 $k\Omega cm^{-1}$	3.3	7.94 $k\Omega cm^{-1}$	3.5

Table 3.6 : Resistivity of CWM (2gr)/ PEDOT:PSS on cotton and TPU substrates.

Number of Coatings	Cotton	Standard Deviation	TPU	Standard Deviation
1 Layer	12.28 $k\Omega cm^{-1}$	2.32	66.94 $k\Omega cm^{-1}$	5.46
2 Layers	15.95 $k\Omega cm^{-1}$	2.87	28.54 $k\Omega cm^{-1}$	2.98
3 Layers	6.91 $k\Omega cm^{-1}$	0.68	6.97 $k\Omega cm^{-1}$	1.28

Table 3.7 : Resistivity of Graphite (1 gr)/PEDOT:PSS on cotton and TPU substrates.

Number of Coatings	Cotton	Standard Deviation	TPU	Standard Deviation
1 Layer	15.26 $k\Omega cm^{-1}$	1.88	6.31 $k\Omega cm^{-1}$	1.09
2 Layers	1.8 $k\Omega cm^{-1}$	0.3	5.72 $k\Omega cm^{-1}$	2.06
3 Layers	1.33 $k\Omega cm^{-1}$	0.32	3.16 $k\Omega cm^{-1}$	0.95

Table 3.8 : Resistivity of Graphite (2 gr)/PEDOT:PSS on cotton and TPU substrates.

Number of Coatings	Cotton	Standard Deviation	TPU	Standard Deviation
1 Layer	2.23 $k\Omega cm^{-1}$	0.75	6.64 $k\Omega cm^{-1}$	1.06
2 Layers	0.8 $k\Omega cm^{-1}$	0.1	4.60 $k\Omega cm^{-1}$	1.09
3 Layers	0.54 $k\Omega cm^{-1}$	0.08	2.25 $k\Omega cm^{-1}$	0.57

Table 3.9 : Resistivity of Graphene (1 gr)/PEDOT:PSS on cotton and TPU substrates.

Number of Coatings	Cotton	Standard Deviation	TPU	Standard Deviation
1 Layer	0.46 $k\Omega cm^{-1}$	0.2	0.76 $k\Omega cm^{-1}$	0.18
2 Layers	0.21 $k\Omega cm^{-1}$	0.03	0.33 $k\Omega cm^{-1}$	0.05
3 Layers	0.14 $k\Omega cm^{-1}$	0.03	0.13 $k\Omega cm^{-1}$	0.03

Table 3.10 : Resistivity of Graphene (2 gr)/PEDOT:PSS on cotton and TPU substrates.

Number of Coatings	Cotton	Standard Deviation	TPU	Standard Deviation
1 Layer	0.096 $k\Omega cm^{-1}$	0.006	1.28 $k\Omega cm^{-1}$	0.3
2 Layers	0.048 $k\Omega cm^{-1}$	0.002	0.056 $k\Omega cm^{-1}$	0.01
3 Layers	0.037 $k\Omega cm^{-1}$	0.002	0.018 $k\Omega cm^{-1}$	0.02

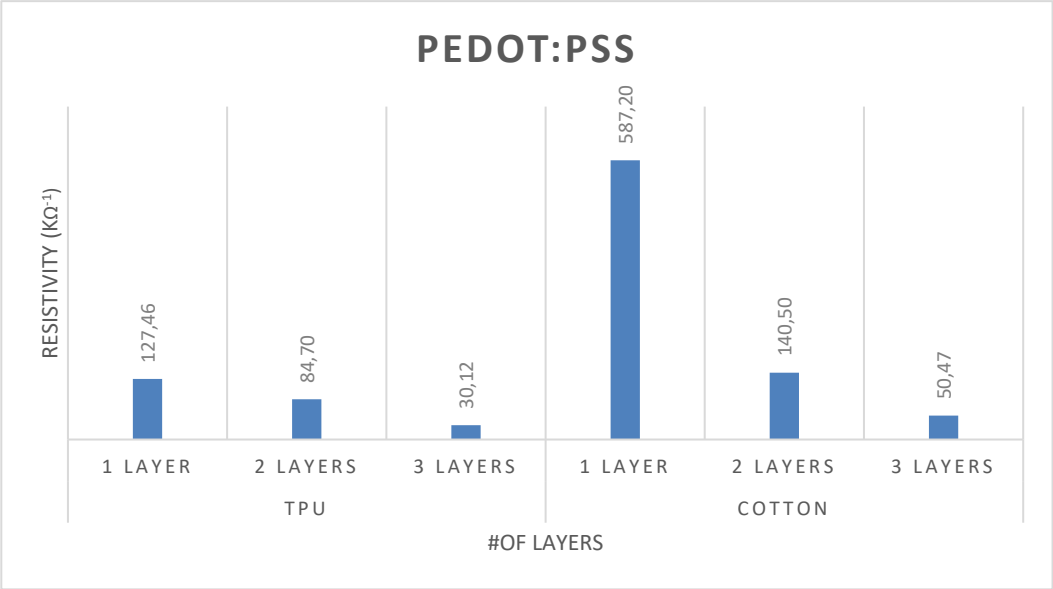

Figure 3.4 : Comparative chart for resistivity vs number of layers for PEDOT:PSS solution coated on TPU and cotton substrates.

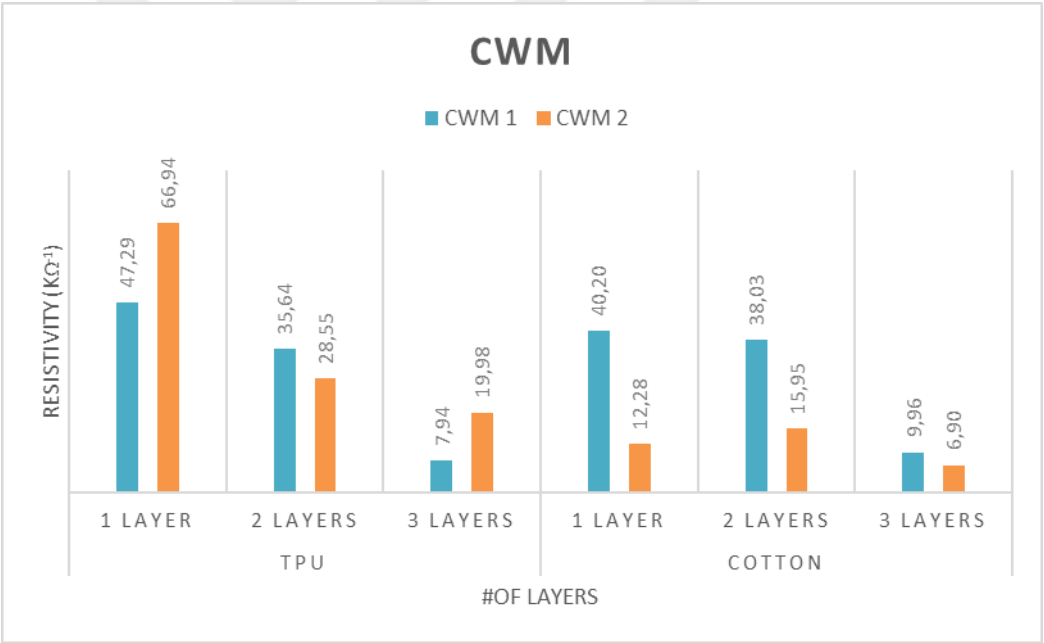

Figure 3.5 : Comparative chart for resistivity vs number of layers for 1 gr and 2 gr of CWM in 10 ml PEDOT:PSS solution coated on TPU and cotton substrates.

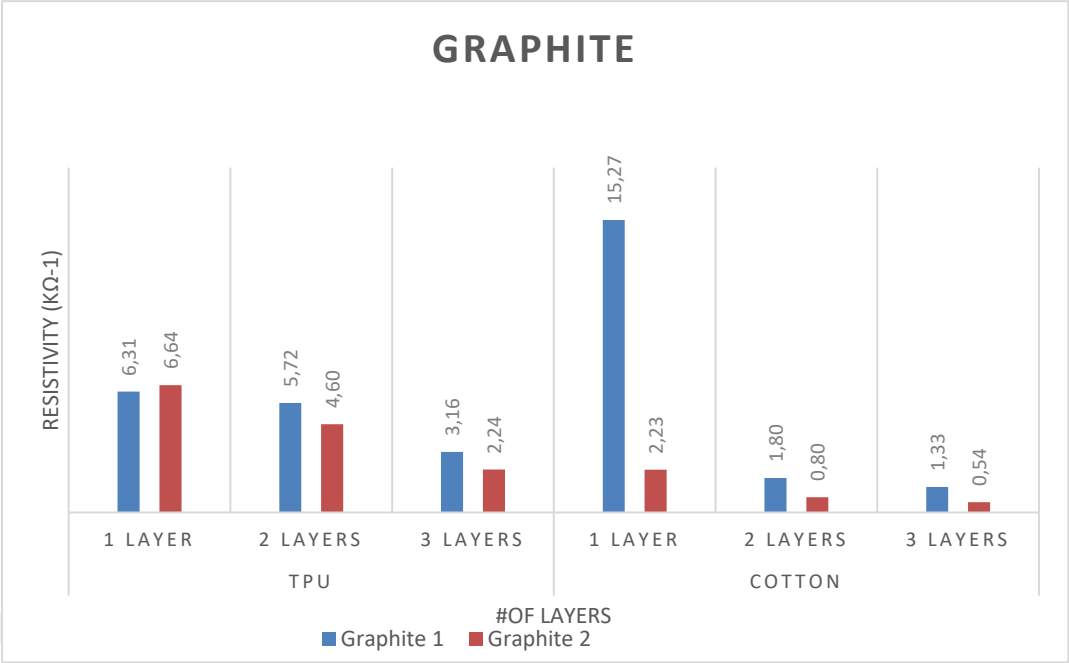

Figure 3.6 : Comparative chart for Resistivity vs number of layers for 1 gr and 2 gr of Graphite in 10 ml PEDOT:PSS solution coated on TPU and cotton substrates.

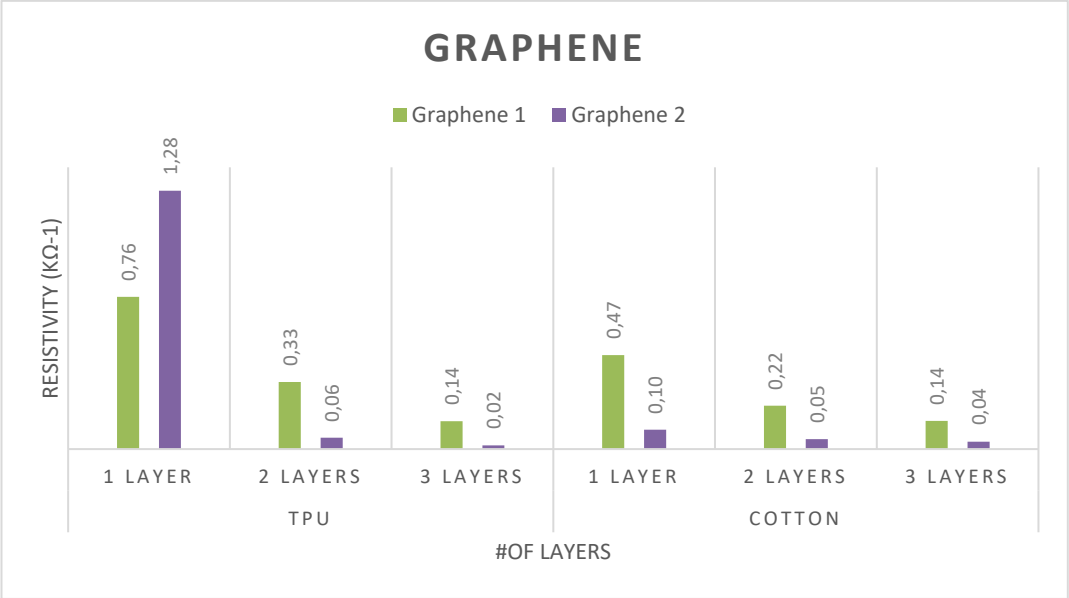

Figure 3.7 : Comparative chart for Resistivity vs number of layers for 1 gr and 2 gr of Graphene in 10 ml PEDOT:PSS solution coated on TPU and cotton substrates.

As can be seen from the results of the resistivity measurements, resistivity decreases as number of layers increases. This can be due to the fact that the surface coverage of the conductive path increases with the number of layers applied. Graphene and graphite do not have any functional groups which will form strong bonds with cotton therefore the adhesion is very weak. However, cotton fabric is highly hydrophilic and fibers act as capillaries to absorb conductive ink onto the cotton fabric surface or into the strands of the fibers by capillary effect, forming hydrogen bonds with the fabric

(Ren et al, 2017). The second and third layers applied on the cotton substrate build up the conductive path that adheres to the surface and decreases the resistivity value.

TPU substrate had its advantages as well as disadvantages. Hydrophobic property of the TPU surface posed some difficulties in the adhesion of conductive ink on the surface. As the number of layers increased the adhesion of conductive ink onto the TPU substrate improved. Smooth surface of TPU film compared to the woven and curvy structure of cotton fabric provided a better base to apply a straight conductive path.

The concentration of conductive particles in the ink dispersion also play a role in the resistivity of the electrode. As the concentration of conductive particles in the ink dispersion increases the resistivity value decreases. PEDOT:PSS, a conductive polymer acts as the carrier base for the ink dispersion. When 3 layers of pure PEDOT:PSS is applied on the substrates the resistivity is around 50 $k\Omega cm^{-1}$ for cotton substrate and 30 $k\Omega cm^{-1}$ for TPU substrate. With the addition of conductive carbon-based particles this value is improved. Graphene gives the best results among all inks prepared. Graphene particles used in this study have particle diameter of 5 µm, graphite particles have particle size of 16-60 µm, cathode waste materials have average particle size of 30 µm. The surface area of 2 grams of graphene is greater than the surface area of 2 grams of graphite and of 2 grams of CWM. Smaller particle size of graphene allows the conductive particles to disperse in a higher concentration throughout the solution and increase the conductivity.

During testing another parameter observed that was influential in resistance of materials was the direction doctor blade was applied. When the blade was applied towards the same direction at each layer application, the electrically conductive pathway was aligned in a more linear direction. If the blade was applied in opposite directions for each layer the alignment was less linear thus causing higher resistivity values. These samples were not included in the final samples used for testing and analysis.

3.4 Electromechanical Test Results

The samples were tested at mechanical tensile tester to characterize their behaviour under strain. Loop tests were performed to measure resistivity under strain and recovery. 5 loops for 5% strain were set up. Young's Modulus for cotton-based

samples was 49.51 N/mm^2 and for TPU based samples 2.40 N/mm^2. Young's Modulus was determined using the equation:

$$E = \frac{Stress}{Strain} = \frac{F/A}{\Delta L/L_0} \quad (3.1)$$

F is the force applied, A is the area of the sample, ΔL is the change in length and L_0 is the original length of the sample.

Resistance under tensile testing was measured with Keithley 2400 and analyzed with free source Sweep Me application. Figures 3.8-3.35 show the SMU Resistance vs. time and $\Delta R/R_0$ vs time graphs of conductive ink (1 gr and 2gr x 2 layers) coated on cotton and TPU substrates.

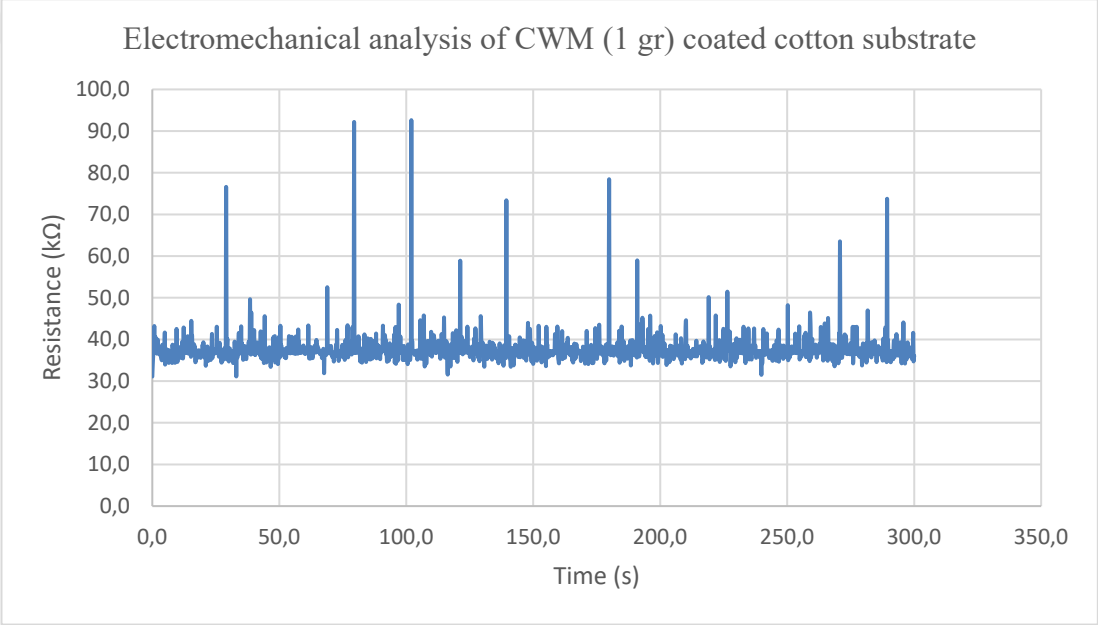

Figure 3.8 : Electromechanical analysis of CWM (1 gr) coated cotton substrate.

The lowest value is 31.12 kΩ and the highest value is 92.63 kΩ for Figure 3.8, where 1 gr concentration of CWM in 10 ml PEDOT:PSS is applied on cotton substrate. As force is applied to the sample the resistance value gradually increases and as the force is removed the resistance decreases. The graph shows a pattern that can be improved by making certain modifications to the ink such as reducing particle size to increase surface area in order form more covalent and van der waals bonds between the substrate and the ink dispersion.

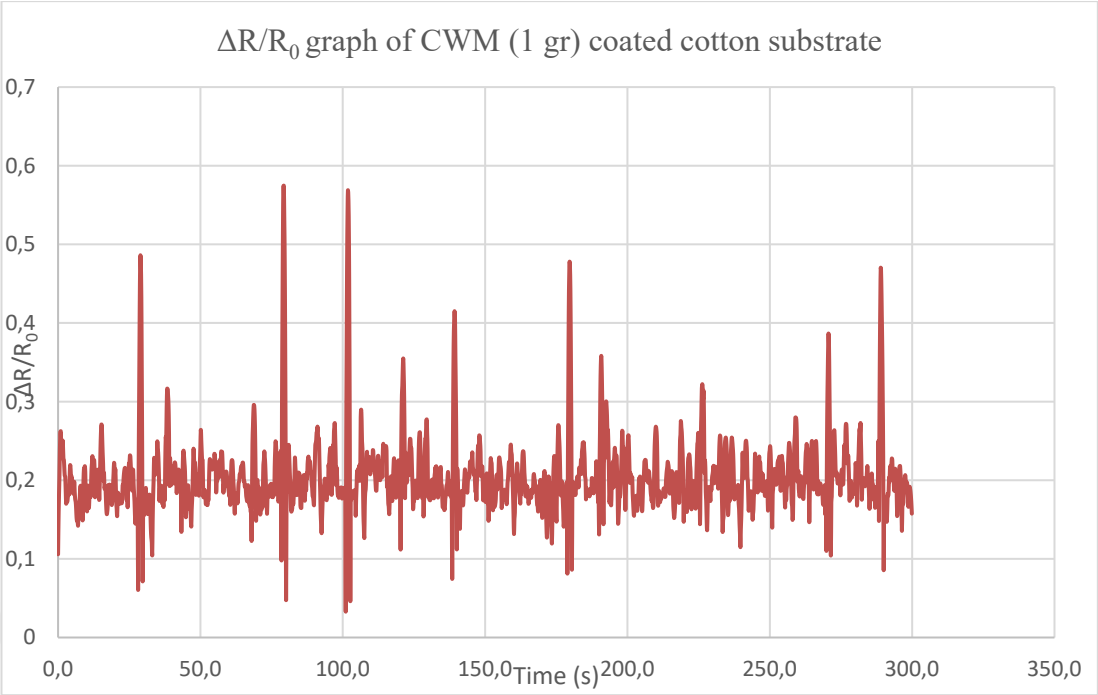

Figure 3.9 : ΔR/R0 vs Time graph of CWM (1 gr) coated cotton substrate.

Figure 3.9 gives ΔR/R0 over time values for CWM (1 gr) on cotton substrate. ΔR/R0 values range between 0.03 and 0.57.

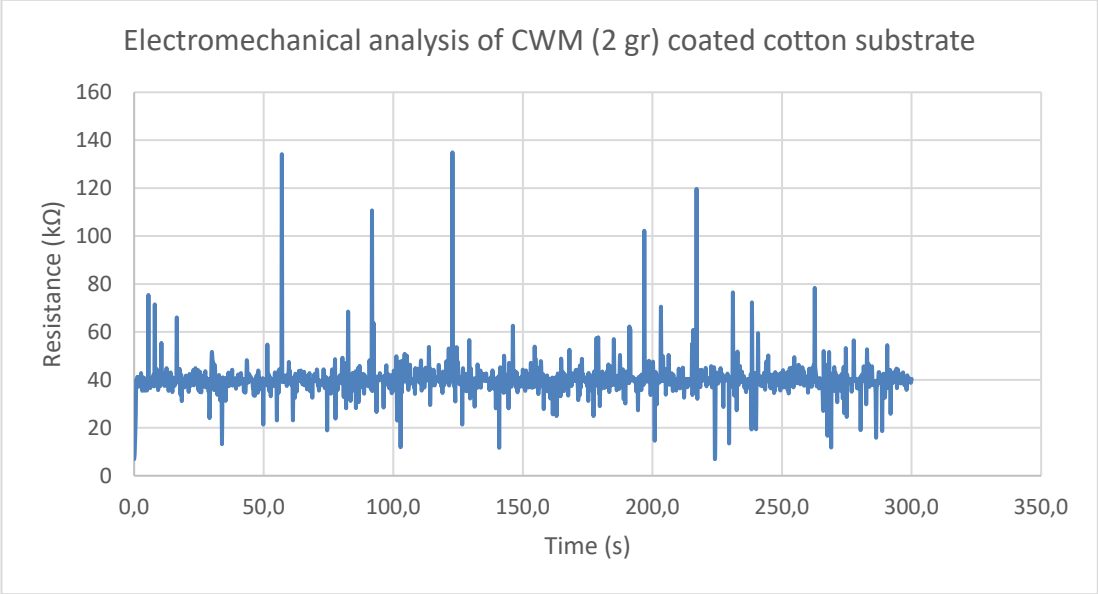

Figure 3.10 : Electromechanical analysis of CWM (2 gr) coated cotton substrate.

Figure 3.10 is similar to Figure 3.8. The concentration of CWM in PEDOT:PSS has increased to 2 gr and thus the lowest resistance value is 6.92 kΩ and the highest resistance value is 272.57 kΩ. The resistance at the end of testing is 38.15 kΩ.

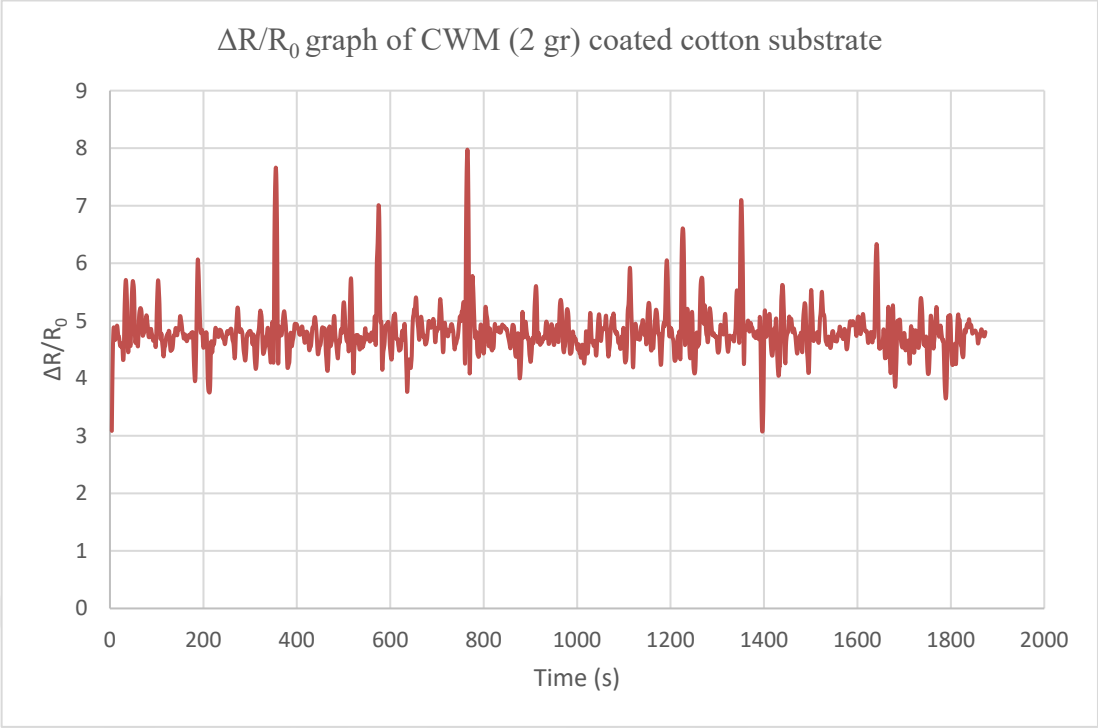

Figure 3.11 : $\Delta R/R_0$ vs Time graph of CWM (2 gr) coated cotton substrate.

Figure 3.11 gives $\Delta R/R_0$ over time values for CWM (2 gr) on cotton substrate. $\Delta R/R_0$ values range between 3.07 and 7.97. The sinus wave is slightly visible every 60 seconds for each of the five cycles.

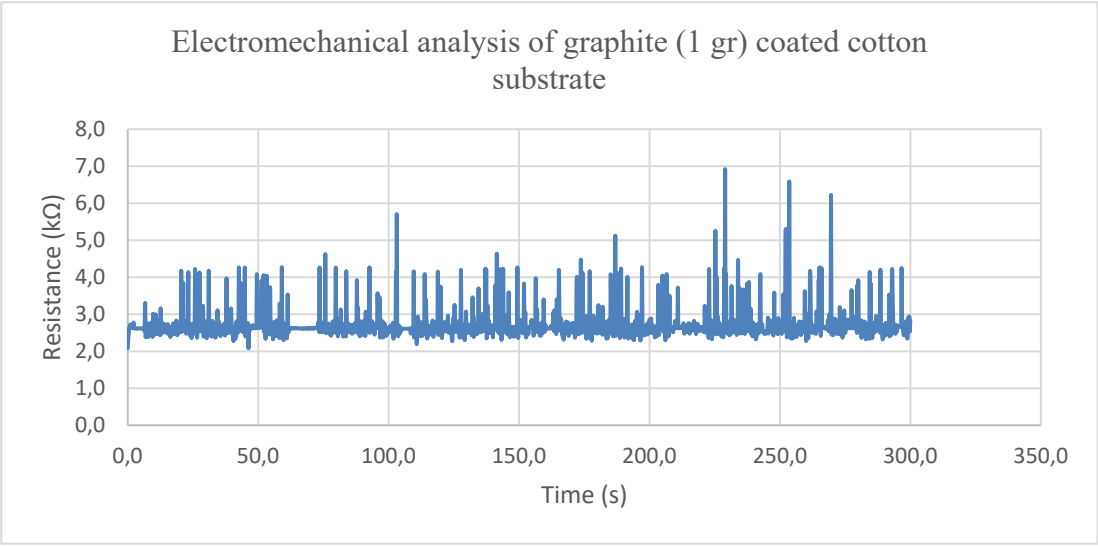

Figure 3.12 : Electromechanical analysis of graphite (1gr) coated cotton substrate.

For 1 gr of graphite in 10 ml PEDOT:PSS the lowest value shown in Figure 3.12 is 2.08 kΩ and the highest value is 6.92 kΩ. Although a slight wave pattern can be discerned from the graph, it is still not a clear pattern that can translate to clean and noise free data. The initial resistance value in this case (2.62 kΩ) is slightly higher than

the resistance at the end of the fifth cycle (2.42 kΩ). This may be due to the realigning of fibers in the cotton fabric.

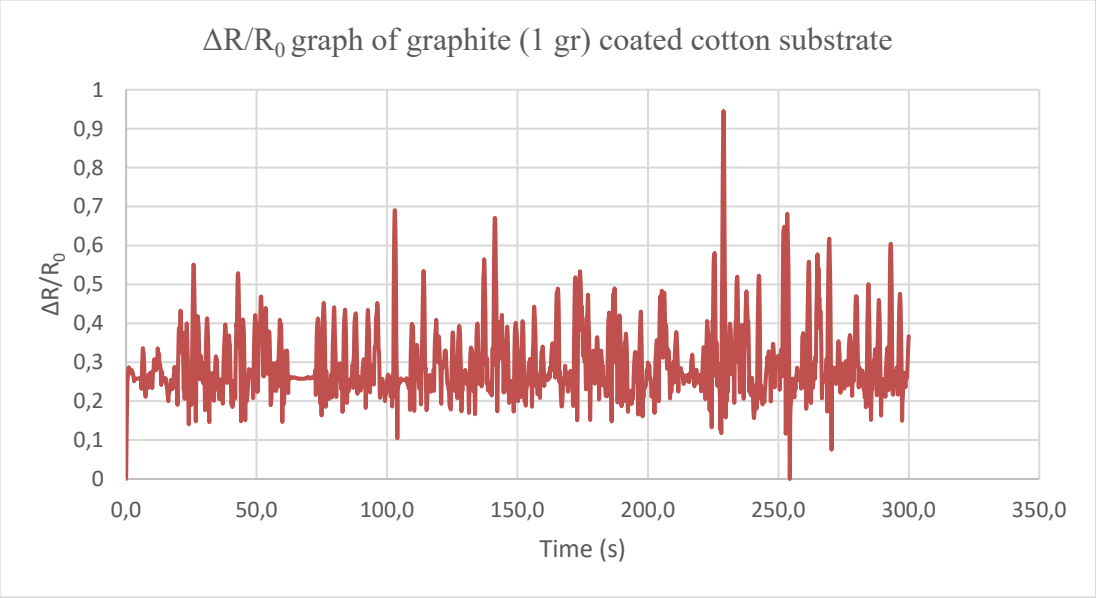

Figure 3.13 : ΔR/R0 vs Time graph of graphite (1 gr) coated cotton substrate.

Figure 3.13 gives ΔR/R0 over time values for graphite (1 gr) on cotton substrate. ΔR/R0 values range between 0.00 and 0.94. The sinus wave is slightly visible every 60 seconds for each of the five cycles.

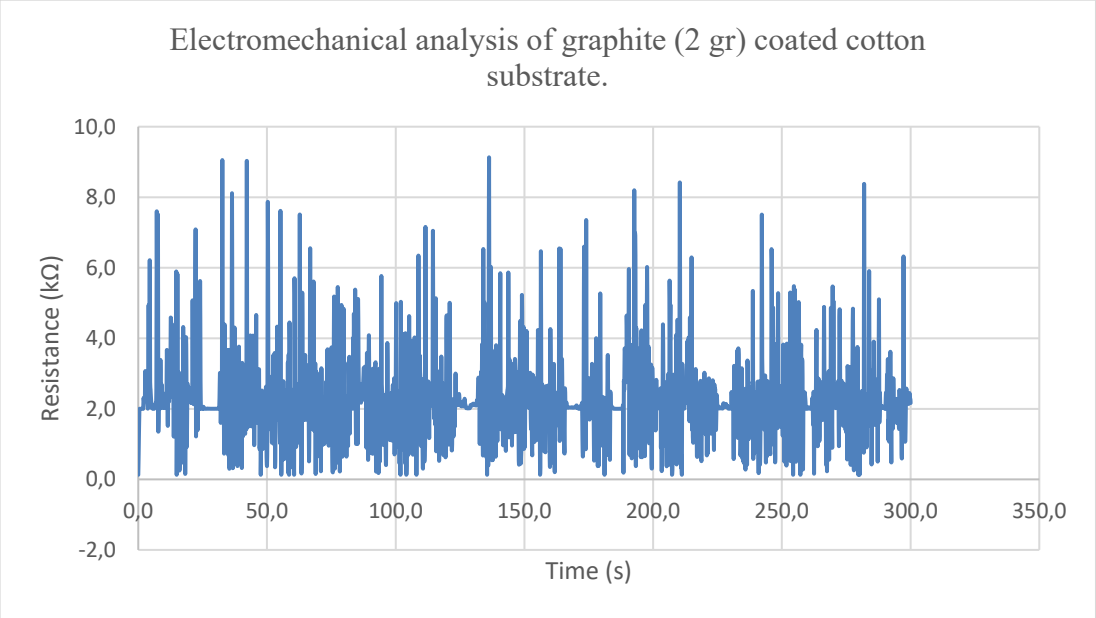

Figure 3.14 : Electromechanical analysis of graphite (2 gr) coated cotton substrate.

For 2 gr of graphite in 10 ml PEDOT:PSS the lowest value shown in Figure 3.14 is 0.2 kΩ and the highest value is 9.13 kΩ. The same concerns about a clear, noise-free signal are also relevant for this case. The wave pattern is discernible, however there are several inconsistencies where the patterns for each cycle do not match each other. The resistance at the beginning and end of testing is 2.00 and 2.03 respectively. This shows that samples made good recovery after 5 cycles.

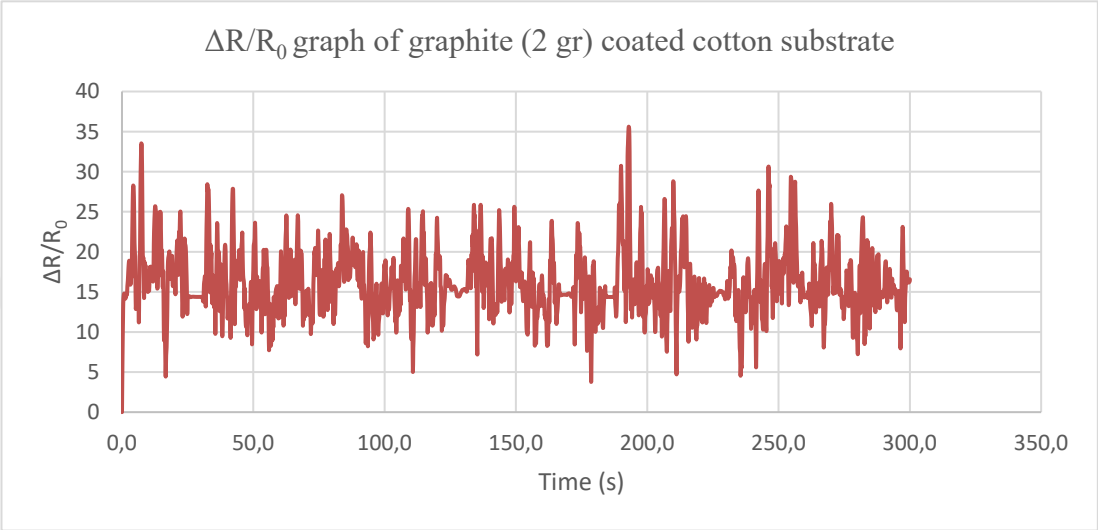

Figure 3.15 : ΔR/R₀ vs Time graph of graphite (2 gr) coated cotton substrate.

Figure 3.15 gives ΔR/R₀ over time values for graphite (2 gr) on cotton substrate. ΔR/R₀ values range between 0.00 and 35.61. Despite the extreme shifts in momentary resistance values, the general graph shows a distinct sinus wave for each of the 5 cycles.

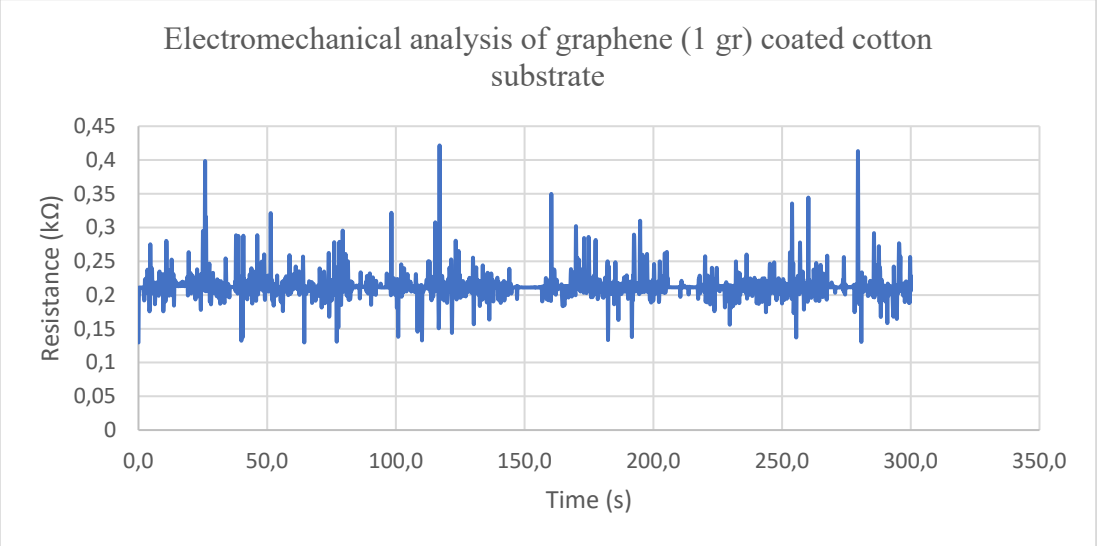

Figure 3.16 : Electromechanical analysis of graphene (1gr) coated cotton substrate.

For 1 gr of graphene in 10 ml PEDOT:PSS the lowest value shown in Figure 3.16 is 0.12 kΩ and the highest value is 0.42 kΩ. The resistance values at the beginning and at the end of testing are very close to each other indication good recovery as well.

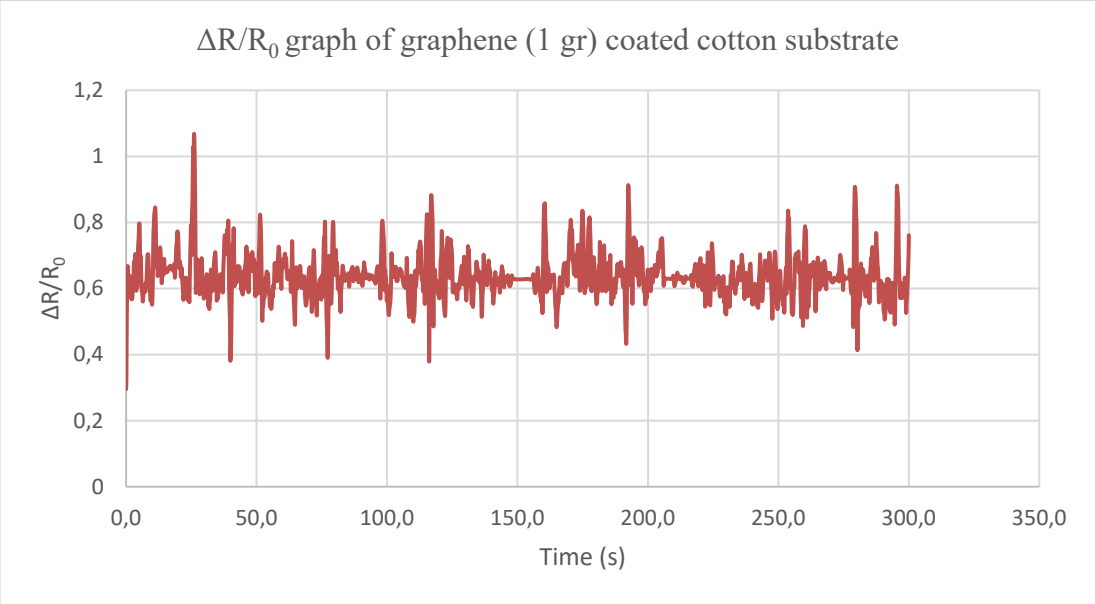

Figure 3.17 : $\Delta R/R_0$ vs Time graph of graphene (1 gr) coated cotton substrate.

Figure 3.17 gives $\Delta R/R_0$ over time values for graphene (1 gr) on cotton substrate. $\Delta R/R_0$ values range between 0.29 and 1.06.

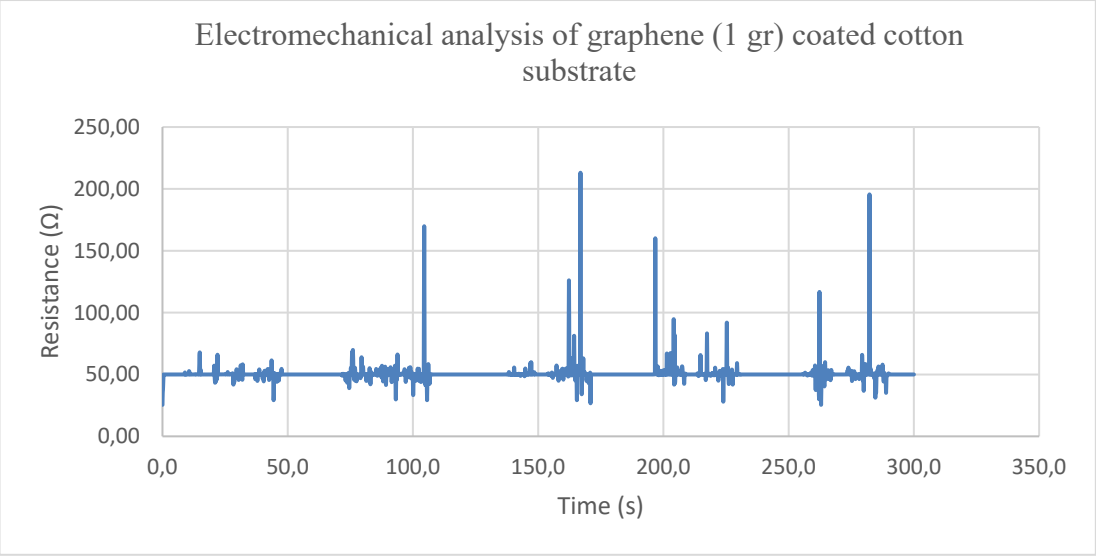

Figure 3.18 : Electromechanical analysis of graphene (2gr) coated cotton substrate.

The graph for 2 gr of graphene in 10 ml PEDOT:PSS shows a clear pattern of five different cycles where resistance increases as force is applied and decreases as it is released. The lowest resistance value is 25.45 Ω and the highest value is 213 Ω. The

resistance values at the beginning and end of testing are the same indicating that these samples also have good recovery.

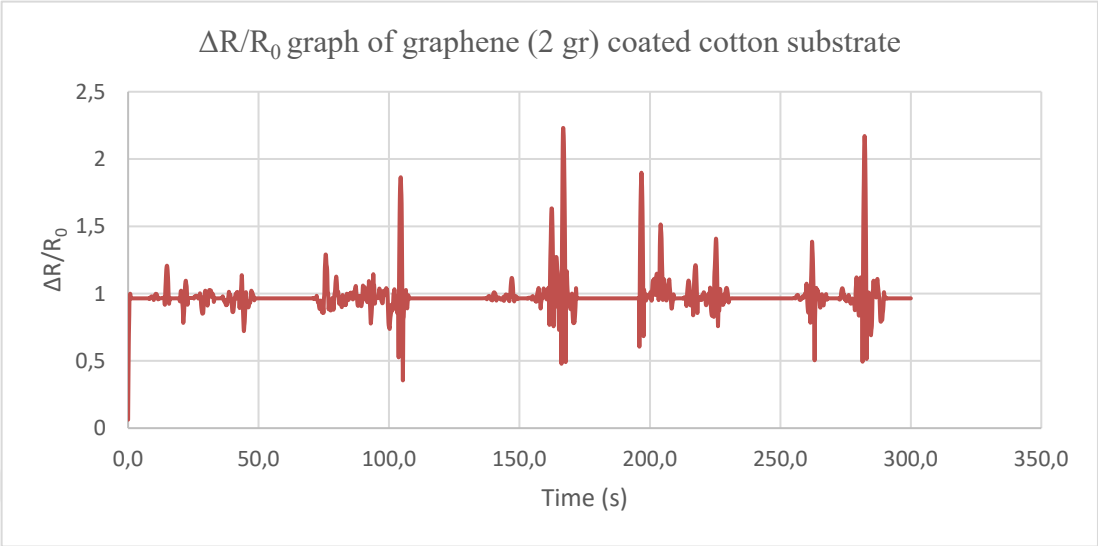

Figure 3.19 : $\Delta R/R_0$ vs Time graph of graphene (2 gr) coated cotton substrate.

Figure 3.19 gives $\Delta R/R_0$ over time values for graphene (2 gr) on cotton substrate. $\Delta R/R_0$ values range between 0.06 and 2.23. With each strain cycle the change in electrical resistance values is clearly observed in the graph.

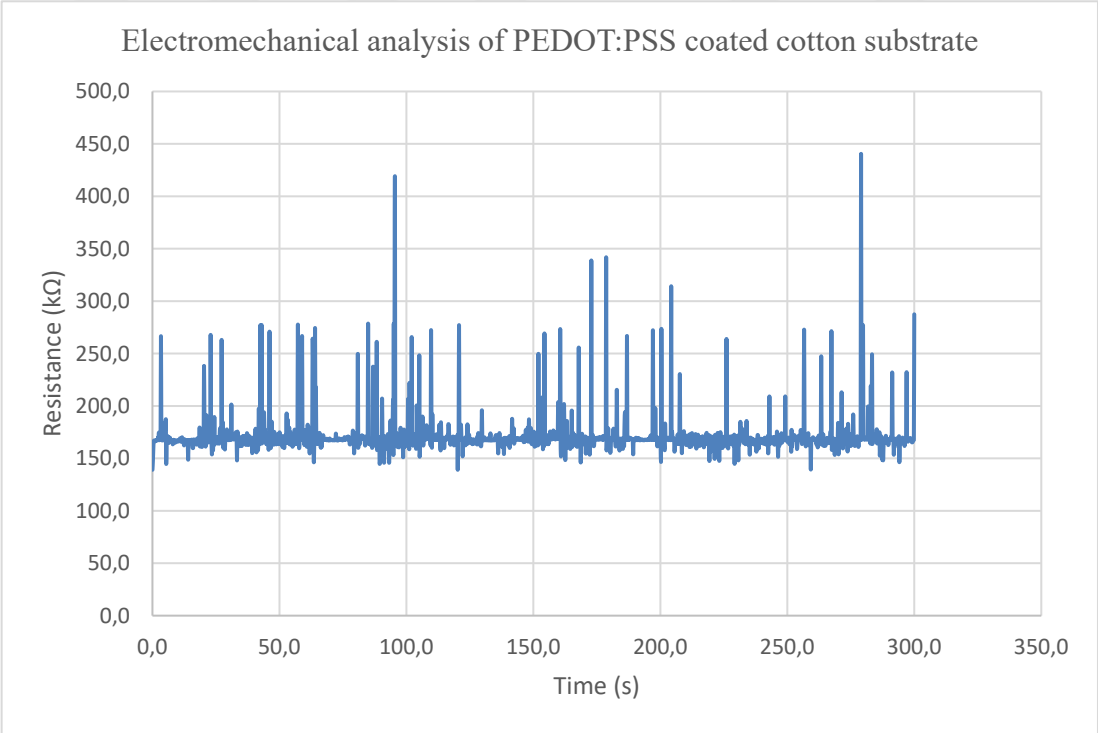

Figure 3.20 : Electromechanical analysis of PEDOT:PSS coated cotton substrate.

As can be seen in Figure 3.20, PEDOT:PSS coated cotton samples have a lowest resistance of 139.11 kΩ and highest resistance value 440.48 kΩ. Although the resistance increases with application of force the results are highly varied and wave pattern is not significant. The resistance value at the end of testing cycles (164.48 kΩ) is slightly lower than the resistance at the beginning (166.44 kΩ) which may be due to the realigning of cotton fibers during application of force.

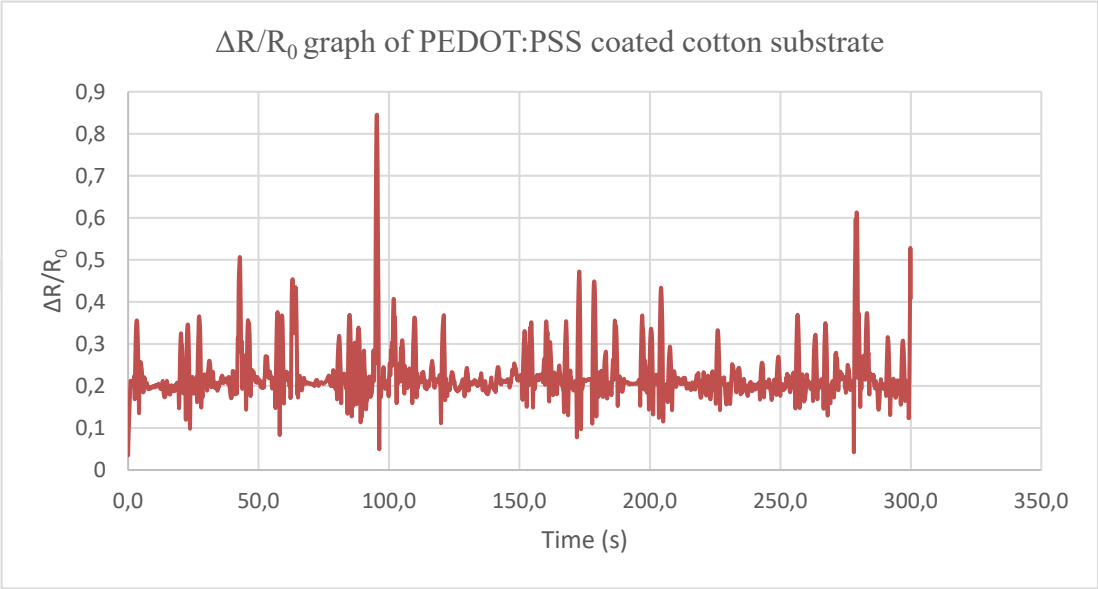

Figure 3.21 : ΔR/R0 vs time graph of PEDOT:PSS coated cotton substrate.

Figure 3.21 gives ΔR/R0 over time values for PEDOT:PSS coated on cotton substrate. ΔR/R0 values range between 0.03 and 0.84. The sinus wave is visible for each of the five cycles.

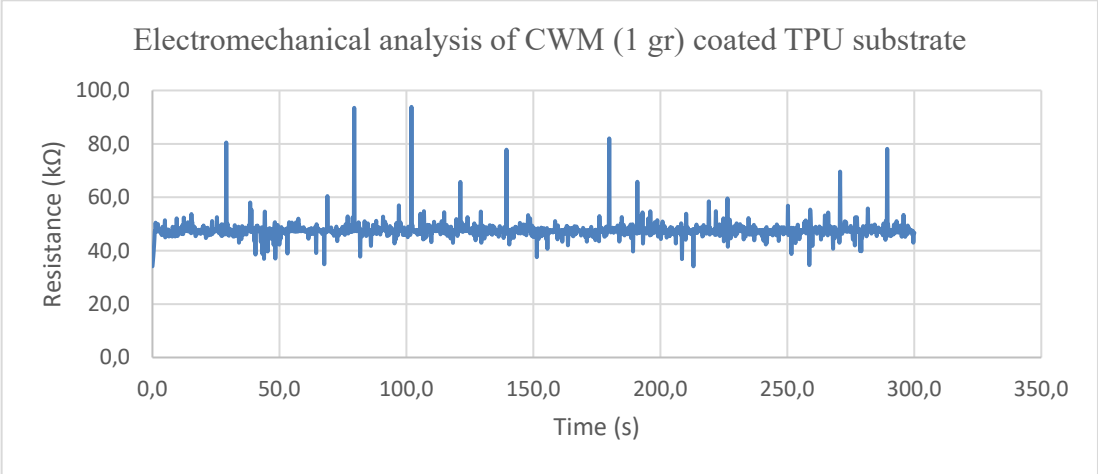

Figure 3.22 : Electromechanical analysis of CWM (1gr) coated TPU substrate.

Figure 3.22 shows that CWM (1 gr) coated TPU samples have lowest resistance value of 34.15 kΩ and highest resistance value of 93.85 kΩ. The resistance at the beginning

of testing is 44.35 kΩ and slightly increases to 47.26 kΩ at the end of testing. This may be due to the increase in size of fractures on the conductive ink coated on the surface of the TPU substrate. Morphological analysis shows a clustered distribution of CWM on TPU described in more detail in the next section.

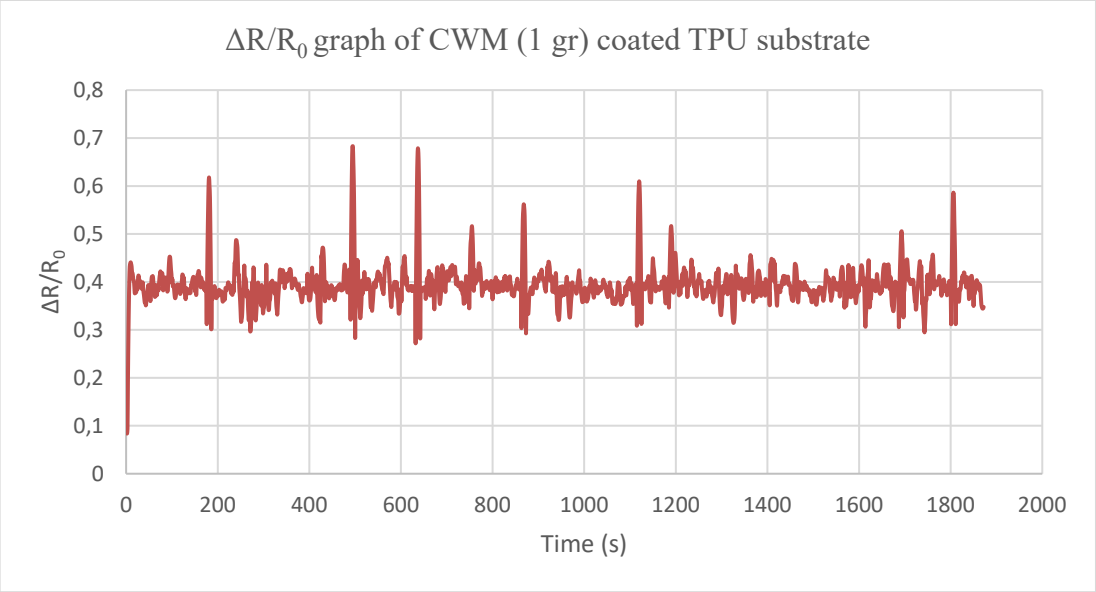

Figure 3.23 : ΔR/R0 vs time graph of CWM (1gr) coated TPU substrate.

Figure 3.23 gives ΔR/R0 over time values for CWM (1 gr) coated on TPU substrate. ΔR/R0 values range between 0.08 and 0.68. The sinus wave is not very clear for each of the five strain cycles.

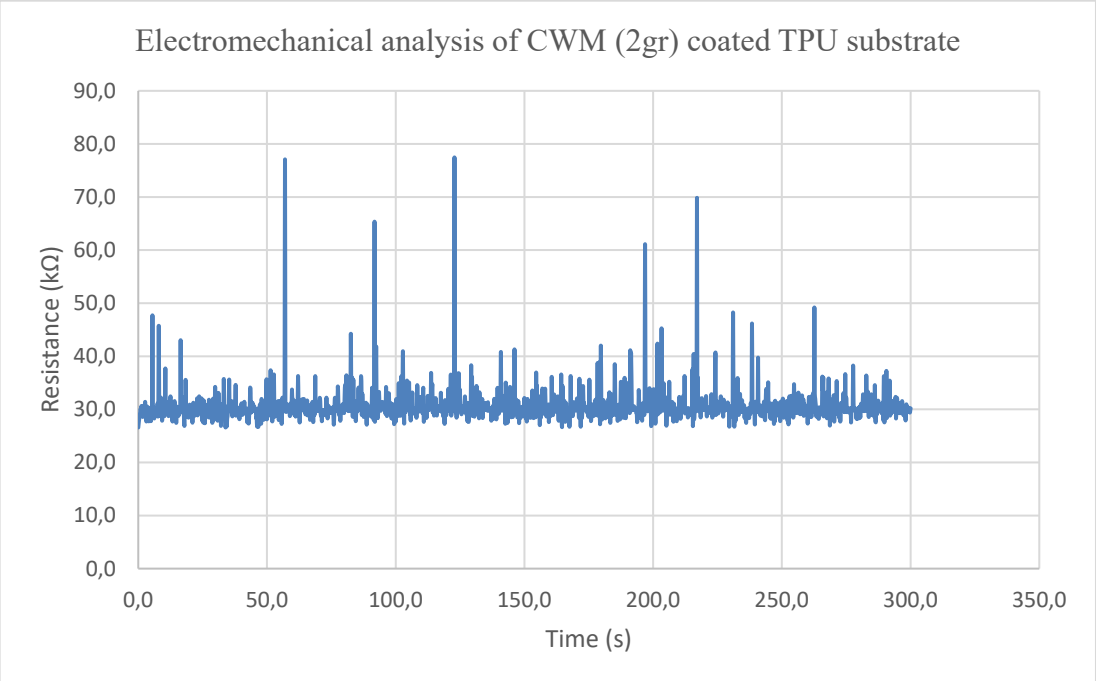

Figure 3.24 : Electromechanical analysis of CWM (2gr) coated TPU substrate.

CWM (2 gr) coated TPU samples have lowest resistance value of 26.58 kΩ and highest resistance value of 77.46 kΩ. Wave patterns are similar to CWM (1 gr) on TPU substrate. CWM forms clusters on TPU causing irregular changes in the resistance as force is applied. The resistance at the beginning of testing is 29.53 kΩ and slightly increases to 30.96 kΩ at the end of testing.

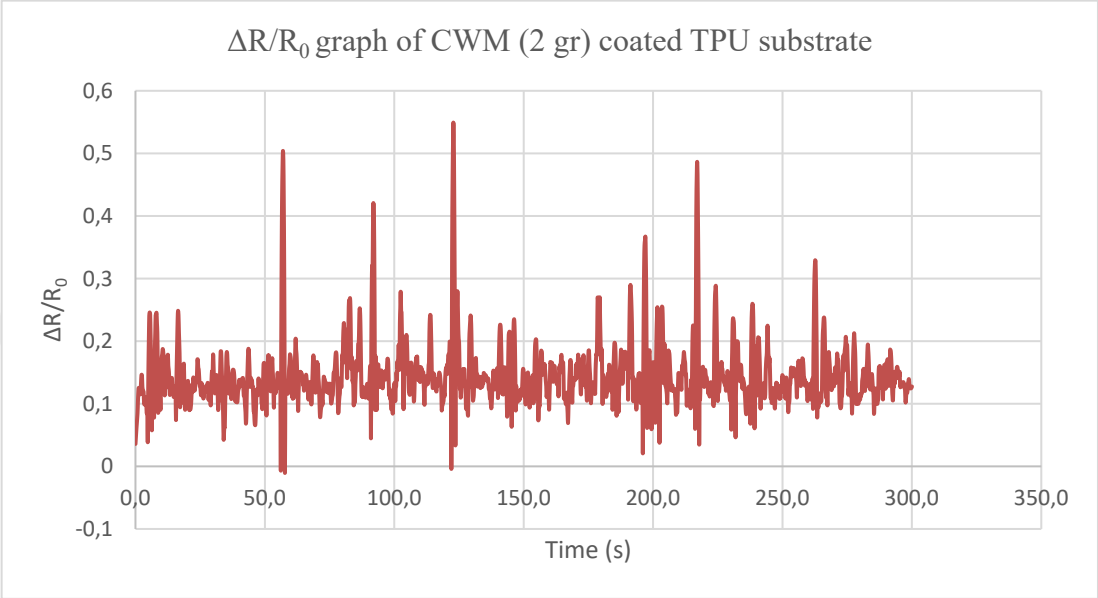

Figure 3.25 : ΔR/R0 vs time graph of CWM (2 gr) coated TPU substrate.

Figure 3.25 gives ΔR/R0 over time values for CWM (2 gr) coated on TPU substrate. ΔR/R0 values range between 0.004 and 0.54. ΔR/R0 graph shows irregularities similar to the resistance vs time graph.

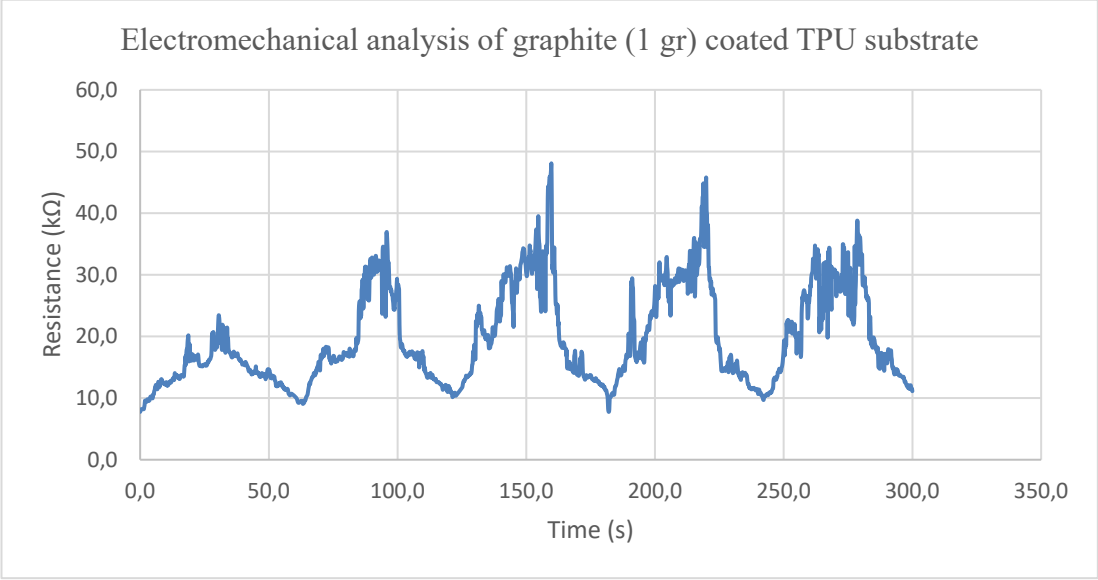

Figure 3.26 : Electromechanical analysis of graphite (1 gr) coated TPU substrate.

Figure 3.26 shows a very clear graph of five cycles of force applied on a TPU substrate coated with 1 gr graphite in 10 ml PEDOT:PSS solution. The lowest resistance value is 7.10 kΩ and the highest resistance value is 48.08 kΩ. Resistance at the beginning and end of testing is similar. Cycle 3 has the highest peak resistance at 48.08 kΩ. This data is noise free and easier to interpret than the data from previous graphs.

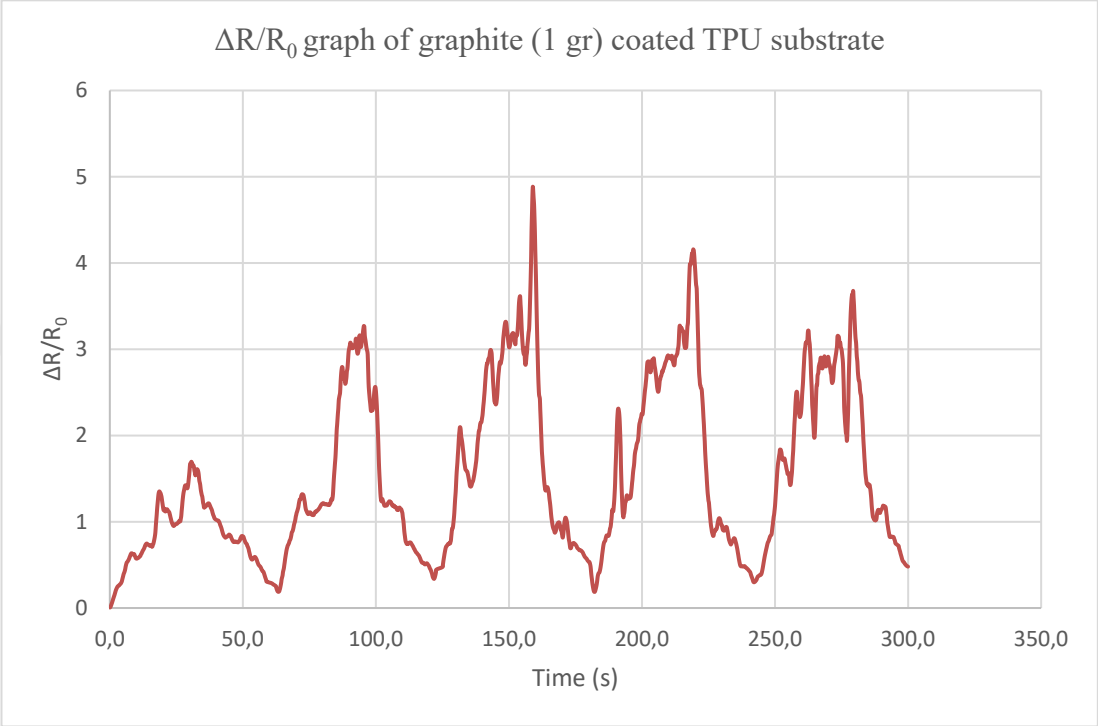

Figure 3.27 : $\Delta R/R_0$ vs time graph of graphite (1 gr) coated TPU substrate.

Figure 3.27 gives $\Delta R/R_0$ over time values for graphite (1 gr) coated on TPU substrate. $\Delta R/R_0$ values range between 0.006 and 4.88. $\Delta R/R_0$ graph shows five distinct sinus waves for each five strain cycle.

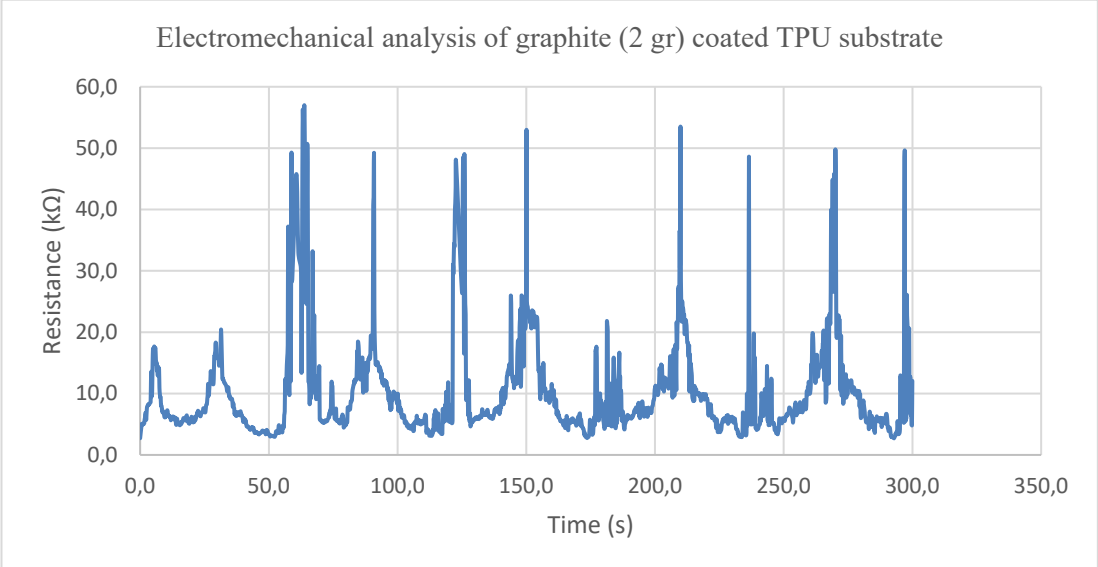

Figure 3.28 : Electromechanical analysis of graphite (2 gr) coated TPU substrate.

Figure 3.28 also shows a distinctive wave pattern. The lowest resistance value is 2.72 kΩ and the highest resistance value is 57.00 kΩ. The resistance at the end of testing cycles is the same as the resistance at the beginning of testing.

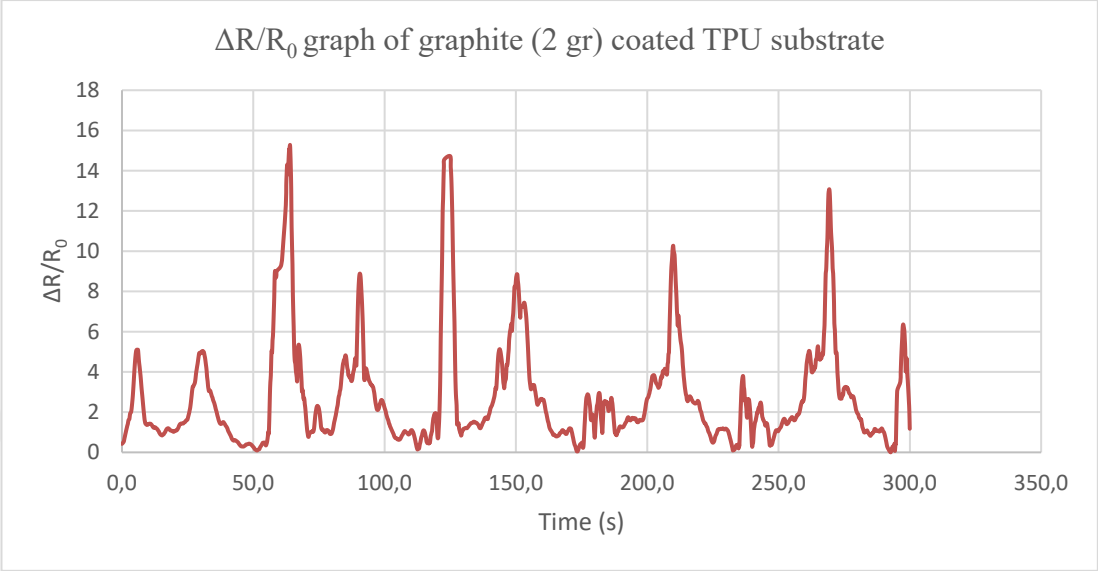

Figure 3.29 : $\Delta R/R_0$ vs time graph of graphite (2 gr) coated TPU substrate.

Figure 3.29 gives $\Delta R/R_0$ over time values for graphite (2 gr) coated on TPU substrate. $\Delta R/R_0$ values range between 0.008 and 15.28. $\Delta R/R_0$ graph shows irregularities such as two peaks within each strain cycle, similar to the resistance vs time graph.

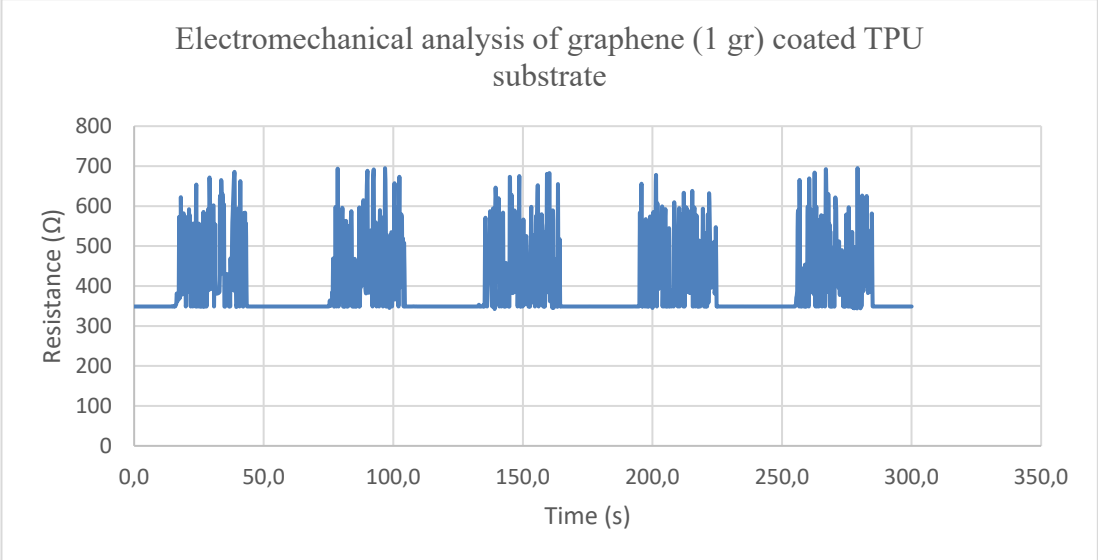

Figure 3.30 : Electromechanical analysis of graphene (1 gr) coated TPU substrate.

Figure 3.30 gives a very clear and repeating wave pattern where each of the five cycles in the testing loop are easily identified. The lowest resistance value is 299 Ω and the

highest resistance value is 695 Ω. The beginning and end of test resistance values are almost identical.

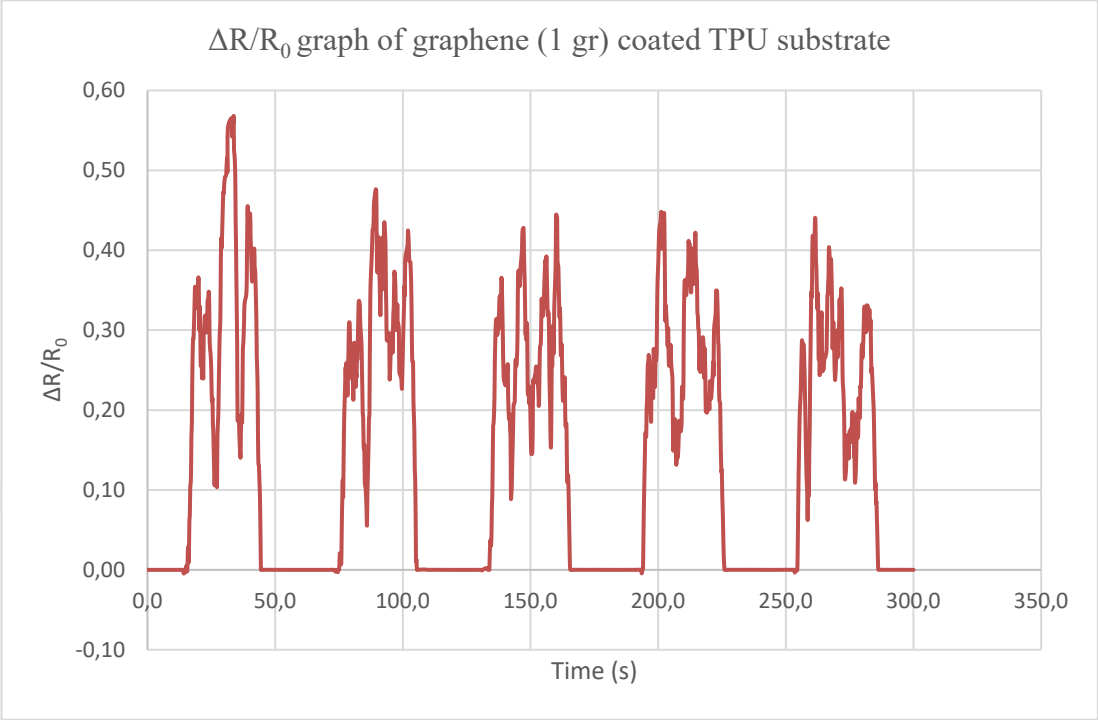

Figure 3.31 : $\Delta R/R_0$ vs time graph of graphene (1 gr) coated TPU substrate.

Figure 3.31 gives $\Delta R/R_0$ over time values for graphene (1 gr) coated on TPU substrate. $\Delta R/R_0$ values range between 0.00 and 0.57. Each strain cycle is clearly visible and easy to interpret.

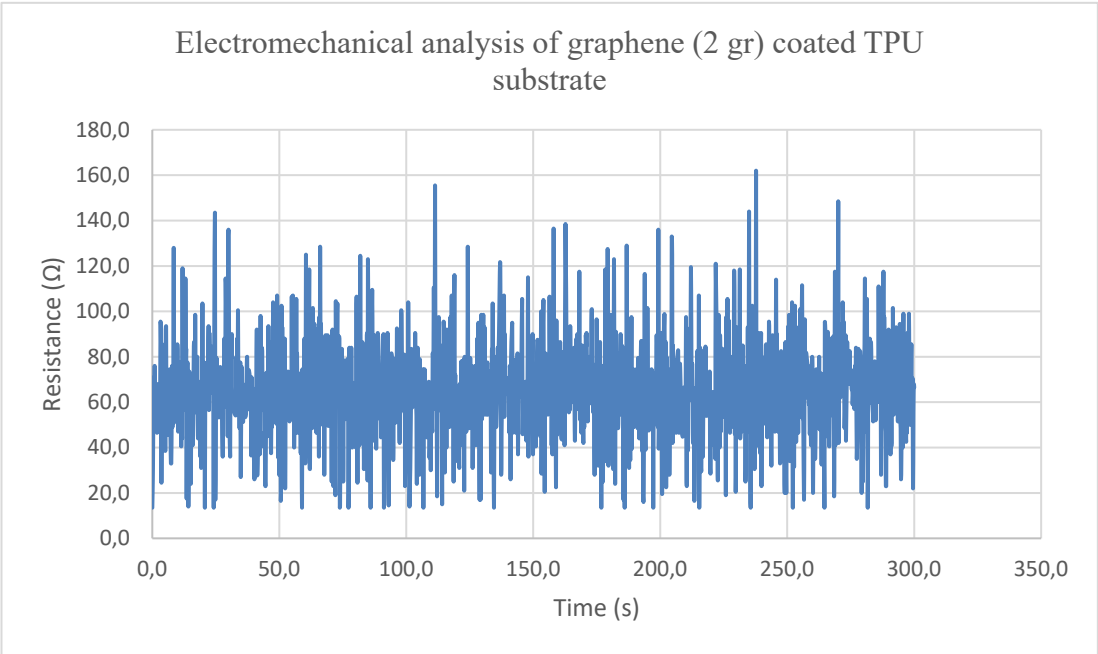

Figure 3.32 : Electromechanical analysis of graphene (2 gr) coated TPU substrate.

The lowest resistance value for 2 gr graphene in 10 ml PEDOT:PSS applied to TPU is 1 Ω and the highest resistance value is 168 Ω. The pattern in Figure 3.32 is not as clear as in Figure 3.30 but the wave pattern can be observed. The irregularities may be due to the fact that graphene (2 gr) has very low resistance values so the change in resistance although it is not very high shows more prominently in the graph. The resistance at the beginning of testing reads at 65 Ω and increases to 66.5 at the end of 5 testing cycles.

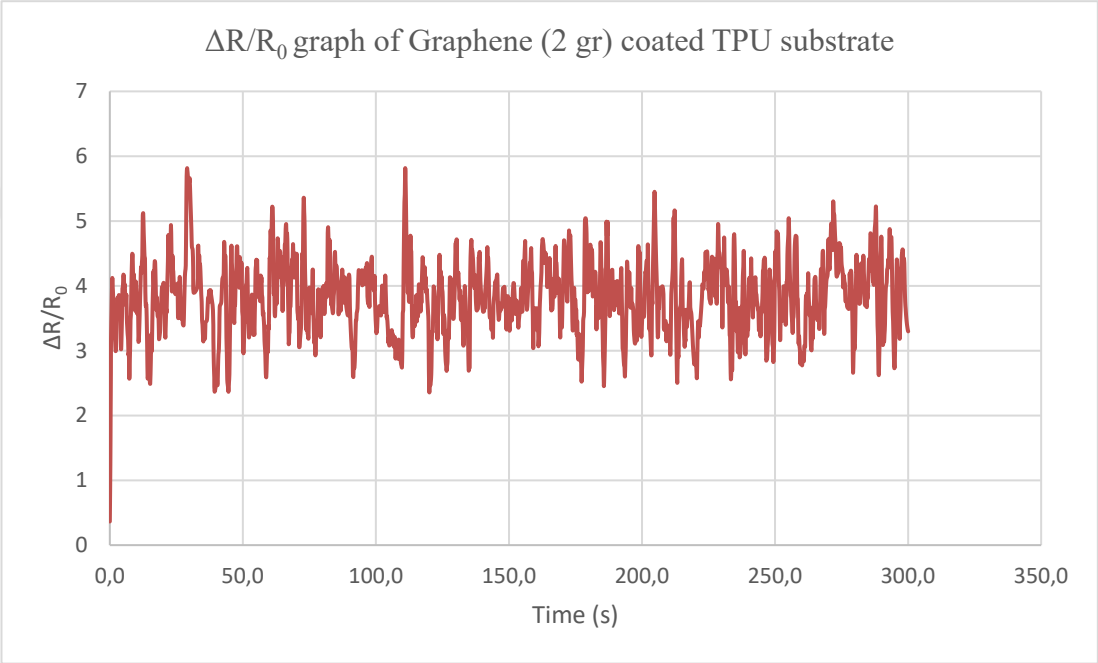

Figure 3.33 : $\Delta R/R_0$ vs time graph of graphene (2 gr) coated TPU substrate.

Figure 3.33 gives $\Delta R/R_0$ over time values for graphene (2 gr) coated on TPU substrate. $\Delta R/R_0$ values range between 0.34 and 5.81. $\Delta R/R_0$ graph shows irregularities similar to the resistance vs time graph.

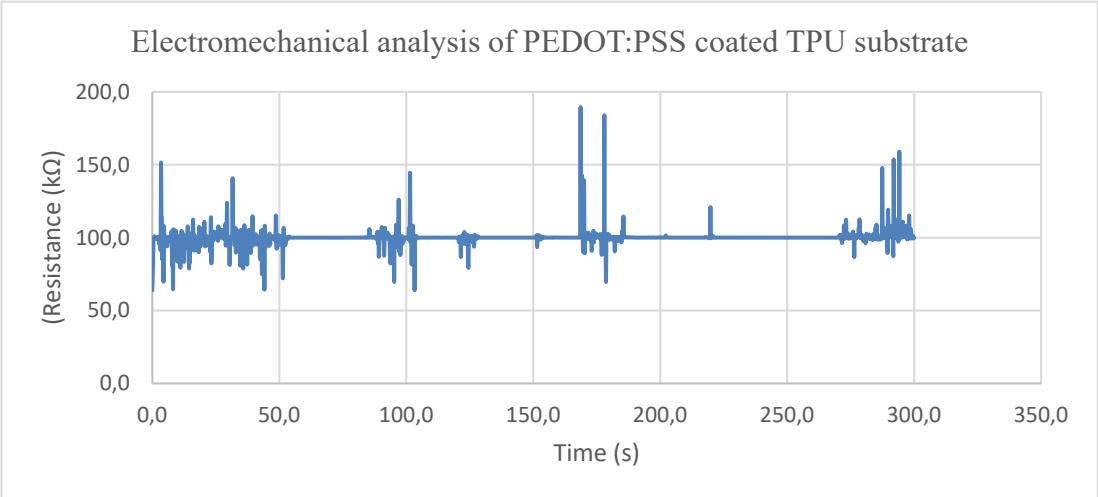

Figure 3.34 : Electromechanical analysis of PEDOT:PSS coated TPU substrate.

The lowest resistance value is 63.90 kΩ and the highest resistance value is 189.50 kΩ for PEDOT:PSS coated TPU samples under strain. When no force is applied the resistance averages at 100 kΩ. The cycles can be seen in the pattern of the graph however they are not repeating patterns such as the patterns in graphene (1 gr).

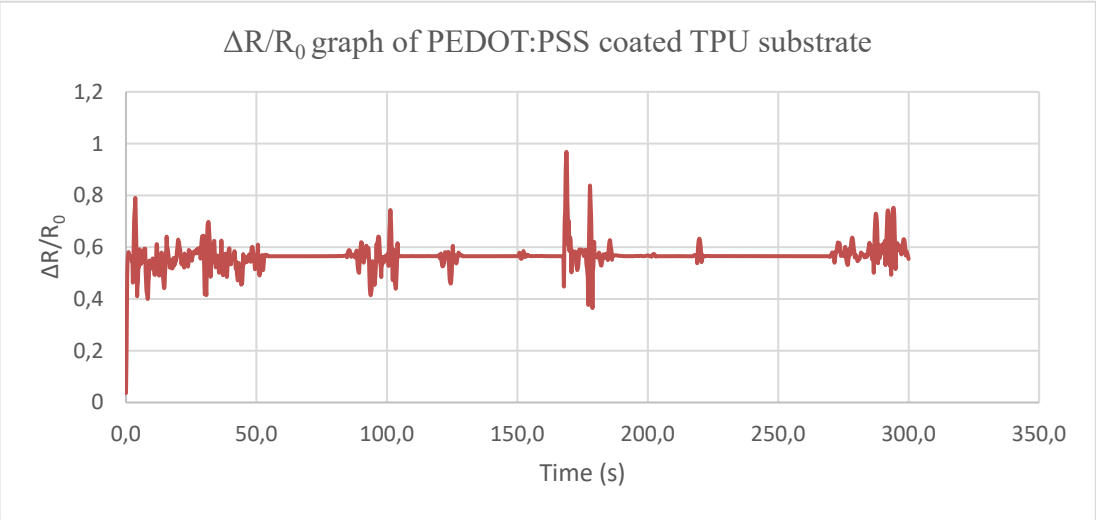

Figure 3.35 : ΔR/R0 vs time graph of PEDOT:PSS coated TPU substrate.

Figure 3.35 gives ΔR/R0 over time values for PEDOT:PSS coated on TPU substrate. ΔR/R0 values range between 0.03 and 0.96. ΔR/R0 graph shows irregularities similar to the resistance vs time graph. After the first strain cycle change of resistance is stable until the peak value of the second and third strain cycles, the fourth cycle is almost non-existent but the material shows some change in resistance in the fifth cycle.

3.5 Morphological Analysis

Samples were viewed under light microscope and analyzed at 0.8x, 1.6x, 2.5x and magnification. Figure 3.36 shows 0,8, 1,6 and 2,5 magnification images of 2 gr/10 ml CWM (2 gr) /PEDOT:PSS solution applied two layers of coatings on cotton and TPU substrates.

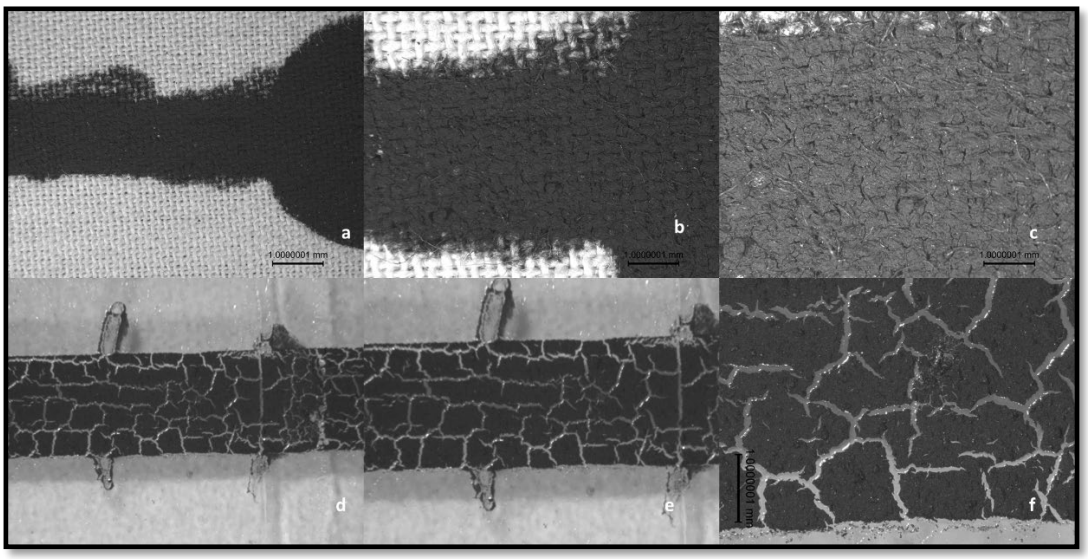

Figure 3.36 : a) 0,8 magnification b) 1,6 magnification c) 2,5 magnification CWM 82 gr)/PEDOT:PSS on cotton substrate d) 0,8 magnification e) 1,6 magnification f) 2,5 magnification CWM (2 gr)/PEDOT:PSS on TPU substrate.

The images show that CWM (2 gr) /PEDOT:PSS coating on TPU substrate form cracks after its dried and the conductive path takes a fractured structure where as on cotton substrate the coating is continuous. The difference is caused by the hydrophobic surface of the TPU film and the hydrophilic structure of the cotton fabric. The resistance values measured by Keithley 2400 signify that cotton coated with CWM (2 gr)/PEDOT:PSS has a lower resistance value of 15.95 $k\Omega cm^{-1}$ compared to TPU at 28.54 $k\Omega cm^{-1}$.

Figure 3.37 shows images of Graphite/PEDOT:PSS ink on cotton and TPU substrates.

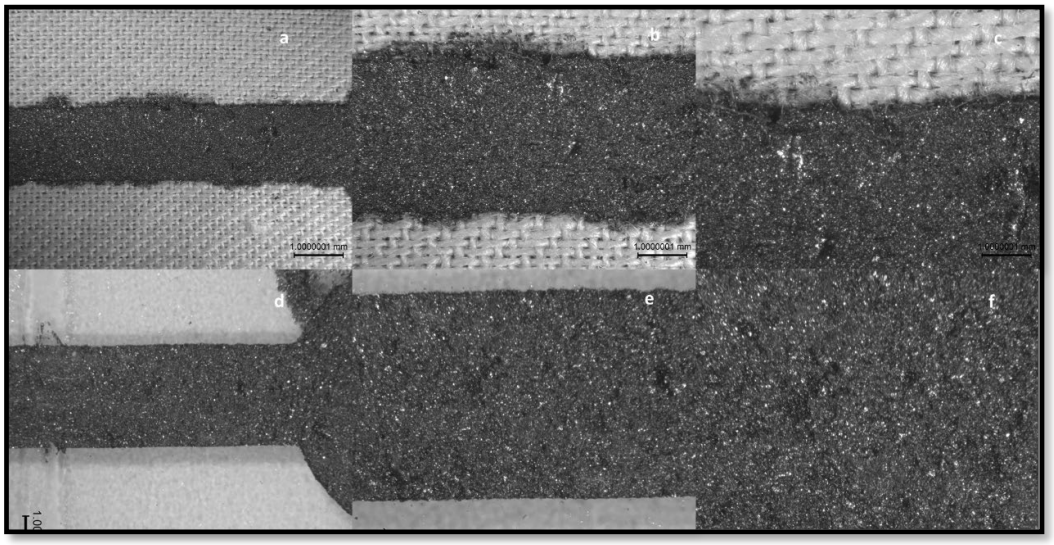

Figure 3.37 : a) 0,8 magnification b) 1,6 magnification c) 2,5 magnification Graphite (2 gr) /PEDOT:PSS on cotton substrate d) 0,8 magnification e) 1,6 magnification f) 2,5 magnification Graphite (2 gr) /PEDOT:PSS on TPU substrate.

The images show that Graphite has a continuous structure on both TPU and cotton substrates. The resistance values are lower in the case of cotton substrates. This may be due to the fact that cotton is hydrophilic and absorbs some of the ink into its fibers and threads, strengthening the bonds the ink forms with the substrate. No significant fractures can be observed on the coating. The graphite particles dispersed in PEDOT:PSS form clusters on some parts of the substrate for both subtrates. Stapel fibers on the surface of the cotton substrate cause some unevenness along the conductive path. With TPU substrate any crease on the film reflects to the conductive path as can be observed in Figure 3.37 (d). Although the ink covers the substrate surface completely it has a grainy texture due to the size and shape of the graphite particles.

Figure 3.38 shows 0,8, 1,6 and 2,5 magnification images of 2 gr/10 ml Graphene/PEDOT:PSS solution applied as two layers of coatings on cotton and TPU substrates.

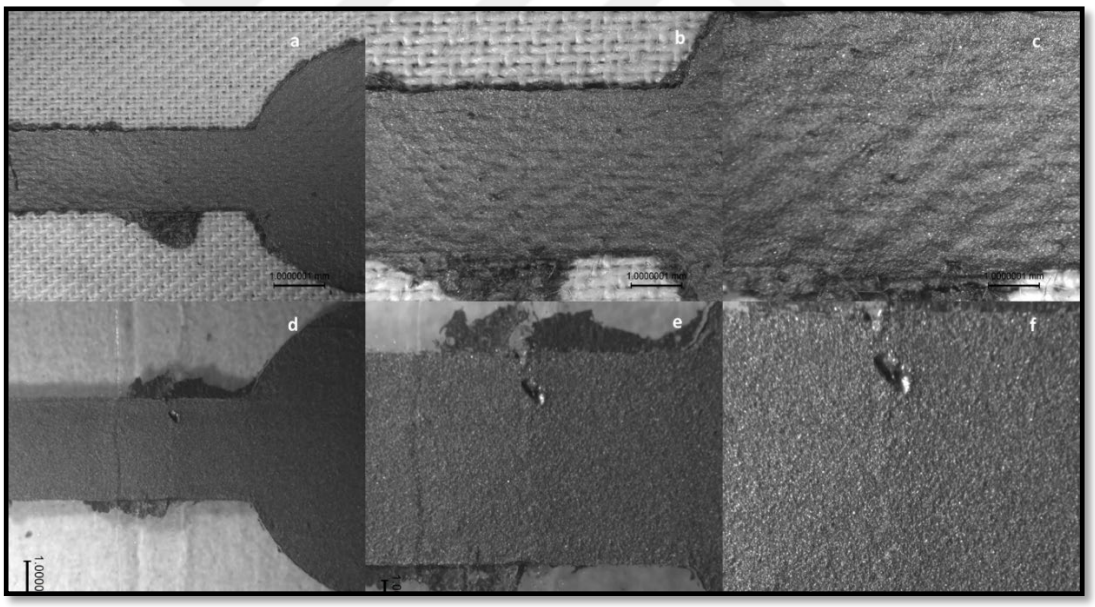

Figure 3.38 : a) 0,8 magnification b) 1,6 magnification c) 2,5 magnification Graphene/PEDOT:PSS on cotton substrate d) 0,8 magnification e) 1,6 magnification f) 2,5 magnification Graphene (2 gr) /PEDOT:PSS on TPU substrate.

Graphene has a lower particle size than CWM and graphite therefore it forms a smoother structure on both substrates. Cotton fabrics woven structure causes a wavy pattern. Resistance values for graphene are lower compared to graphite and CWM inks. For both substrates the resistance values are very close to each other (0.048 $k\Omega cm^{-1}$cotton and 0.056 $k\Omega cm^{-1}$ for TPU). When the probe is applied directly on to

the conductive path the tip of the probe causes a dent on the conductive path. This image is clearly visible on Figure 3.38 d, e and f. This may cause problems in application especially for TPU film because the conductive layer cannot penetrate the surface of the film. It would be easily scraped off unless further preventive measures are taken, such as coating a protective layer over the flexible electrode. Since cotton substrate has absorbed some of the ink into its structure, it will not lose its conductivity completely even if the outer layer is partially scraped off although an increase in resistance may be observed under such conditions.

Figure 3.39 shows 0,8, 1,6 and 2,5 magnification images of PEDOT:PSS solution applied two layers of coatings on cotton and TPU substrates.

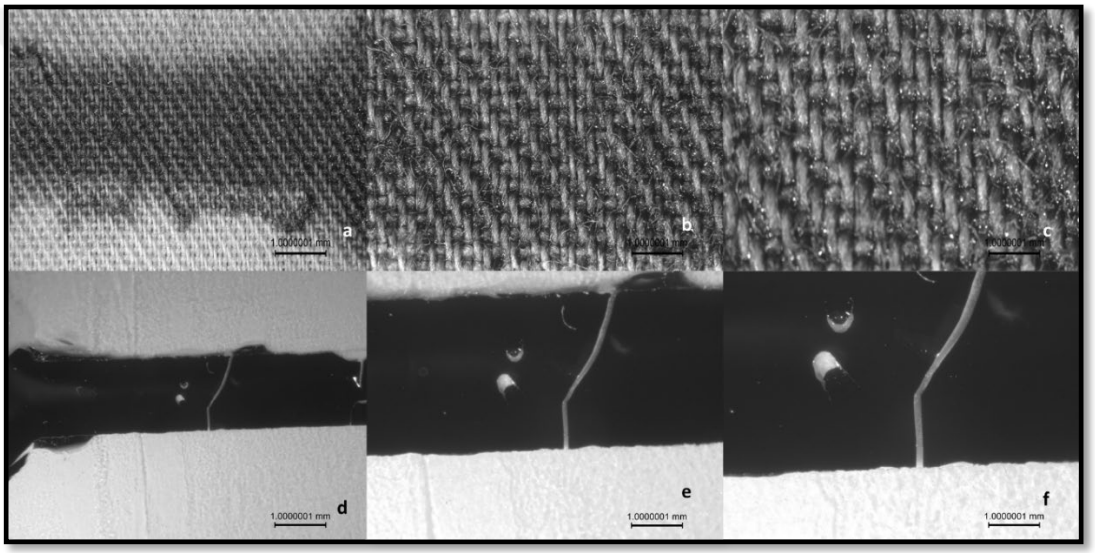

Figure 3.39 : a) 0,8 magnification b) 1,6 magnification c) 2,5 magnification PEDOT:PSS on cotton substrate d) 0,8 magnification e) 1,6 magnification f) 2,5 magnification PEDOT:PSS on TPU substrate.

Two layers of PEDOT:PSS coating on cotton and TPU substrates forms a very different structure compared to the other three ink formulations with carbon-based particles that are used in this study. Cotton absorbs most of the fluid and the images show dark spots and light spots on the woven structure where the ink is distributed unevenly. The connection points between weft and warp yarns that placed lower have a darker colour and the tops of the yarns have a lighter colour. Ink seems to coagulate in lower points. TPU sample shows a deep fracture as well as the dents caused by the probe tips. With TPU samples the design of the electrode is transferred clearly onto the substrate. The edges are sharp and clean whereas with cotton samples due to the

wicking properties of cotton, ink is wicked outside the designed path and the pattern looks dispersed. This can be observed in all cotton samples.

Samples were also analyzed according to the concentration of the ink solution and number of coatings applied. Figures 3.40 to 3.47 show images of 1gr/10ml and 2 gr/10 ml concentration ink solutions applied in different number of coatings on cotton and TPU substrates.

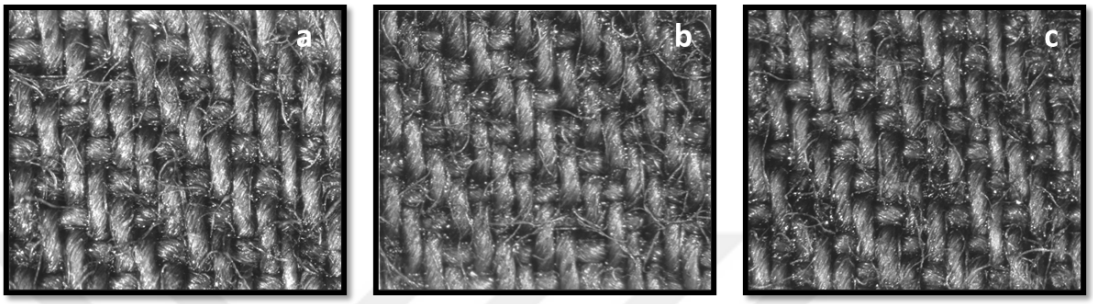

Figure 3.40 : Cotton substrate with PEDOT:PSS a) 1 layer of coating, b) 2 layers of coating, c) 3 layers of coating.

The images show a better surface coverage for 2 layers and 3 layers of coating with ink coagulating at junction points. At 1 layer of coating the top surface of the yarns are not covered by the conductive ink.

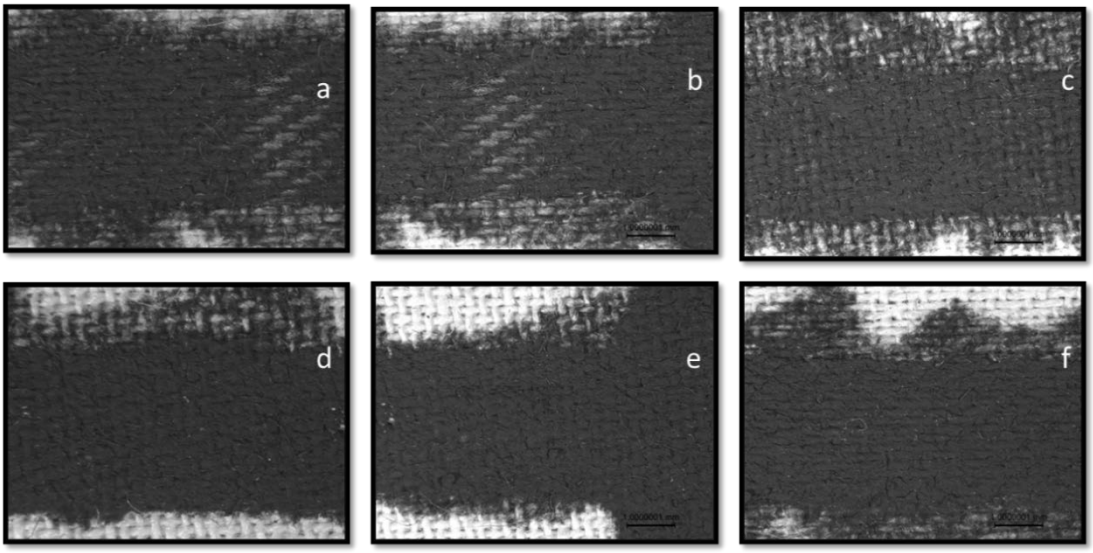

Figure 3.41 : Cotton substrate with CWM/PEDOT:PSS a) 1 gr/10ml 1 layer of coating, b) 1 gr/10ml 2 laters of coatings, c) 1 gr/10ml 3 layers of coatings, d) 2 gr/10ml 1 layer of coating, e) 2 gr/10ml 2 layers of coatings, f) 2 gr/10ml 3 layers of coatings.

As can be seen in Figure 3.41, surface coverage increases with the increase in the number of layers of coating. As the concentration of CWM particles in the ink solution

increases, coverage also increases. In figures 3.41 a and b some white patches can be observed in the conductive path but d and e show a fully covered conductive path.

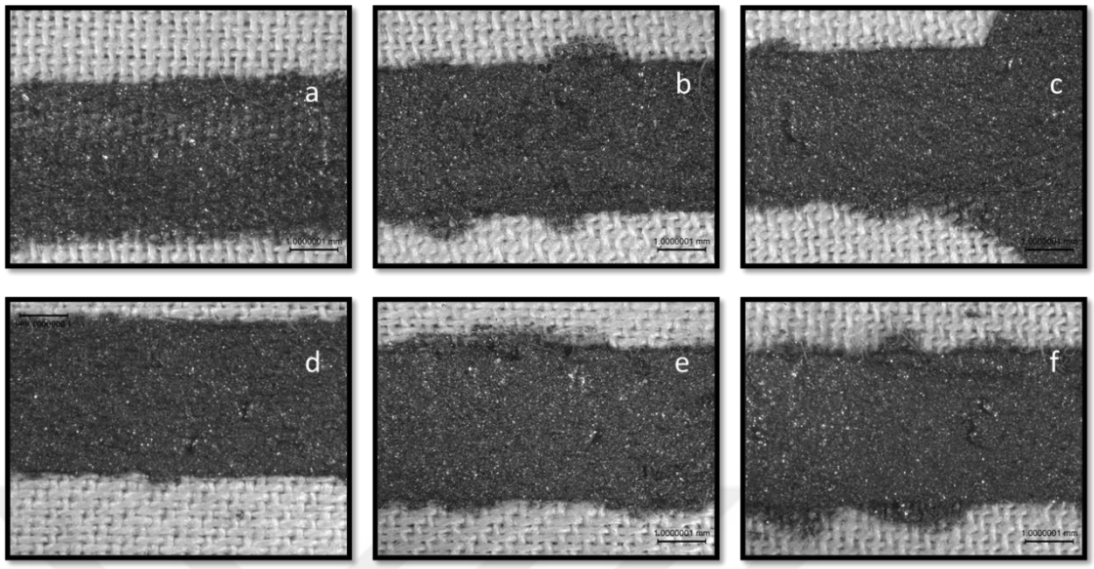

Figure 3.42 : Cotton substrate Graphite/PEDOT:PSS a) 1 gr/10ml 1 layer of coating, b) 1 gr/10ml 2 layers of coatings, c) 1 gr/10ml 3 layers of coatings, d) 2 gr/10ml 1 layer of coating, e) 2 gr/10ml 2 layers of coatings, f) 2 gr/10ml 3 layers of coatings.

At 1 layer of coating of graphite (1 gr)/PEDOT:PSS white patches can be seen on the cotton substrate (Fig. 3.42 (a)).

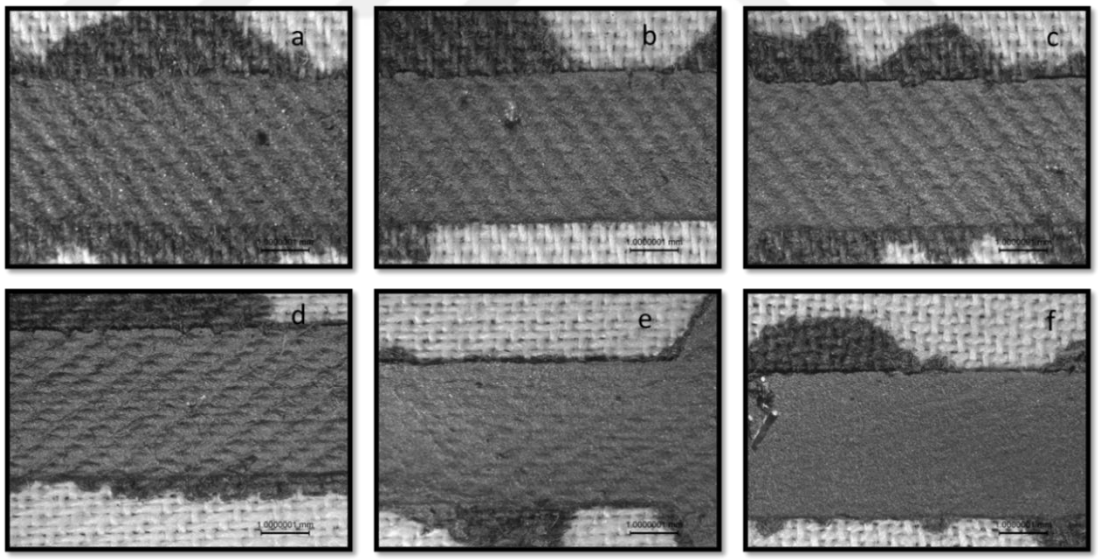

Figure 3.43 : Cotton substrate Graphene/PEDOT:PSS a) 1 gr/10ml 1 layer of coating, b) 1 gr/10ml 2 layers of coatings, c) 1 gr/10ml 3 layers of coatings, d) 2 gr/10ml 1 layer of coating, e) 2 gr/10ml 2 layers of coatings, f) 2 gr/10ml 3 layers of coatings.

The weave of the cotton substrate is more pronounced in Fig. 3.43 a, b, c and d. As the concentration and the number of layers increase coverage increases and the weave structure is not as easily observed in Fig. 3.43 f.

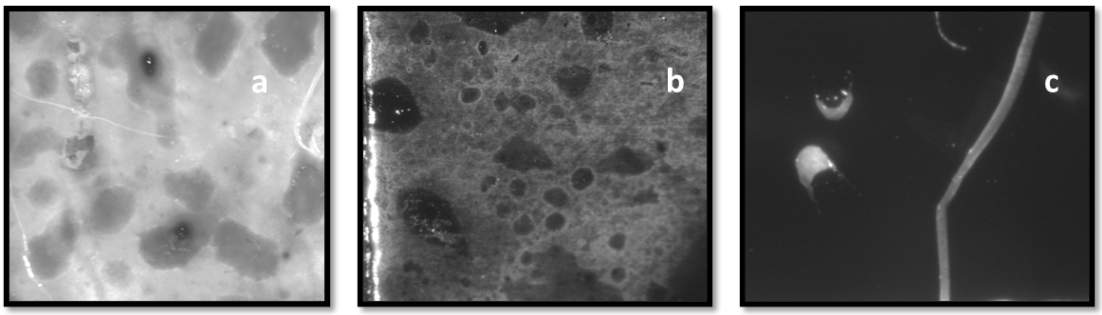

Figure 3.44 : TPU substrate PEDOT:PSS a) 1 layer of coating, b) 2 layers of coatings, c) 3 layers of coatings.

PEDOT:PSS film on TPU substrate shows a clear image of the effect of number of layers on substrate coverage. In Figure 3.44 (a) a very thin and almost transparent film is produced on the TPU surface. In Figure 3.44 (b) a slightly thicker and opaque film can be seen and in Figure 3.44 (c) a dark layer of PEDOT:PSS film is observed. Figure 3.44 (a) shows hairline fractures on the film surface. Figure 3.44 (c) a deep fracture is visible. These fractures may be due to the high elasticity of the substrate and may form while the samples are being handled for analysis.

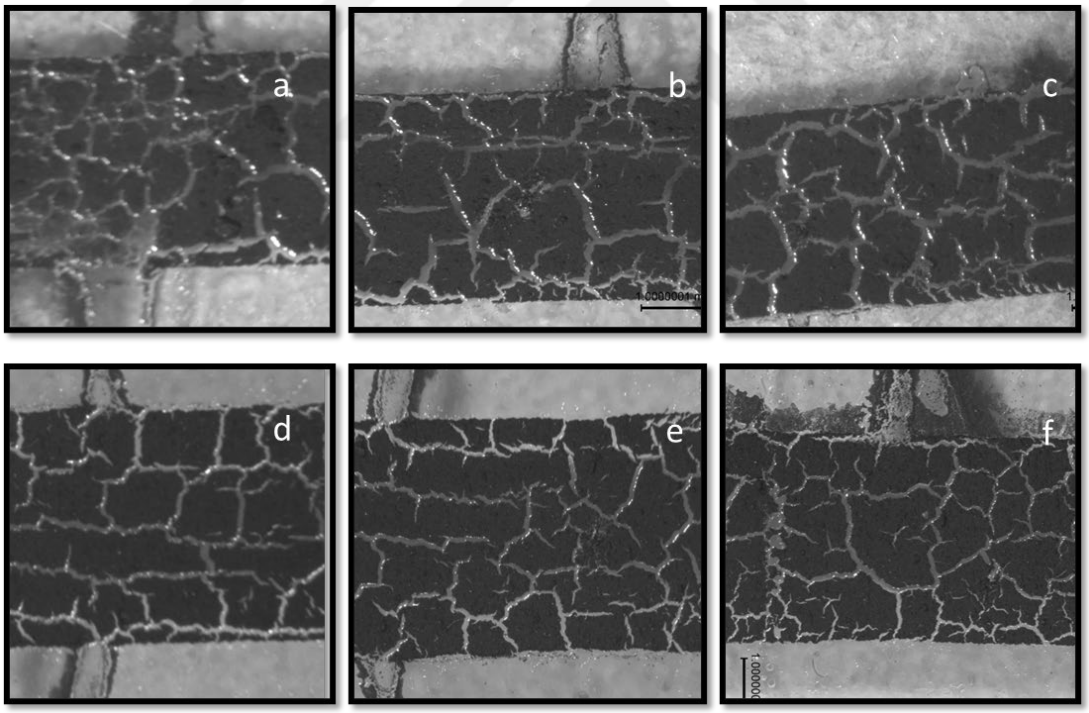

Figure 3.45 : TPU substrate CWM/PEDOT:PSS a) 1 gr/10ml 1 layer of coating, b) 1 gr/10ml 2 layers of coatings, c) 1 gr/10ml 3 layers of coatings, d) 2 gr/10ml 1 layer of coating, e) 2 gr/10ml 2 layers of coatings, f) 2 gr/10ml 3 layers of coatings.

CWM /PEDOT:PSS dispersion forms a fractured surface on the TPU film.

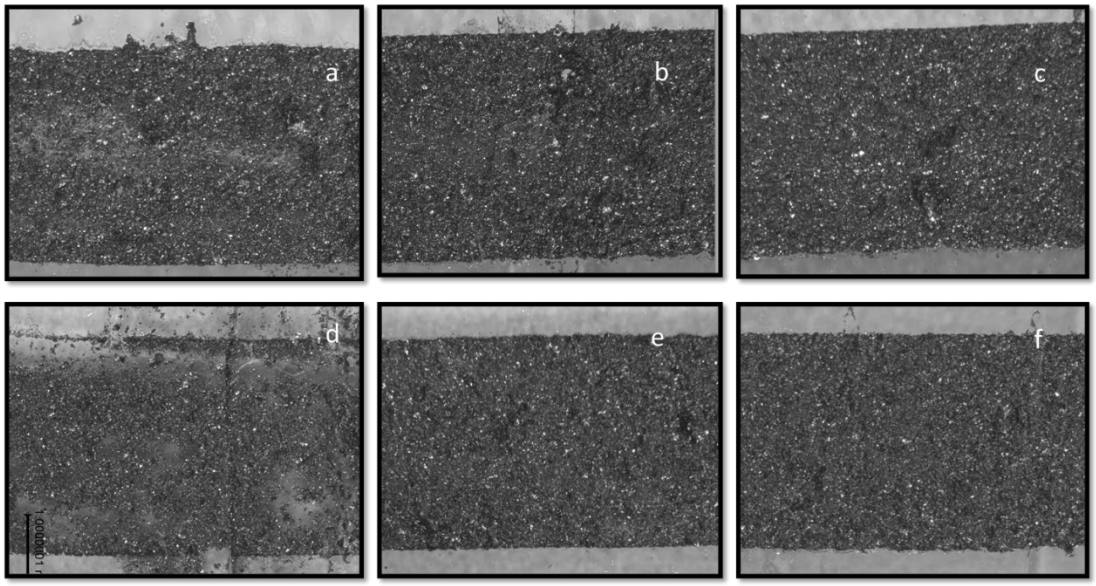

Figure 3.46 : 1.6 magnification TPU substrate Graphite/PEDOT:PSS a) 1 gr/10ml 1 coating, b) 1 gr/10ml 2 coatings, c) 1 gr/10ml 3 coatings, d) 2 gr/10ml 1 coating, e) 2 gr/10ml 2 coatings, f) 2 gr/10ml 3 coatings.

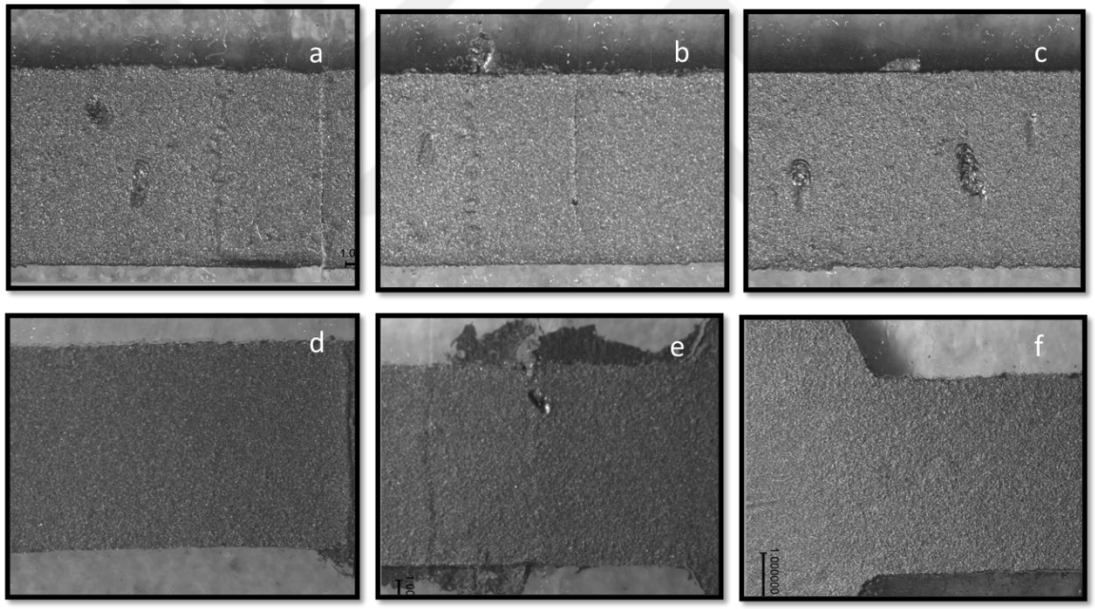

Figure 3.47 : 1.6 magnification TPU substrate Graphene/PEDOT:PSS a) 1 gr/10ml 1 coating, b) 1 gr/10ml 2 coatings, c) 1 gr/10ml 3 coatings, d) 2 gr/10ml 1 coating, e) 2 gr/10ml 2 coatings, f) 2 gr/10ml 3 coatings.

Adhesion of the ink film is determined by the reciprocal interactions of polar and nonpolar (dispersive) components between polymer films and inks. The greater the similarity between the polar and dispersive components of inks, coating and substrates, the better the wetting and adhesion on the surface of printing substrate (Aydemir et al., 2021).

3.6 Contact Angle Measurements

Cotton and TPU substrates were coated with 3 different dispersions to observe superamphiphobic properties. The results for contact angle measurements of coated substrates for water are given in Table 3.11 and for oil in Table 3.12.

Table 3.11 : Average values for contact angles of coated TPU and cotton substrates (Water).

Cotton Substrate	
Control Sample	Not detected
Tubiguard coated	142.37˚
Tubiguard and zinc stearate coated	143.33˚
Tubiguard and SiO_2 coated	131.47˚
TPU Substrate	
Control sample	101.54˚
Tubiguard coated	116.93˚
Tubiguard and zinc stearate coated	124.66˚
Tubiguard and SiO_2 coated	115.13˚

Table 3.12: Average values for contact angles of coated TPU and cotton substrates (Oil).

Cotton Substrate	
Control Sample	Not detected
Tubiguard coated	134,96˚
Tubiguard and zinc stearate coated	135,33˚
Tubiguard and SiO_2 coated	127.75˚

Table 3.12 (continued) : Average values for contact angles of coated TPU and cotton substrates (Oil).

TPU Substrate	
Control sample	59˚
Tubiguard coated	83,51˚
Tubiguard and zinc stearate coated	79,54˚
Tubiguard and SiO_2 coated	85,8˚

In order to achieve superamphiphobic properties the contact angles should be over 150 degrees (Chu and Seeger, 2010). The improvement of hydrophobicity of hydrophilic cotton substrates is considerably good. There is some improvement on TPU hydrophobicity but not nearly as good as cotton substrate. Only one coat of amphiphobic dispersion was applied on the substrates. The surfaces were not treated with other methods such as sandpaper degradation. The hydrophobicity could be improved with several layers of coating. Figure 3.48 shows images from contact angle measurements for cotton and TPU substrates for water, and Figure 3.49 shows images from contact angle measurements for cotton and TPU substrates for oil.

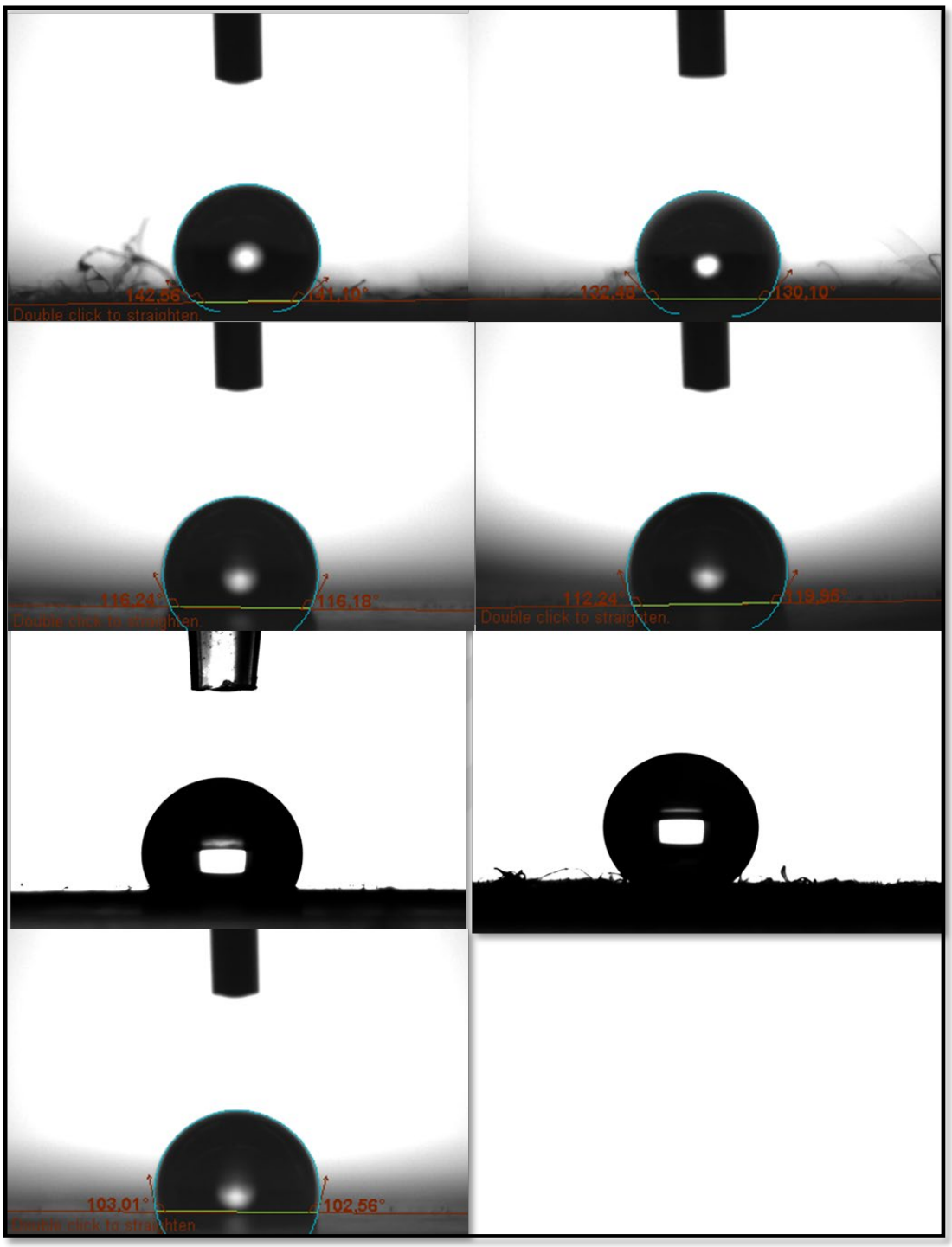

Figure 3.48 : a) CA of cotton with ZnSt b) cotton with SiO_2 c) TPU with zinc stearate d) TPU with SiO_2 e)TPU with tubiguard f) cotton with tubiguard g)TPU control sample for water.

Staple fibers on the surface of the cotton substrate are clearly visible in Figure 3.48 (a), (b) and (f).

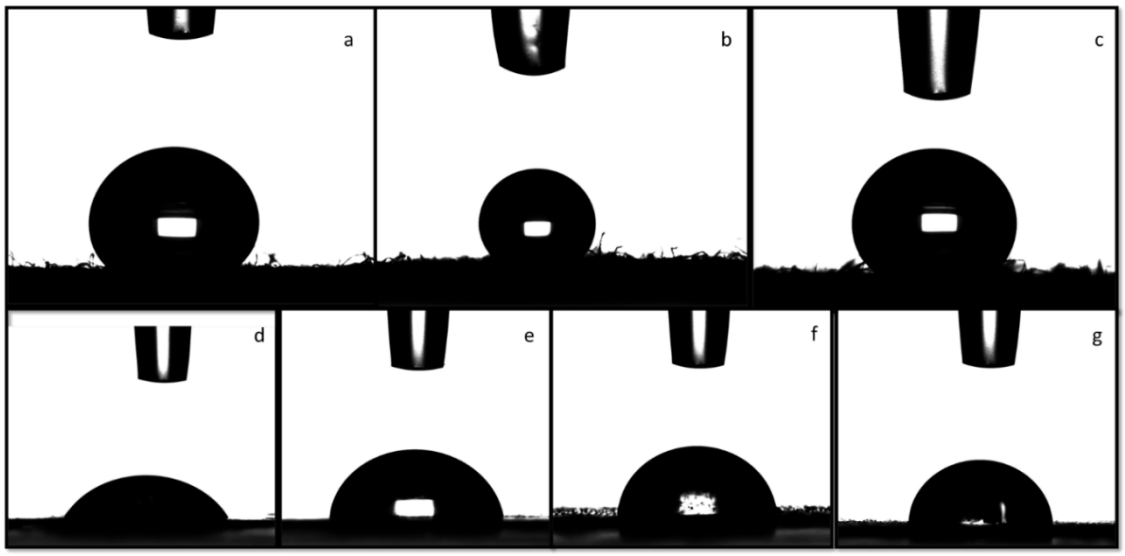

Figure 3.49 : Contact angles for cotton and TPU substrates for oil a) cotton coated with tubiguard b) cotton coated with tubiguard ZnSt dispersion c) cotton coated with tubiguard SiO_2 dispersion d) TPU control sample e) TPU coated with tubiguard f) TPU coated with tubiguard ZnSt dispersion g) TPU coated with tubiguard SiO_2 dispersion.

As in Figure 3.48 staple fibers on the surface of the cotton substrate are clearly visible in Figure 3.49 (a), (b) and (c). In figure 3.49 (f) microhierarchical structures can be observed on the surface of TPU coated with tubiguard ZnSt dispersion. Cotton substrate in its pure form is highly hydrophilic and oleophilic. The contact angle measurement for untreated cotton substrate shows no contact angle detected, in other words the cotton material fully absorbs water and oil droplets. TPU in its pure form is hydrophobic with a 101˚ contact angle. Oleophilic characteristic of TPU substrate is less compared to cotton but still the 59˚ contact angle is not high enough to be characterized as oleophobic. The contact angle measurements show that coated cotton fabric yields better results than coated TPU substrate. ZnSt added Tubiguard dispersion provides higher amphiphobic properties to the substrates. Cotton, due to its fibrous composition and the microhiearchical structure formed by the staple fibers on the substrate surface enable cotton to gain amphiphobic properties. In order to be called superamphiphobic the contact angle should be equal to or higher than 150˚, cotton contact angle values are above 130˚ for both water and oil experiments but the results can be improved in further studies.

CONCLUSION

In this study carbon-based flexible electrodes were printed on textile (cotton fabric) and polymer (TPU film) surfaces. Seven different ink dispersions were prepared using carbon-based conductive materials and a conductive polymer. PEDOT:PSS, a highly conductive polymer, was used as a carrier for the carbon-based ink dispersions. Graphite, graphene and CWM particles were dispersed in the conductive PEDOT:PSS polymer in two different weight percentages. Viscosity of the inks were measured using PCE RVI-2 digital viscosimeter. Density of CWM, graphite and graphene particles were measured using a gas pcynometer, Micromeritics - ACCUPYC II 1340. The inks were applied to the substrate surface using doctor blade. Three different samples were prepared depending on the number of conductive ink layers applied on the surface. Resistivity of each sample was measured by two probe method using Keithley 2400 Source Meter. Electromechanical properties of samples were measured using Shimadzu - AGS-X tensile testing device and a free online application “Sweep Me” .

Viscosity of the inks increases as the weight-volume fraction of the carbon based particles in the dispersion increases. As particle size decreases, the surface to volume ratio increases thus increasing the degree of interactions between the particles (Koca et al, 2018). Graphene has smaller particle size than Graphite and CWM therefore the viscosity of graphene/PEDOT:PSS dispersion is higher than Graphite and CWM. Graphene dispersion has the highest viscosity among all dispersions.

Density of particles and resistance of pressed carbon-based powders were measured. Graphene has the lowest density (2.07 g/cm^3) and CWM has the highest density (2.47 g/cm^3). Pressed graphene disc has the lowest resistance with 3.01 Ω and CWM has the highest resistance with 8.13 Ω.

Conductive inks applied on cotton and TPU substrates were analyzed with Fourier transform infrared spectroscopy (FT-IR) with a full-scale spectrum between 400 cm-1 and 4000 cm-1 wavenumbers. The spectra for cotton substrate-based samples and TPU based samples were analyzed separately. There are no significant peaks relevant

to any functional groups in the FTIR spectrum of graphite or graphene, therefore the inks show similar characteristics with PEDOT:PSS spectra. Graphite and CWM spectra are very similar because the main material of cathodes of recycled batteries is a graphite rod. The differences may be due to the irregularities found in recycled CWM composition.

Resistance measurements of 7 types of ink applied on 2 different substrates were taken. Graphene gives the best results among all inks prepared. 2 gr of graphene in 10 ml PEDOT:PSS had an average resistance of 0.037 kΩcm-1 on cotton substrate and 0.018 kΩcm-1on TPU substrate. 2 gr of graphite measured average resistance of 0.54 kΩcm-1for cotton substrates and 2.25 kΩcm-1for TPU substrate. 2 gr of CWM measured average resistance of 6.91 kΩcm-1 for cotton substrates and 6.97 kΩcm-1 for TPU substrates. PEDOT:PSS doped with DMSO measured average resistance of 50.47 kΩcm-1 for cotton substrates and 30.12 kΩcm-1 for TPU substrates.

Smooth surface of TPU film compared to the woven and curvy structure of cotton fabric provided a better base to apply a straight conductive path. Hydrophobic property of the TPU surface posed some difficulties in the adhesion of conductive ink on the surface. cotton fabric is highly hydrophilic and fibers act as capillaries to absorb conductive ink onto the cotton fabric surface or into the strands of the fibers by capillary effect, forming hydrogen bonds with the fabric. The concentration of conductive particles in the ink dispersion also play a role in the resistivity of the electrode. As the concentration of conductive particles in the ink dispersion increases the resistivity value decreases. PEDOT:PSS, a conductive polymer acts as the carrier base for the ink dispersion. When 3 layers of pure PEDOT:PSS is applied on the substrates the resistivity is around 50 kΩcm-1 for cotton substrate and 30 kΩcm-1 for TPU substrate. With the addition of conductive carbon-based particles this value is improved.

The samples were tested at mechanical tensile tester to characterize their behaviour under strain. Loop tests were performed to measure resistivity under strain and recovery. 5 loops for 3 mm strain were setup. Strain for cotton substrates was measured at 50% and for TPU substrates at 60%. The results showed that resistance increases as force is applied. Both TPU and cotton based samples recovered from force applied. The resistances at the beginning and ending of testing cycles were either similar or slightly different from each other indicating good recovery. The best wave patterns

were observed in graphite (1 and 2 gr) and graphene 1 gr applied on TPU. The other samples also showed wave patterns but the presence of irregularities made the graphs less easy to interpret.

Samples were viewed under light microscope and analyzed at 0.8x, 1.6x, 2.5x and magnification. CWM (2 gr) /PEDOT:PSS coating on TPU substrate form cracks after its dried and the conductive path takes a fractured structure where as on cotton substrate the coating is continuous. The difference is caused by the hydrophobic surface of the TPU film and the hydrophilic structure of the cotton fabric. Adhesion of the ink film is determined by the reciprocal interactions of polar and nonpolar (dispersive) components between polymer films and inks. The greater the similarity between the polar and dispersive components of inks, coating and substrates, the better the wetting and adhesion on the surface of printing substrate.

The images show that Graphite has a continuous structure on both TPU and cotton substrates. The resistance values are lower in the case of cotton substrates. This may be due to the fact that cotton is hydrophilic and absorbs some of the ink into its fibers and threads, strengthening the bonds the ink forms with the substrate. No significant fractures can be observed on the coating. The graphite particles dispersed in PEDOT:PSS form clusters on some parts of the substrate for both subtrates. Stapel fibers on the surface of the cotton substrate cause some unevenness along the conductive path. With TPU substrate any crease on the film reflects to the conductive path as can be observed in Figure 3.27 (d). Although the ink covers the substrate surface completely it has a grainy texture due to the size and shape of the graphite particles.

Graphene has a lower particle size than CWM and graphite therefore it forms a smoother structure on both substrates. It would be easily scraped off unless further preventive measures are taken, such as coating a protective layer over the flexible electrode. Since cotton substrate has absorbed some of the ink into its structure, it will not lose its conductivity completely even if the outer layer is partially scraped off although an increase in resistance may be observed under such conditions.

Surface coverage increases with the increase in the number of layers of coating. As the concentration of CWM particles in the ink solution increases, coverage also increases. With TPU samples the design of the electrode is transferred clearly onto the substrate.

The edges are sharp and clean where as with cotton samples due to the wicking properties of cotton, ink is wicked outside the designed path and the pattern looks dispersed.

Cotton and TPU substrates were coated with 3 different dispersions to observe superamphiphobic properties. Contact angles for water and oil droplets were measured using Theta Lite by Biolin Scientific in BTU Chemical Engineering and BTU Central Laboratories. The improvement of hydrophobicity of hydrophilic cotton substrates is considerably good. There is some improvement on TPU hydrophobicity but it is not nearly as good as cotton substrate. Cotton substrate in its pure form is highly hydrophilic and oleophilic. The contact angle measurement for untreated cotton substrate shows no contact angle detected, in other words the cotton material fully absorbs water and oil droplets. TPU in its pure form is hydrophobic with a 101˚ contact angle. Oleophilic characteristic of TPU substrate is less compared to cotton but still the 59˚ contact angle is not high enough to be characterized as oleophobic. The contact angle measurements show that coated cotton fabric yields better results than coated TPU substrate. ZnSt added Tubiguard dispersion provides higher amphiphobic properties to the substrates. Cotton, due to its fibrous composition and the microhiearchical structure formed by the staple fibers on the substrate surface enable cotton to gain amphiphobic properties. Tubiguard and zinc stearate coated cotton substrate has a 143.33˚ CA with water and 135,33˚ CA with oil. Tubiguard and zinc stearate coated TPU substrate has an average CA of 124.66 for water and 79,54˚ for oil. TPU coated with tubiguard and SiO_2 has CA of 85.8 . Oleophobic and hydrophobic properties could be improved by increasing weight percentage of ZnSt and SiO_2 and by applying more than one layer of amphiphobic coating.

The findings of this thesis study show that as the particle size of conductive materials decrease and the surface area increases, the conductive ink dispersion and substrate displays better performance. Properties of the substrate such as hydrophilicity or hydrophilicity, fibrous or film structure also affect the outcome of the sensor. Cotton coated with Tubiguard and zinc stearate dispersion had the highest contact angles for both water and oil showing superior amphiphobic properties. Graphene and PEDOT:PSS dispersion shows excellent morphological, electrical and electromechanical properties. Properties of CWM sensors can be improved by reducing the size of CWM particles. 3 layers of 2 gr of CWM in 10 ml PEDOT:PSS

printed on cotton substrate gave good resistance values at resting state, however electromechanical properties would need to be improved under strain. The results gained from this thesis study indicate that although graphene has superior characteristics, CWM can be a sustainable alternative in manufacturing flexible sensors. CWM can be utilized in applications where less sensitivity is required. It has environmental benefits because it is obtained from recycled materials, as well as cost benefits. Sustainable use of resources and zero-waste policies make CWM worthy of further research and development.

REFERENCES

Acosta Maya, S. (2000). The Sony walkman. *Revista Universidad EAFIT*, 36(117), 19-27.

Ajana, B. (2017). Digital health and the biopolitics of the Quantified Self. *Digital health*, *3*, 2055207616689509.

Antikainen, A., Reijonen, J., Lagerbom, J., Lindroos, M., Pinomaa, T., & Lindroos, T. (2022). Single-Track Laser Scanning as a Method for Evaluating Printability: The Effect of Substrate Heat Treatment on Melt Pool Geometry and Cracking in Medium Carbon Tool Steel. Journal of Materials Engineering and Performance, 1-15.

Aroganam, G., Manivannan, N., & Harrison, D. (2019). Review on wearable technology sensors used in consumer sport applications. *Sensors*, *19*(9).

Aydemir, C., Altay, B. N., & Akyol, M. (2021). Surface analysis of polymer films for wettability and ink adhesion. Color Research & Application, 46(2), 489-499.

Bae, G. Y., Pak, S. W., Kim, D., Lee, G., Kim, D. H., Chung, Y., & Cho, K. (2016). Linearly and highly pressure-sensitive electronic skin based on a bioinspired hierarchical structural array. *Advanced Materials*, *28*(26), 5300-5306.

Bedeloğlu, A., &Taş, M. (2016). Grafen ve grafen üretim yöntemleri. Afyon Kocatepe Üniversitesi Fen ve Mühendislik Bilimleri Dergisi, 16(3), 544-554.

Bohunicky, B., & Mousa, S. A. (2010). Biosensors: the new wave in cancer diagnosis. *Nanotechnology, science and applications*, 1-10.

Borkowski, S., Sandrick, C., Wagila, K., Goller, C., Ye, C., & Zhao, L. (2016). Magicbands in the magic kingdom: customer-centric information technology implementation at disney. *Journal of the International Academy for Case Studies*, *22*(3), 143.

Boutry, C. M., Nguyen, A., Lawal, Q. O., Chortos, A., Rondeau-Gagné, S., & Bao, Z. (2015). A sensitive and biodegradable pressure sensor array for cardiovascular monitoring. *Advanced Materials*, 27(43), 6954-6961.

Buechley, L., & Eisenberg, M. (2008). The LilyPad Arduino: Toward wearable engineering for everyone. *IEEE Pervasive Computing*, *7*(2), 12-15.

Caldara, M., Colleoni, C., Guido, E., Re, V., & Rosace, G. (2016). Optical monitoring of sweat pH by a textile fabric wearable sensor based on covalently bonded litmus-3-glycidoxypropyltrimethoxysilane coating. *Sensors and Actuators B: Chemical*, 222, 213-220.

Castillo-Henríquez, L., Brenes-Acuña, M., Castro-Rojas, A., Cordero-Salmerón, R., Lopretti-Correa, M., & Vega-Baudrit, J. R. (2020). Biosensors for the detection of bacterial and viral clinical pathogens. *Sensors*, *20*(23), 6926.

Cao, M., Su, J., Fan, S., Qiu, H., Su, D., & Li, L. (2021). Wearable piezo-resistive pressure sensors based on 3D graphene. *Chemical Engineering Journal*, 406, 126777.

Chen, S., Wu, N., Lin, S., Duan, J., Xu, Z., Pan, Y., ... & Zhou, J. (2020). Hierarchical elastomer tuned self-powered pressure sensor for wearable multifunctional cardiovascular electronics. *Nano Energy*, 70, 104460.

Chen, W., & Huang, Y. (2022). Advanced three-dimensional graphene-based piezoresistive sensors in wearable devices. In *Journal of Physics: Conference Series* (Vol. 2174, No. 1, p. 012019). IOP Publishing.

Chen, Y., Lu, B., Chen, Y., & Feng, X. (2015). Breathable and stretchable temperature sensors inspired by skin. Scientific reports, 5(1), 1-11.

Cherrington, R., Goodship, V., & Middleton, B. (2016). Design and Manufacture of Plastic Components for Multifunctionality: Structural Composites, Injection Molding, and 3D Printing, p.40, Elsevier

Chiang, C. K., Park, Y. W., Heeger, A. J., Shirakawa, H., Louis, E. J., & MacDiarmid, A. G. (1978). Conducting polymers: Halogen doped polyacetylene. *The Journal of Chemical Physics*, *69*(11), 5098-5104.

Choi, W., Lahiri, I., Seelaboyina, R., & Kang, Y. S. (2010). Synthesis of graphene and its applications: a review. Critical Reviews in Solid State and Materials Sciences, 35(1), 52-71.

Chu, Z., & Seeger, S. (2014). Superamphiphobic surfaces. *Chemical Society Reviews*, *43*(8), 2784-2798.

Chung, D. D. L. (2002). Review graphite. *Journal of materials science*, 37(8), 1475-1489.

Cima, M. J. (2014). Next-generation wearable electronics. *Nature biotechnology*, 32(7), 642-643.

Comini, E. (2021). Achievements and challenges in sensor devices. *Frontiers in Sensors*, *1*, 607063.

Costa, J. C., Spina, F., Lugoda, P., Garcia-Garcia, L., Roggen, D., & Münzenrieder, N. (2019). Flexible sensors—from materials to applications. *Technologies*, *7*(2), 35.

Cotur, Y., Kasimatis, M., Kaisti, M., Olenik, S., Georgiou, C., & Güder, F. (2020). Stretchable composite acoustic transducer for wearable monitoring of vital signs. *Advanced functional materials*, 30(16), 1910288.

Currano, L. J., Sage, F. C., Hagedon, M., Hamilton, L., Patrone, J., & Gerasopoulos, K. (2018). Wearable sensor system for detection of lactate in sweat. *Scientific reports*, 8(1), 1-11.

Dagdeviren, C., Su, Y., Joe, P., Yona, R., Liu, Y., Kim, Y. S., ... & Rogers, J. A. (2014). Conformable amplified lead zirconate titanate sensors with enhanced piezo-electric response for cutaneous pressure monitoring. *Nature communications*, 5(1), 1-10.

De France, K., Zeng, Z., Wu, T., & Nyström, G. (2021). Functional materials from nanocellulose: utilizing structure–property relationships in bottom-up fabrication. Advanced Materials, 33(28), 2000657.

Dehghani-Sanij, A. R., Tharumalingam, E., Dusseault, M. B., & Fraser, R. (2019). Study of energy storage systems and environmental challenges of batteries. *Renewable and Sustainable Energy Reviews*, *104*, 192-208.

Desai, P. R., Desai, P. N., Ajmera, K. D., & Mehta, K. (2014). A review paper on oculus rift-a virtual reality headset. *arXiv preprint arXiv:1408.1173*.

Ding, Y. R., Xue, C. H., Guo, X. J., Wang, X., Jia, S. T., & An, Q. F. (2022). Flexible superamphiphobic film with a 3D conductive network for wearable strain sensors in humid conditions. *ACS Applied Electronic Materials*, *4*(1), 345-355.

Dolibog, P., Pietrzyk, B., Kierszniok, K., & Pawlicki, K. (2022, February). Comparative analysis of human body temperatures measured with noncontact and contact thermometers. In *Healthcare* (Vol. 10, No. 2, p. 331). MDPI.

Dolson, C. M., Harlow, E. R., Phelan, D. M., Gabbett, T. J., Gaal, B., McMellen, C., ... & Seshadri, D. R. (2022). Wearable Sensor Technology to Predict Core Body Temperature: A Systematic Review. *Sensors*, *22*(19), 7639.

Due, B. L. (2014). *The future of smart glasses: An essay about challenges and possibilities with smart glasses* (Vol. 1, pp. 1-21). København, Denmark: Centre of Interaction Research and Communication Design, University of Copenhagen.

Duocastella, M., Kim, H., Serra, P., & Piqué, A. (2012). Optimization of laser printing of nanoparticle suspensions for microelectronic applications. Applied Physics A, 106, 471-478.

Erdem, Ö., Eş, I., Akceoglu, G. A., Saylan, Y., & Inci, F. (2021). Recent advances in microneedle-based sensors for sampling, diagnosis and monitoring of chronic diseases. *Biosensors*, *11*(9), 296.

Erdonmez, F. S., & Bedeloğlu, A. Ç. (2023). Textile-Based Flexible and Wearable Sensors. Flexible and Wearable Sensors: Materials, Technologies, and Challenges, 253.

Eswaraiah, V., Balasubramaniam, K., & Ramaprabhu, S. (2011). Functionalized graphene reinforced thermoplastic nanocomposites as strain sensors in structural health monitoring. *Journal of Materials Chemistry*, 21(34), 12626-12628.

Fernandes, T. G., Diogo, M. M., & Cabral, J. M. (2013). Stem Cell Bioprocessing: For Cellular Therapy, Diagnostics and Drug Development. Elsevier.

Ferrone, A., Maita, F., Maiolo, L., Arquilla, M., Castiello, A., Pecora, A., ... & Colace, L. (2016, June). Wearable band for hand gesture recognition based on strain sensors. In 2016 6th IEEE International Conference on Biomedical Robotics and Biomechatronics (BioRob) (pp. 1319-1322). IEEE.

Fonseca, L., Corujo, D., Xavier, W., & Gonçalves, P. (2022). On the Development of a Wearable Animal Monitor. *Animals*, *13*(1), 120.

Galpayage Dona, D. G., Wang, M., Liu, M., Motta, N., Waclawik, E., & Yan, C. (2012). Recent advances in fabrication and characterization of graphene-polymer nanocomposites. Graphene, 1(2), 30-49.

Gao, L., Zhu, C., Li, L., Zhang, C., Liu, J., Yu, H. D., & Huang, W. (2019). All paper-based flexible and wearable piezoresistive pressure sensor. *ACS applied materials & interfaces*, *11*(28), 25034-25042.

Gautschi, G. (2002). Piezoelectric sensors. In *Piezoelectric Sensorics* (pp. 73-91). Springer, Berlin, Heidelberg.

Geim, A. K. (2009). Graphene: status and prospects. *science*, *324*(5934), 1530-1534.

Ghaffari, S., Aliofkhazraei, M., Darband, G. B., Zakeri, A., & Ahmadi, E. (2019). Review of superoleophobic surfaces: Evaluation, fabrication methods, and industrial applications. Surfaces and Interfaces, 17, 100340.

Gioberto, G. (2015). *Measuring joint movement through garment-integrated wearable sensing* (Doctoral dissertation, University of Minnesota).

Godfrey, A. (Ed.). (2021). *Digital Health: Exploring Use and Integration of Wearables*. Academic Press.

Grabis, D. W. (1980). The LCD Market: The origin and underlying reasons for the growth of liquid crystal display technology in the USA--focus: electronic watch and calculator applications. Golden Gate University.

Guler, S. D., Gannon, M., & Sicchio, K. (2016). *Crafting wearables: Blending technology with fashion*. Apress.

Hailstone, J., & Kilding, A. E. (2011). Reliability and validity of the Zephyr™ BioHarness™ to measure respiratory responses to exercise. *Measurement in Physical Education and Exercise Science*, *15*(4), 293-300.

Han, T. H., Kim, H., Kwon, S. J., & Lee, T. W. (2017). Graphene-based flexible electronic devices. *Materials Science and Engineering: R: Reports*, *118*, 1-43.

Hatamie, A., Angizi, S., Kumar, S., Pandey, C. M., Simchi, A., Willander, M., & Malhotra, B. D. (2020). Textile based chemical and physical sensors for healthcare monitoring. Journal of the Electrochemical Society, 167(3), 037546.

Heo, J. S., Hossain, M. F., & Kim, I. (2020). Challenges in design and fabrication of flexible/stretchable carbon-and textile-based wearable sensors for health monitoring: A critical review. Sensors, 20(14), 3927.

Herzer, N., Hoeppener, S., & Schubert, U. S. (2010). Fabrication of patterned silane based self-assembled monolayers by photolithography and surface reactions on silicon-oxide substrates. *Chemical Communications*, 46(31), 5634-5652.

Homayounfar, S. Z., & Andrew, T. L. (2020). Wearable sensors for monitoring human motion: a review on mechanisms, materials, and challenges. *SLAS TECHNOLOGY: Translating Life Sciences Innovation*, *25*(1), 9-24.

Hong, S. Y., Lee, Y. H., Park, H., Jin, S. W., Jeong, Y. R., Yun, J., ... & Ha, J. S. (2016). Stretchable active matrix temperature sensor array of polyaniline nanofibers for electronic skin. *Advanced materials*, 28(5), 930-935.

Hossain, S. Z., Luckham, R. E., Smith, A. M., Lebert, J. M., Davies, L. M., Pelton, R. H., ... & Brennan, J. D. (2009). Development of a bioactive paper sensor for detection of neurotoxins using piezo-electric inkjet printing of sol− gel-derived bioinks. *Analytical chemistry*, 81(13), 5474-5483.

Hsieh, Y. L. (2007). Chemical structure and properties of cotton. Cotton: Science and technology, 3-34.

Url-1 <https://polymerdatabase.com/polymer%20classes/Polyurethane%20type.html Accessed November 20, 2022.

Url-2 <https://www.hleewainwright.com/ Accessed February 12, 2022.

Url-3 <https://www.keyence.com/ss/products/measure/sealing/coater-type/spray.jsp Accessed December 8, 2022.

Url-4 <https://www.maximizemarketresearch.com/market-report/global-printed-and-flexible-sensors-market/36362/ Accessed December 18, 2022.

Url-5 <https://www.precedenceresearch.com/printed-and-flexible-sensors-market. Accessed December 18, 2022.

Url-5 <https://www.sigmaaldrich.com/TR/en/product/aldrich/307564

Accessed November 20, 2022.

Hu, L., Song, J., Yin, X., Su, Z., & Li, Z. (2020). Research progress on polymer solar cells based on PEDOT: PSS electrodes. *Polymers*, *12*(1), 145.

Hu, Q., Nag, A., Xu, Y., Han, T., & Zhang, L. (2021). Use of graphene-based fabric sensors for monitoring human activities. *Sensors and Actuators A: Physical*, *332*, 113172.

Huang, Y., Fan, X., Chen, S. C., & Zhao, N. (2019). Emerging technologies of flexible pressure sensors: materials, modeling, devices, and manufacturing. Advanced functional materials, 29(12), 1808509.

Huang, J., Hao, Y., Zhao, M., Qiao, H., Huang, F., Li, D., & Wei, Q. (2021). Biomass-based wearable and Self-powered pressure sensor for human motion detection. Composites Part A: Applied Science and Manufacturing, 146, 106412.

Hughes-Riley, T., Dias, T., & Cork, C. (2018). A historical review of the development of electronic textiles. *Fibers*, *6*(2), 34.

Homayounfar, S. Z., & Andrew, T. L. (2020). Wearable sensors for monitoring human motion: a review on mechanisms, materials, and challenges. SLAS TECHNOLOGY: Translating Life Sciences Innovation, 25(1), 9-24.

Iguchi, S., Mitsubayashi, K., Uehara, T., & Ogawa, M. (2005). A wearable oxygen sensor for transcutaneous blood gas monitoring at the conjunctiva. Sensors and Actuators B: Chemical, 108(1-2), 733-737.

Islam, R., Khair, N., Ahmed, D. M., & Shahariar, H. (2019). Fabrication of low cost and scalable carbon-based conductive ink for E-textile applications. *Materials Today Communications*, *19*, 32-38.

Ismail, W. M. I. W., Razab, M. K. A. A., & Masri, M. N. (2016). Effect of Cathode Waste Material Concentration in Conductive Paint Coating. *J. Trop. Resour. Sustain. Sci*, *4*, 78-81.

Jian, M., Wang, C., Wang, Q., Wang, H., Xia, K., Yin, Z., ... & Zhang, Y. (2017). Advanced carbon materials for flexible and wearable sensors. Science China Materials, 60(11), 1026-1062.

Kang, M., Kim, J., Jang, B., Chae, Y., Kim, J. H., & Ahn, J. H. (2017). Graphene-based three-dimensional capacitive touch sensor for wearable electronics. *ACS nano*, *11*(8), 7950-7957.

Kazani, I., Hertleer, C., De Mey, G., Schwarz, A., Guxho, G., & Van Langenhove, L. (2012). Electrical conductive textiles obtained by screen printing. Fibres & Textiles in Eastern Europe, 20(1), 57-63.

Keum, K., Heo, J. S., Eom, J., Lee, K. W., Park, S. K., & Kim, Y. H. (2021). Highly sensitive textile-based capacitive pressure sensors using PVDF-HFP/ionic liquid composite films. Sensors, 21(2), 442.

Khan, S., Lorenzelli, L., & Dahiya, R. S. (2014). Technologies for printing sensors and electronics over large flexible substrates: A review. *IEEE Sensors Journal*, *15*(6), 3164-3185.

Kim, H. H., Mazumder, M., Lee, S. J., & Lee, M. S. (2020). Laboratory Evaluation of Sustainable PMA Binder Containing Styrene-Isoprene-Styrene (SIS) and Thermoplastic Polyurethane. *Sustainability*, *12*(23), 10057.

Kim, Y., & Oh, J. H. (2020). Recent progress in pressure sensors for wearable electronics: From design to applications. *Applied Sciences*, 10(18), 6403.

Kite-Powell, J. (2016). Polar: The original fitness tracker and heart rate monitor. Forbes.

Koca, H. D., Doganay, S., Turgut, A., Tavman, I. H., Saidur, R., & Mahbubul, I. M. (2018). Effect of particle size on the viscosity of nanofluids: A review. Renewable and Sustainable Energy Reviews, 82, 1664-1674.

Koch, K., Bhushan, B., Jung, Y. C., & Barthlott, W. (2009). Fabrication of artificial Lotus leaves and significance of hierarchical structure for superhydrophobicity and low adhesion. Soft Matter, 5(7), 1386-1393.

Kramar, A., & González-Benito, F. J. (2022). Cellulose-Based Nanofibers Processing Techniques and Methods Based on Bottom-Up Approach—A Review. Polymers, 14(2), 286.

Krol, P. (2007). Synthesis methods, chemical structures and phase structures of linear polyurethanes. Properties and applications of linear polyurethanes in polyurethane elastomers, copolymers and ionomers. *Progress in materials science*, *52*(6), 915-1015.

Kwak, Y. H., Kim, W., Park, K. B., Kim, K., & Seo, S. (2017). Flexible heartbeat sensor for wearable device. *Biosensors and Bioelectronics*, 94, 250-255.

Li, L., Zheng, J., Chen, J., Luo, Z., Su, Y., Tang, W., ... & Li, H. (2020). Flexible pressure sensors for biomedical applications: from ex vivo to in vivo. Advanced Materials Interfaces, 7(17), 2000743.

Li, S., Li, R., González, O. G., Chen, T., & Xiao, X. (2021). Highly sensitive and flexible piezoresistive sensor based on c-MWCNTs decorated TPU electrospun fibrous network for human motion detection. Composites Science and Technology, 203, 108617.

Li, X. P., Li, Y., Li, X., Song, D., Min, P., Hu, C., ... & Yu, Z. Z. (2019). Highly sensitive, reliable and flexible piezoresistive pressure sensors featuring polyurethane sponge coated with MXene sheets. *Journal of colloid and interface science*, *542*, 54-62.

Li, Y., Samad, Y. A., Taha, T., Cai, G., Fu, S. Y., & Liao, K. (2016). Highly flexible strain sensor from tissue paper for wearable electronics. *ACS sustainable chemistry & engineering*, 4(8), 4288-4295.

Li, P., Tao, C. A., Wang, B., Huang, J., Li, T., & Wang, J. (2018). Preparation of graphene oxide-based ink for inkjet printing. Journal of nanoscience and nanotechnology, 18(1), 713-718.

Li, Y., Yang, Z., Wang, G., & Yang, C. (2020). Research on piezo-electric pressure sensor for shock wave load measurement. ISA transactions, 104, 382-392.

Li, L., Han, L., Hu, H., & Zhang, R. (2023). A review on polymers and their composites for flexible electronics. Materials Advances.

Liu, G., Chen, X., Li, X., Wang, C., Tian, H., Chen, X., ... & Shao, J. (2021). Flexible, equipment-wearable piezoelectric sensor with piezoelectricity calibration enabled by in-situ temperature self-sensing. *IEEE Transactions on Industrial Electronics*, *69*(6), 6381-6390.

Long, Z., Liu, X., Xu, J., Huang, Y., & Wang, Z. (2022). High-Sensitivity Flexible Piezoresistive Pressure Sensor Using PDMS/MWNTS Nanocomposite Membrane Reinforced with Isopropanol for Pulse Detection. *Sensors*, *22*(13), 4765.

Lower, E. S. (1982). Zinc stearate: its properties and uses, *Pigment & Resin Technology*, Vol. 11 No. 6, pp. 9-14

Luo, J., Zhang, L., Wu, T., Song, H., & Tang, C. (2021). Flexible piezo-electric pressure sensor with high sensitivity for electronic skin using near-field electrohydrodynamic direct-writing method. *Extreme Mechanics Letters*, 48, 101279.

Malmivaara, M. (2009). The emergence of wearable computing. In *Smart clothes and wearable technology* (pp. 3-24). Woodhead Publishing.

Manjakkal, L., Sakthivel, B., Gopalakrishnan, N., & Dahiya, R. (2018). Printed flexible electro-chemical pH sensors based on CuO nanorods. *Sensors and Actuators B*: Chemical, 263, 50-58.

Manjakkal, L., Dervin, S., & Dahiya, R. (2020). Flexible potentiometric pH sensors for wearable systems. *RSC advances*, *10*(15), 8594-8617.

Mann, S. (1997). Smart clothing: The wearable computer and wearcam. *Personal Technologies*, *1*, 21-27.

Mannoor, M. S., Tao, H., Clayton, J. D., Sengupta, A., Kaplan, D. L., Naik, R. R., ... & McAlpine, M. C. (2012). Graphene-based wireless bacteria detection on tooth enamel. *Nature communications*, 3(1), 1-9.

Marco, S., Samitier, J., Ruiz, O., Morante, J. R., & Esteve, J. (1996). High-performance piezo-resistive pressure sensors for biomedical applications using very thin structured membranes. Measurement science and technology, 7(9), 1195.

Miah, M. R., Yang, M., Hossain, M. M., Khandaker, S., & Awual, M. R. (2022). Textile-based flexible and printable sensors for next generation uses and their contemporary challenges: A critical review. Sensors and Actuators A: Physical, 113696.

Mishra, R. B., El-Atab, N., Hussain, A. M., & Hussain, M. M. (2021). Recent progress on flexible capacitive pressure sensors: From design and materials to applications. *Advanced materials technologies*, *6*(4), 2001023.

Murray, H. H. (2006). Kaolin applications. *Developments in clay science*, *2*, 85-109.

Nag, A., Mukhopadhyay, S. C., & Kosel, J. (2017). Wearable flexible sensors: A review. *IEEE Sensors Journal*, 17(13), 3949-3960.

Nag, A., & Mukhopadhyay, S. C. (2021). The fabrication of printed flexible sensors: challenges and possible outcomes. In *Printed and Flexible Sensor Technology: Fabrication and applications* (pp. 59-82). IOP Publishing. mo

Nagamine, K., Mano, T., Nomura, A., Ichimura, Y., Izawa, R., Furusawa, H., ... & Tokito, S. (2019). Noninvasive sweat-lactate biosensor emplsoying a hydrogel-based touch pad. *Scientific reports*, 9(1), 1-8.

Nasiri, S., & Khosravani, M. R. (2020). Progress and challenges in fabrication of wearable sensors for health monitoring. *Sensors and Actuators A: Physical*, 312, 112105.

Neinhuis, C., & Barthlott, W. (1997). Characterization and distribution of water-repellent, self-cleaning plant surfaces. Annals of botany, 79(6), 667-677.

Nimbalkar, S. M. (2015). Pulse Oximetry. *Journal of Neonatology*, *29*(3), 29-34.

Nossier, S. A., Rizk, M. R. M., Moussa, N. D., & el Shehaby, S. (2019). Enhanced smart hearing aid using deep neural networks. *Alexandria Engineering Journal*, *58*(2), 539-550.

Ohta, S., Komagata, S., Seki, J., Saeki, T., Morishita, S., & Asaoka, T. (2013). All-solid-state lithium ion battery using garnet-type oxide and Li3BO3 solid electrolytes fabricated by screen-printing. *Journal of Power Sources*, 238, 53-56.

Orth, M., Post, R., & Cooper, E. (1998, April). Fabric computing interfaces. I*n CHI 98 conference summary on human factors in computing system*s (pp. 331-332).

Oseledchik, M., Ivleva, M., & Ivlev, V. (2017, June). Knowledge as a non-equilibrium dynamic system. *In 2nd International Conference on Contemporary Education, Social Sciences and Humanities* (ICCESSH 2017) (pp. 1-5). Atlantis Press.

Pang, C., Lee, G. Y., Kim, T. I., Kim, S. M., Kim, H. N., Ahn, S. H., & Suh, K. Y. (2012). A flexible and highly sensitive strain-gauge sensor using reversible interlocking of nanofibres. *Nature materials*, 11(9), 795-801.

Parameswaran, C., & Gupta, D. (2019). Large area flexible pressure/strain sensors and arrays using nanomaterials and printing techniques. Nano Convergence, 6(1), 1-23.

Park, D. Y., Joe, D. J., Kim, D. H., Park, H., Han, J. H., Jeong, C. K., ... & Lee, K. J. (2017). Self-powered real-time arterial pulse monitoring using ultrathin epidermal piezo-electric sensors. *Advanced Materials*, 29(37), 1702308.

Park, S. W., Das, P. S., Chhetry, A., & Park, J. Y. (2017). A flexible capacitive pressure sensor for wearable respiration monitoring system. *IEEE Sensors Journal*, 17(20), 6558-6564.

Park, S., & Jayaraman, S. (2003). Smart textiles: Wearable electronic systems. *MRS bulletin*, 28(8), 585-591.

Park, S., Mackenzie, K., & Jayaraman, S. (2002, June). The wearable motherboard: a framework for personalized mobile information processing (PMIP). In *proceedings of the 39th annual design automation conference* (pp. 170-174).

Phiri, J., Johansson, L. S., Gane, P., & Maloney, T. (2018). A comparative study of mechanical, thermal and electrical properties of graphene-, graphene oxide-and reduced graphene oxide-doped microfibrillated cellulose nanocomposites. Composites Part B: Engineering, 147, 104-113.

Pierre Claver, U., & Zhao, G. (2021). Recent progress in flexible pressure sensors based electronic skin. Advanced Engineering Materials, 23(5), 2001187.

Portella, E. H., Romanzini, D., Angrizani, C. C., Amico, S. C., & Zattera, A. J. (2016). Influence of stacking sequence on the mechanical and dynamic mechanical properties of cotton/glass fiber reinforced polyester composites. Materials Research, 19, 542-547.

Prieto-Avalos, G., Cruz-Ramos, N. A., Alor-Hernández, G., Sánchez-Cervantes, J. L., Rodríguez-Mazahua, L., & Guarneros-Nolasco, L. R. (2022). Wearable devices for physical monitoring of heart: a review. *Biosensors*, *12*(5), 292.

Qiu, H., Wang, X., & Xie, F. (2017, November). A survey on smart wearables in the application of fitness. In *2017 IEEE 15th Intl Conf on Dependable, Autonomic and Secure Computing, 15th Intl Conf on Pervasive Intelligence and Computing, 3rd Intl Conf on Big Data Intelligence and*

Computing and Cyber Science and Technology Congress (DASC/PiCom/DataCom/CyberSciTech) (pp. 303-307). IEEE.

Quirós-Solano, W. F., Gaio, N., Silvestri, C., Pandraud, G., & Sarro, P. M. (2016). PEDOT: PSS: a conductive and flexible polymer for sensor integration in organ-on-chip platforms. *Procedia Engineering*, *168*, 1184-1187.

Rehman, W. U., Rasheed, T., Naveed, A., & Ali, A. (2022). Thermoplastic polyurethane/rutile titanium dioxide composites tuned for hydrophobicity with effective reinforcement. Journal of Polymer Research, 29(5), 188.

Ren, J., Wang, C., Zhang, X., Carey, T., Chen, K., Yin, Y., & Torrisi, F. (2017). Environmentally-friendly conductive cotton fabric as flexible strain sensor based on hot press reduced graphene oxide. Carbon, 111, 622-630.

Ren, Z., Yang, J., Qi, D., Sonar, P., Liu, L., Lou, Z., ... & Wei, Z. (2021). Flexible sensors based on organic–inorganic hybrid materials. *Advanced Materials Technologies*, 6(4), 2000889.

Sahoo, B., Yoon, K., Seo, J., & Lee, T. (2018). Chemical and physical pathways for fabricating flexible superamphiphobic surfaces with high transparency. *Coatings*, 8(2), 47.

Sang Tran, T., Dutta, N. K., & Roy Choudhury, N. (2019). Graphene-based inks for printing of planar micro-supercapacitors: A review. *Materials*, 12(6), 978.

Scott, S. M., & Ali, Z. (2021). Fabrication methods for microfluidic devices: An overview. Micromachines, 12(3), 319.

Seneviratne, S., Hu, Y., Nguyen, T., Lan, G., Khalifa, S., Thilakarathna, K., ... & Seneviratne, A. (2017). A survey of wearable devices and challenges. *IEEE Communications Surveys & Tutorials*, *19*(4), 2573-2620.

Sergio, M., Manaresi, N., Tartagni, M., Guerrieri, R., & Canegallo, R. (2002, June). A textile based capacitive pressure sensor. In SENSORS, 2002 IEEE (Vol. 2, pp. 1625-1630). IEEE.

Shi, H., Liu, C., Jiang, Q., & Xu, J. (2015). Effective approaches to improve the electrical conductivity of PEDOT: PSS: a review. *Advanced Electronic Materials*, 1(4), 1500017.

Shimokura, R. (2018). Hearing Aids. In *An Excursus into Hearing Loss*. IntechOpen.

Shirakawa, H., McDiarmid, A., & Heeger, A. (2003). Twenty-five years of conducting polymers. *Chemical communications*, *2003*(1), 1-4.

Shirley, J. A., Florence, S. E., Sreeja, B. S., Padmalaya, G., & Radha, S. (2020). Zinc oxide nanostructure-based textile pressure sensor for wearable applications. *Journal of Materials Science: Materials in Electronics*, 31(19), 16519-16530.

Skyrme et al, October 2022, Wearable Sensors 2023-2033, IDTechEx Research, Retrieved December 10, 2022, from

https://www.idtechex.com/en/research-report/wearable-sensors-2023-2033/893

Smith, R. E., Totti, S., Velliou, E., Campagnolo, P., Hingley-Wilson, S. M., Ward, N. I., ... & Crean, C. (2019). Development of a novel highly conductive and flexible cotton yarn for wearable pH sensor technology. *Sensors and Actuators B: Chemical*, 287, 338-345.

Souri, H., Banerjee, H., Jusufi, A., Radacsi, N., Stokes, A. A., Park, I., ... & Amjadi, M. (2020). Wearable and stretchable strain sensors: materials, sensing mechanisms, and applications. *Advanced Intelligent Systems*, *2*(8), 2000039.

Su, Y., Ma, C., Chen, J., Wu, H., Luo, W., Peng, Y., ... & Li, H. (2020). Printable, highly sensitive flexible temperature sensors for human body temperature monitoring: a review. *Nanoscale research letters*, 15(1), 1-34.

Sun, K., Zhang, S., Li, P., Xia, Y., Zhang, X., Du, D., ... & Ouyang, J. (2015). Review on application of PEDOTs and PEDOT: PSS in energy conversion and storage devices. Journal of Materials Science: Materials in Electronics, 26, 4438-4462.

Sundén, B. (2019). *Hydrogen, batteries and fuel cells*. Chapter 4, Battery technologies, 57-79, Academic Press.

Syduzzaman, M. D., Patwary, S. U., Farhana, K., & Ahmed, S. (2015). Smart textiles and nano-technology: a general overview. *J. Text. Sci. Eng*, *5*(1).

Tadyszak, K., Wychowaniec, J. K., & Litowczenko, J. (2018). Biomedical applications of graphene-based structures. *Nanomaterials*, *8*(11), 944.

Takamatsu, S., Imai, T., Yamashita, T., Kobayashi, T., Miyake, K., & Itoh, T. (2011, October). Flexible fabric keyboard with conductive polymer-coated fibers. In SENSORS, 2011 IEEE (pp. 659-662). IEEE.

Tas, M., Altin, Y., & Bedeloglu, A. C. (2019). Reduction of graphene oxide thin films using a stepwise thermal annealing assisted by L-ascorbic acid. Diamond and Related Materials, 92, 242-247.

Üner, İ., & GÜRCÜM, B. (2019). Conductive ink applications on electronic textiles. Pamukkale University *Journal Of Engineering Sciences-Pamukkale Universitesi Muhendislik Bilimleri Dergisi*, 25(7).

Valle-Lopera, D. A., Castaño-Franco, A. F., Gallego-Londoño, J., & Hernández-Valdivieso, A. M. (2017). Test and fabrication of piezoresistive sensors for contact pressure measurement. Revista Facultad de Ingeniería Universidad de Antioquia, (82), 47-52.

Wan, S., Bi, H., Zhou, Y., Xie, X., Su, S., Yin, K., & Sun, L. (2017). Graphene oxide as high-performance dielectric materials for capacitive pressure sensors. *Carbon*, *114*, 209-216.

Wang, K., Li, J., Li, W., Wei, W., Zhang, H., & Wang, L. (2019). Highly active Co-based catalyst in nanofiber matrix as advanced sensing layer for high selectivity of flexible sensing device. *Advanced Materials Technologies*, 4(2), 1800521.

Wang, K., Wei, W., Lou, Z., Zhang, H., & Wang, L. (2019). 1D/2D heterostructure nanofiber flexible sensing device with efficient gas detectivity. *Applied Surface Science*, 479, 209-215.

Wang, T. W., & Lin, S. F. (2020). Wearable piezo-electric-based system for continuous beat-to-beat blood pressure measurement. *Sensors*, 20(3), 851.

Wiklund, J., Karakoç, A., Palko, T., Yiğitler, H., Ruttik, K., Jäntti, R., & Paltakari, J. (2021). A review on printed electronics: Fabrication methods, inks, substrates, applications and environmental impacts. *Journal of Manufacturing and Materials Processing*, 5(3), 89.

Wilson, S., & Laing, R. (2018). Wearable technologies: Present and future. In *91st world conference of the textile institute, Leeds, UK*.

Wu, S. (2022). An Overview of Hierarchical Design of Textile-Based Sensor in Wearable Electronics. *Crystals*, 12(4), 555.

Wu, X., Ma, Y., Zhang, G., Chu, Y., Du, J., Zhang, Y., ... & Huang, J. (2015). Thermally stable, biocompatible, and flexible organic field-effect transistors and their application in temperature sensing arrays for artificial skin. *Advanced Functional Materials*, 25(14), 2138-2146.

Yang, T., Xie, D., Li, Z., & Zhu, H. (2017). Recent advances in wearable tactile sensors: Materials, sensing mechanisms, and device performance. Materials Science and Engineering: R: Reports, 115, 1-37.

Yang, G., Pang, G., Pang, Z., Gu, Y., Mäntysalo, M., & Yang, H. (2018). Non-invasive flexible and stretchable wearable sensors with nano-based enhancement for chronic disease care. *IEEE reviews in biomedical engineering*, *12*, 34-71.

Yang, Y., Yang, X., Yang, Y., & Yuan, Q. (2018). Aptamer-functionalized carbon nanomaterials electro-chemical sensors for detecting cancer relevant biomolecules. *Carbon*, 129, 380-395**.**

Yang, C., Zhang, D., Wang, D., Chen, X., & Luan, H. (2022). Ultra-sensitive, stretchable, and bidirectional wearable strain sensor for human motion detection. Journal of Materials Chemistry C, 10(18), 7076-7086.

Yetisen, A. K., Moreddu, R., Seifi, S., Jiang, N., Vega, K., Dong, X., ... & Koch, A. W. (2019). Dermal tattoo biosensors for colorimetric metabolite detection. *Angewandte Chemie*, *131*(31), 10616-10623.

Yildirim, E., Wu, G., Yong, X., Tan, T. L., Zhu, Q., Xu, J., ... & Yang, S. W. (2018). A theoretical mechanistic study on electrical conductivity enhancement of DMSO treated PEDOT: PSS. *Journal of Materials Chemistry C*, *6*(19), 5122-5131.

Yoon, J. H., Kim, S. M., Park, H. J., Kim, Y. K., Oh, D. X., Cho, H. W., ... & Choi, B. G. (2020). Highly self-healable and flexible cable-type pH sensors for real-time monitoring of human fluids. *Biosensors and Bioelectronics*, 150, 111946.

Zazoum, B., Batoo, K. M., & Khan, M. A. A. (2022). Recent advances in flexible sensors and their applications. Sensors, 22(12), 653.

Zhang, X., Lei, S. H. E. N., & Ying, T. A. N. G. (2020). Research on the design of smart mountaineering gear based on solar power technology. *Textile and Apparel*, *30*(4), 231-238.

Zhang, X., Ke, L., Zhang, X., Xu, F., Hu, Y., Lin, H., & Zhu, J. (2022). Breathable and Wearable Strain Sensors Based on Synergistic Conductive Carbon Nanotubes/Cotton Fabrics for Multi-directional Motion Detection. ACS Applied Materials & Interfaces, 14(22), 25753-25762.

Zhang, J. W., Zhang, Y., Li, Y. Y., & Wang, P. (2022). Textile-based flexible pressure sensors: A review. *Polymer Reviews*, *62*(1), 65-94.

Zhao, S., Ran, W., Wang, D., Yin, R., Yan, Y., Jiang, K., ... & Shen, G. (2020). 3D dielectric layer enabled highly sensitive capacitive pressure sensors for wearable electronics. *ACS applied materials & interfaces*, 12(28), 32023-32030.

Zhong, B., Kuang, P., & Yu, J. (2022). Graphene oxide: Synthesis and properties. In *Graphene Oxide-Metal Oxide and Other Graphene Oxide-based Composites in Photocatalysis and Electrocatalysis* (pp. 31-64). Elsevier.

Zhu, B., Li, X., Zhou, L., & Su, B. (2022). An overview of wearable and implantable electrochemical glucose sensors. *Electroanalysis*, *34*(2), 237-245.